Solvent dependent growth of one-dimensional crystalline β-FeOOH nanorods

by

MAHABUBUR RAHMAN CHOWDHURY

Thesis submitted in fulfilment of the requirements for the degree

DOCTOR TECHNOLOGIAE: ENGINEERING: CHEMICAL

in the

FACULTY OF ENGINEERING

at the

CAPE PENINSULA UNIVERSITY OF TECHNOLOGY

Cape Town Campus

Supervisor: Assoc. Prof. V.G. Fester

Co-supervisor: Assoc. Prof. G.M. Kale (University of Leeds, UK)

February 2014

*"Read! In the name of your Lord Who has created (**all that exists**). He has created man from a clot (**a piece of thick coagulated blood**). Read! And your Lord is the Most Generous. Who has taught (**the writing**) by the pen. He has taught man which he knew not" [Al-Quran, 96: 1-5]*

"A saint is a sinner who keeps on trying" – N. R. Mandela

DECLARATION

I, Mahabubur Rahman Chowdhury, hereby declare that the contents of this thesis represent my own unaided work, and that the thesis has not previously been submitted for academic examination towards any qualification. Furthermore, it represents my own opinions and not necessarily those of the National Research Foundation and Cape Peninsula University of Technology.

Mahabubur Rahman Chowdhury

10 February 2014

Signed

Date

Solvent dependent growth of 1-D crystalline β-FeOOH nanorods

by

Mahabubur Rahman Chowdhury

ABSTRACT

Several authors have reported on the use of alcohols – water /or mixed solvents to synthesise metal oxide nanoparticles. However, no systematic study has been carried out to evaluate the effect of mixed solvent on the particle characteristics, although considerable research has been reported, a gap still exists with regard to the effect of the alcohols as solvents on the growth kinetics of nanoparticles. To address these issues, four different alcohols, namely, methanol (MeOH), ethanol (EtOH), propanol (PrOH) and butanol (BuOH) were used as solvents in the synthesis of β-FeOOH particles.

The effect of organic solvents on the growth kinetics of β-FeOOH nanorods has been evaluated for the first time in this study. Two-stage growth of akaganeite nanorods has been observed in BuOH and PrOH. The first growth stage follows a typical power law representing Ostwald ripening (OR) kinetic. The second stage was found to be asymptotic and obeyed oriented attachment (OA) kinetic. The proof of the OA kinetic also comes from the HRTEM images of the synthesised particles. Simultaneous occurrence of the two mechanisms was observed in the growth of the particles synthesised in EtOH and MeOH. The rate constants for OR kinetic, K_{OR}, was found to be higher than the rate constant for OA kinetic, K_{OA}, for different solvents used.

The use of a mixed solvent is a new approach in the synthesis and processing of materials. Various researchers have stated that the surface tension of the solvent plays an important role in the formation of uniform nanorods. However, the effect of surface tension was not correlated with the particle growth, earlier, though the dielectric properties of the mixed solvents were only taken into account. Additionally, no quantitative or qualitative relationship was presented between surface tension and particle growth in the literature. In this work an attempt to correlate these two parameters (surface tension and particle growth) with the concentration of the precursor and temperature was made, resulting in an exponential relationship between K_{OR} for the particle growth and surface tension of the alcohols. Furthermore, the relationship between surface tension and particle growth was validated by an independent study using statistically designed experiments to account for the influence of various process variables on the particle growth. The findings in this study obtained from both theoretical and experimental work provides an insight into the relationship between solvent surface tension and particle growth interactions, producing a new piece of information that will further promote our understanding of the formation mechanisms of β-FeOOH growth.

The transformation temperature of akaganeite (β-FeOOH) nanorods to hematite (α-Fe_2O_3) particles was found to be solvent dependent. Thermogravimetric analysis and differential scanning calorimetry were performed to evaluate the effect of alcohol on the thermodynamic stability of the particles. Alcohol as solvent played a significant role in the dehydration property of the synthesised particles. The percentage mass loss of the particles at 300˚C decreases linearly with increasing carbon number in the linear alkyl chain of the solvent.

The effect of alcohol type on the particle morphology was found to be more pronounced at higher $FeCl_3$ concentrations (>0.5M). Splitting of β-FeOOH nanorods was observed at $FeCl_3$ concentration of 0.7M in BuOH. In PrOH, rectangular morphologies were obtained whereas nanoribbons resulted in surfactant-free conditions. It was found that the nature of anions (chloride vs. nitrate and sulphate) in the precursor salt also influenced the morphology.

DEDICATION

To my dearest parents

Late Shafiqur Rahman Chowdhury and Arnis Akhter Chowdhury

To my dearest younger brothers

Ashiqur Rahman Chowdhury and Mashukur Rahman Chowdhury

To the love of my life

I could not have finished this work in time without your support and sacrifice

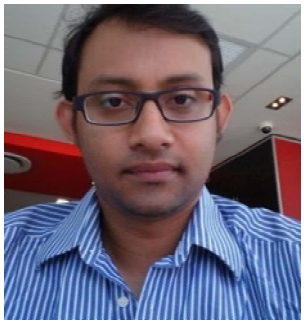

BIOGRAPHICAL SKETCH

Mahabubur Rahman Chowdhury was born in Dhaka, Bangladesh. He attended Khilgaon Government High School in Dhaka where he matriculated in 2002. He obtained his Bachelor of Technology (*cum laude*) in Chemical Engineering at CPUT in 2008. Both the SAIMM (Southern African Institute of Mining and Metallurgy) and SAIChE (South African Institution of Chemical Engineers) presented him with awards for exceptional academic achievement during his undergraduate studies. He was awarded a Master of Technology degree (passed with 73%) in Chemical Engineering in 2010, and received several postgraduate merit scholarships from the University. He also received an innovation scholarship from the National Research Foundation (NRF) of South Africa. While at the University he has worked as a research assistant/metallurgist, student tutor, lecturer, and supervisor for Bachelor of Technology research projects. His master's study has generated two published papers. The data generated from his study were included in engineering design software by an international engineering design company (ESDU). The developed correlation is used in "Pipe Tool" slurry pipeline design software. After completion of his master's degree, he enrolled for a doctorate in Chemical Engineering in 2011 under the supervision of Prof. Veruscha Fester (CPUT, RSA) and Prof. Girish Kale (University of Leeds, UK). A paper have been published so far from this work and another paper has been accepted for consideration in reputed journal.

PUBLICATIONS

1. Chowdhury, MR & Fester, VG 2012, Modelling pressure losses for Newtonian and non-Newtonian laminar and turbulent flow in long square edged orifices, Chemical engineering research and design, vol 90, pp. 863-869.
2. Chowdhury, MR, Fester, VG & Kale, GM 2014, Growth kinetics evaluation of hydrothermally synthesised β-FeOOH nanorods, Journal of crystal growth, vol 387, pp. 57-65.
3. Chowdhury, MR, Fester, VG, Kale, GM & Cespedes, O, Effect of experimental conditions on the synthesis of β-FeOOH nanostructures, Journal of nanoparticle research, (accepted).
4. Fester, VG, Chowdhury, MR & Ludicello, F 2010, Pressure loss and discharge coefficients for non-Newtonian fluids in long orifices, 18th International conference on hydrotransport, BHR group, Rio de Janeiro.

PRESENTATIONS

1. Chowdhury, MR & Fester, VG 2010, Modelling pressure losses for Newtonian and non-Newtonian laminar and turbulent flow in long square edged orifices, 18th international hydrotransport conference, Rio de Janeiro, Brazil.
2. Chowdhury, MR & Fester, VG 2012, Relationship between solvent surface tension and particle growth, CPUT post graduate conference, Cape Town, R.S.A.
3. Chowdhury, MR, Fester, VG & Kale, GM 2013, Relationship between solvent surface tension and particle growth, Nanotechnology, Cancun, Mexico.

ACKNOWLEDGEMENTS

I am grateful to:

- ALLAH the ALMIGHTY, for giving me strength and courage to pursue the highest degree.
- Prof. Veruscha Fester, for giving me the opportunity to pursue this degree under her supervision.
- Prof. Girish Kale, for his advice.
- All the crazies from the leodies flat in UK
- Dr Franscious Cummings from UCT, for helping with TEM images and microscopic analysis.
- Ronel August from UCT for assisting with the XRD analysis.
- Berita Blaauw Combrinck (CPUT) for her splendid laboratory work.
- Unitemp, South Africa, for their excellent professionalism in delivering the parts on time.
- Jackie from CJ labs for delivering the chemicals timeously.
- Steven Mudenda (PhD student at the University of Leeds, UK) for his assistance during my time at Leeds.
- All other staff of the Material Science and Technology group who contributed to this work.

The financial assistance of the Cape Peninsula University of Technology (CPUT) and the National Research Foundation (NRF) towards the research are acknowledged. Opinions expressed in this thesis and the conclusions arrived at are those of the author and are not necessarily attributable to the Cape Peninsula University of Technology or the National Research Foundation.

TABLE OF CONTENTS

LIST OF TABLES

TERMS AND CONCEPT

1-D nanorod: A rod shaped particles having both dimensions in nanometer scale.

Hydrothermal synthesis: A synthesis technique for crystallization of nanomaterials by utilizing high temperature and high pressure.

Nanowire: Practically similar to nanorod but have aspect ratios higher than 10

Ostwald ripening: Growth of bigger particles by dissolution of and re-deposition of smaller particles in solution.

Oriented attachment: A recently observed phenomenon where the particle shape or size changes by attaching different particles together crystallographically.

Supercritical water: Water at a temperature and pressure above its critical point.

LIST OF ABBREVIATIONS

1-D	One dimensional
CHP	Continuous hydrothermal synthesis
CHS	Continuous hydrothermal plant
CTAB	Cetyltrimethylammonium bromide
CVD	Chemical vapour deposition
EDS	Energy dispersive spectroscopy
FEG	Field emission gun
GRIGC	Grain rotation induced grain coalescence
HS	Hydrothermal synthesis
LSW	Lifshitz-Slyozov-Wagner
OA	Oriented attachment
OR	Ostwald ripening
NCW	Near critical water
NR	Nanorod
NT	Nanotube
NW	Nanowire
SCW	Supercritical water
SDD	Silicon drift detector
SEM	Scanning electron microscope
TEM	Transmission electron microscope
TGA	Thermogravimetric analysis

VLS	Vapour-liquid-solid
XRD	XRay diffraction

LIST OF SYMBOLS

Symbol	Description	Unit
C	Solute concentration	M
D	Particle diameter	m
d	Particle diameter	m
d_e	Equivalent diameter	m
d_o	Initial particle diameter	m
e	Electron charge	C
G	Gibbs free energy	kJ/mol
h	Planck's constant	-
K	Boltzmann's constant	-
K_{OA}	Growth rate constant	$min^{-1/3}$
K_{OR}	Growth rate constant	min^{-1}
L	Particle length	m
L_{AV}	Average particle length	m
T	Temperature	˚C
t	Time	s
GREEK SYMBOLS		
ε	Dielectric constant	-

ε_o	Permittivity in vacuum	-
μ	Viscosity	Pa.s
μ	Chemical potential	J
γ	Interfacial energy	j/m^2
σ	Surface tension	N/m
φ_{AV}	Average diameter	m

Chapter 1

Introduction

1.1 Background

Metal oxide nanoparticles often exhibit enhanced chemical, thermal, optical, electrical and magnetic properties, which make them useful in different catalysis, pigments, coatings and inks applications (Darr & Poliakoff, 1999). Iron oxide nanoparticles have promising potential in imaging technique (Jun et al., 2007). Non-spherical nanoparticles have become attractive because of their anisotropic behaviour (Jiang et al., 2010).

One-dimensional (1-D) nanomaterials such as nanowires, nanotubes, nanorods and nanoribbons have unusual properties, such as photochemical, photophysical and electron transport properties (Liu et al., 2006) and have been extensively investigated as building blocks for many functional applications, ranging from molecular nanosensors and nanoscale electronics to nanocomputing (Persson et al., 2004). Akaganeite (β-FeOOH) is a type of iron oxy hydroxide which has applications in different technological fields. One dimensional β-FeOOH nanorods and nano wires were synthesised in which surfactants were used to direct growth, achieve uniformity and prevent aggregation of the product. However, one-step surfactant-free synthesis of 1-D β-FeOOH is not common (Wei & Nan, 2011). There are several studies pertaining to the novel morphological features of a-Fe_2O_3 nanoparticles, but the same for β-FeOOH are almost non-existent, despite its different applications (application in lithium batteries, Shao et al., 2005; hydro-processing of coals, Cornell & Schwertmann, 2003; precursor to ferromagnetic materials, (xiong et al., 2003; etc.). Published literature provides strong evidence that β-FeOOH particle formation strongly

depends on the experimental conditions, however, no attempts have been made to describe mathematically how these factors impact the characteristics of the synthesised particles. Despite the number of studies conducted on the synthesis of β-FeOOH particles, there is a lack of a standardised synthesis procedure for preparation of a specific particle size systematically. Therefore, particles were synthesised systematically to derive mathematical relationships between experimental conditions and particle growth.

The particle size and morphology strongly control the magnetic and optical properties of 1-D nanoparticles. Different intriguing applications of metal oxide nanoparticles often depend on specific physical characteristics of the nanoparticles such as size, morphology and crystallinity. These physical characteristics are subject to the method employed to fabricate these particles (Kandori et al., 2002). Several techniques exist to fabricate 1-D nanostructures such as template-directed synthesis (Kim et al., 2002), vapour-solid (VS) or vapour-liquid-solid (VLS) growth (Pan et al., 2001), hydrothermal or solvothermal method (Wang & Li, 2002) and the solution-liquid-solution method (Holmes et al., 2000). Hydrothermal synthesis possesses several advantages over other manufacturing techniques, including high purity (> 99.5%) and chemical homogeneity, small particle size (< 5 nm possible), narrow particle size distribution, single-step processing, low energy usage, fast reaction times, low- cost equipment, the ability to generate metastable compounds, and importantly, no calcination is required for many materials since they are fully crystallised by the reaction (Byrappa & Adschiri, 2007). Because of all these advantages, the hydrothermal method was chosen to synthesise 1-D β-FeOOH and α-Fe_2O_3 particles in this study.

Several authors have reported the use of alcohols for nanoparticle synthesis. Chen et al. (2008) synthesised hematite nanoplates using alcohols as solvents. They reported that alcohol played an important role in controlling nanoplate sizes. Liu et al. (2006) reported the synthesis of 1-D α-Fe_2O_3 nanorods and tubes in the presence of butanol and different surfactants (L113B and SPAN 80). Together with the surfactant, it was believed that butanol played an important role in obtaining the rod-like

structure. Shao et al. (2005) reported the synthesis of arrayed akaganeite nanorods and hexagram shaped particles using ethanol as solvent. The authors reported that the surface tension of the ethanol-water mixture was low enough to form β-FeOOH nanorods. Fester et al. (2008) reported use of alcohols in the synthesis of 1-D α-Fe_2O_3 nanorods and concluded that 1-D α-Fe_2O_3 nanorods could be synthesised without a surfactant only in butanol. Vorkapic and Matsoukas (1998) studied the role of alcohols in the preparation of titania colloids and reported that alcohol played a significant role in the synthesis of the particles. Verdon and co-worker (1995) found that the presence of ethanol improved the dehydration properties of the particles significantly, compared with those synthesised without ethanol. Liang et al., (2010) developed a continuous hydrothermal method to produce single crystal iron oxide nanoparticles using ferric nitrate and isopropanol (IPA). The degree of crystallinity and crystal size decreased with increasing amount of IPA, indicating that the presence of alcohol mainly affected the crystallization process. A correlation between the type of alcoholic solvent and the growth mechanism of the β-FeOOH nanoparticles is lacking which makes this study relevant.

Surface tension of alcohol plays an important role in the formation of uniform nanorods. A low surface tension of solvent can promote the growth of β-FeOOH nanorods (Shao et al., 2005, Fester et al., 2008). Addition of medium which can lower the surface tension of precursor solution can alter the thermodynamic properties of the reaction system and subsequently affect the nucleation kinetics, which would result in various morphology and particle sizes. The application of alcohol / water mixture during the synthesis of different metal oxide nanoparticles can be found in the literature. However the effect of mixed solvent properties on the growth of 1-D β-FeOOH nanorods was not evaluated despite of its numerous industrial and scientific applications. Dielectric constants of the mixed solvents were related to particle nucleation and growth in all cases. Coulombic interaction is weaker in water and solvent with high dielectric constant values (Israelachvili, 1992). This phenomenon makes the application of the dielectric constant only, to relate particle growths susceptible. On the hypothesis that a quantitative and / or qualitative relationship between alcohol surface tension and particle growth exists, the effect of four

different alcohols on the growth kinetics of β-FeOOH nanorods has been evaluated. Empirical correlations have been developed to further illustrate the relationships between the solvent surface tension and particle growth.

1.2 Objectives of the study

The objectives of the study can be summarised as:

1. To conduct a systematic study to evaluate the effect of alcohol on the β-FeOOH particle morphology and growth mechanism under different hydrothermal processing conditions, i.e. solvent ratio, precursor concentration and type and temperature.
2. To establish a quantitative and / or qualitative relationship between particle growth and solvent surface tension.

1.3 Delineation of the study

The following was not included in this study:

- Applications of the synthesised particles.
- Use of nonpolar solvent to synthesise the particles.

Chapter 2

Literature review

2.1 Introduction

This chapter presents a brief review of literature on different synthesis techniques to obtain iron oxide nanoparticles. One-dimensional nanostructures are reviewed. Effect of surfactant and nature of alcohol used as solvent on the morphology of the synthesized iron oxide nanoparticles is discussed. A comprehensive review of different growth kinetics is offered. Fundamentals of different characterisation techniques are also briefly given.

2.2 Iron oxides

One of the common compounds that exists as a natural mineral and can also be fabricated synthetically is iron oxide. There are 16 types of iron oxides are known to date (Cornell & Schwertmann, 2003) and these are noted in Table 2.1.

2.2.1 Structure of iron oxides

Iron oxides are crystalline except schwertmannite and ferrihydrite, which are poorly crystalline. The structural chemistry of iron compounds is diverse; this is reflected in their large number of atomic structures. Figure 2.1 presents the structures of common iron compounds. Virtually all the phases of iron compounds can be formed from chemical solutions, alluding to a complicated chemistry of formation (Almeida, 2010). The high versatility of iron chemistry in an aqueous medium originates from two factors: 1) the occurrence of two oxidation states, Fe^{2+} and Fe^{3+} which are stable on a large range of

acidity and, 2) the high reactivity of iron complexes towards acid-base and condensation phenomena (Jolivet et al., 2006).

Table 2.1 Various types of iron oxides (Azhar, 2007)

Oxides	**Oxyhydroxides and hydroxides**
Hematite, α-Fe_2O_3	Goethite, α-FeOOH
Magnetite, Fe_3O_4	Lepidocrocite, ϒ-FeOOH
Maghemite, ϒ-Fe_2O_3	Akaganeite, β-FeOOH
β-Fe_2O_3	Schwertmannite, $Fe_{16}O_{16}(OH)y(SO_4).nH_2O$
Wustite, FeO	δ-FeOOH
	Feroxyhyte, δ'-FeOOH
	High pressure, FeOOH
	Ferrihydrite, $Fe_5HO_8.4H_2O$
	Bernalite, $Fe(OH)_3$
	$Fe(OH)_2$
	Green rusts

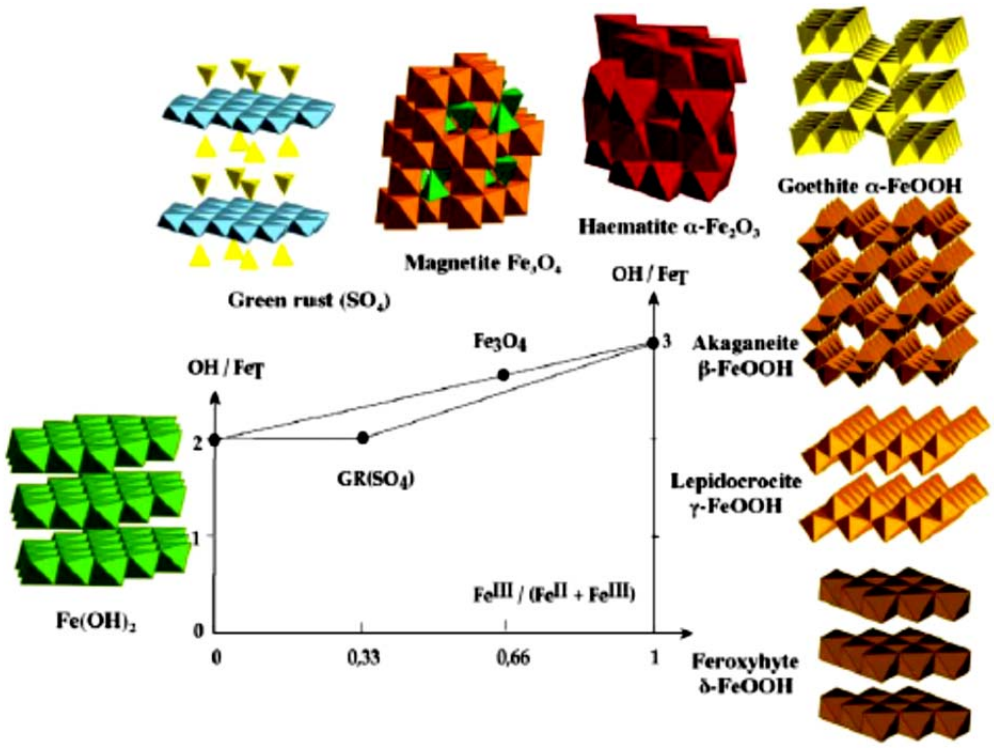

Figure 2.1 Different phases of iron oxides and hydroxides formed as a function of hydroxylation ratio and composition (Jolivet et al., 2006)

2.2.2 Hematite α – Fe_2O_3

Hematite is the oldest known of the iron oxides and is widespread in rocks and soils. It is also known as ferric oxide, iron sesquioxide, red ochre, specularite, specular iron ore, kidney ore, or martite. Hematite is blood-red in colour if finely divided, and black or grey if coarse (Teja & Koh, 2009). Hematite is extremely stable at ambient conditions and often is the end product of the transformation of other iron oxides. It is isostructural with corundum. The unit cell is hexagonal with a = 0.5034 nm and c = 1.375 nm. There are six formula units in a unit cell of hematite. The structure of iron oxides consists of hexagonal close-packed arrays of oxygen ions stacked along the {001} direction. Fe^{3+} ions are arranged in such a way that two filled sites are followed by a vacant site in the {001} plane, thus forming six fold rings (Cornell & Schwertmann, 2000; Aronniemi et al., 2003). Crystal structure of hematite is presented in Figure 2.2.

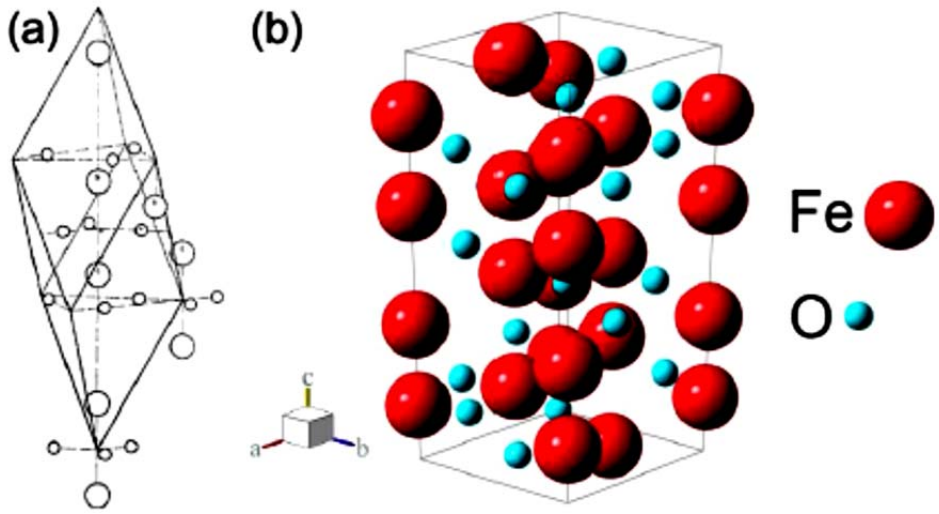

Figure 2.2 Crystal structure of hematite: a) arrangement of atoms, b) unit cell model (Pauling & Hendricks, 1925)

2.2.3 Akaganeite – β-FeOOH

Akaganeite was first discovered in Japan, and the mineral is named after the Akagane mine in Iwate, Japan (Murad, 1979). Akaganeite is typically obtained as a product of the hydrolysis of ferric chloride solution at low pH between 1.2 and 1.9 (Deliyanni et al., 2001). It cannot be synthesized at pH above 5; at higher pH the OH^- ions compete for the structural sites than the Cl^- ion (Cornell & Schwertmann, 2000). Akaganeite is a fine-grained material with a large specific surface area (Cornell & Schwertmann, 2000). The crystal structure of akaganeite (Figure 2.3) was first shown by Mackay (1960) to be related to the hollandite structure, with additional chloride anions occupying channels parallel to the crystallographic c-axis. Chloride ion originates from the precursor, ferric chloride. β-FeOOH exhibits a monoclinic crystal structure with space group I4/m (tetragonal symmetry), a = 10.480 Å, b = 10.480 Å and c = 3.023 Å (Almeida, 2010). Akaganeite normally displays two morphologies: somatoidal or cigar shaped and rod-like crystals. Somatoidal particles are frequently twinned but the rod like crystals are not (Cornell & Schwertmann, 2000).

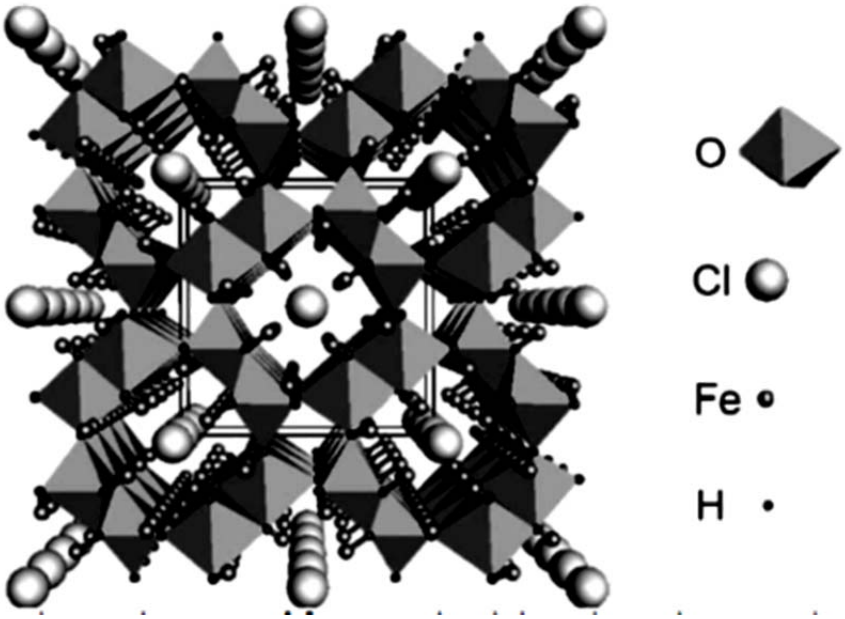

Figure 2.3 The crystal structure of akaganeite (Stahl et al., 2003)

2.2.4 Applications of α-Fe_2O_3 and β-FeOOH

Three forms of the iron oxides can be used in a number of applications. But owing to the nature of this work, applications of hematite (α-Fe_2O_3) and akaganeite (β-FeOOH) alone are highlighted. Hematite has been used as catalysts for a number of industrially important reactions, including the synthesis of NH_3 (Haber process), high temperature water gas shift reaction, and the de-sulfurisation of natural gas. Other reactions include the dehydrogenation of ethyl benzene to styrene, the Fisher-Tropsch synthesis for hydrocarbons, the oxidation of alcohols, and the large-scale manufacture of butadiene (Cornell & Schwertmann, 2000, Azhar Uddin et al., 2008). It is a semiconductor and can catalyse oxidation/reduction reactions (Al-Sayari et al., 2007) and also been used as a support material for gold in catalysts for the oxidation of carbon monoxide at low temperature (Zhong et al., 2007). Hematite (α-Fe_2O_3) has also been used as a photo-catalyst for the degradation of chlorophenol and azo-dyes (Bandara et al., 2007). All three forms of iron oxide are commonly used in synthetic pigments in paints, ceramics, and porcelain (Cornell & Schwertmann, 2000).

The α-, β-, γ-type, iron oxyhydroxides have distinctive properties and these materials have been widely used as electrode materials and precursors in lithium batteries (Flynn, 1984; Kanno et al., 1996; Amine et al., 1999). Akaganeite (β-FeOOH) possesses a large, tunnel-type structure where iron atoms are strongly bonded to the framework (Amine at al., 1999), and lithium can be intercalated and extracted freely in the tunnels (2 X 2) during discharge and charge processes. Akaganeite exhibits good electrochemical performance with a high theoretical discharge capacity of 283 $mAhg^{-1}$, which makes it a promising electrode material. It is also a semiconductor with a band gap of 2.12 eV (White, 1990), and can be used in oxidation/reduction reactions, hydro-processing of coal (Cornell & Schwertmann, 2003) and in the preparation of ferromagnetic materials such as γ-Fe_2O_3 (Xiong et al., 2003).

The fabrication technique plays a key role in determining the particle size and shape, size distribution, surface chemistry and hence the applications of the iron oxide (Jiang et al., 2010). In addition, the preparation method also determines the degree of structural defects or impurities present in the particles, and the distribution of such defects (Tartaj et al., 2003). Hence, several synthesis routes have been developed to obtain proper control over the physical and magnetic properties (Tartaj et al., 2003).

2.3 1-D nanostructure overview

1-D nanostructure represents a cluster of nano-materials with highly anisotropic morphologies. Nanowires (aspect ratio > 10), nanorods (aspect ratio < 10), belts, ribbons and hollow tubes are typical examples of 1-D nanostructure. One-dimensional nanostructures are considered ideal model systems for investigating the dependence of optical, electrical, magnetic and mechanical properties on size and morphology (Almeida, 2010).

2.3.1 Particle formation mechanisms and applications of 1-D nanostructures

Understanding the growth mechanism of nanostructures is of critical importance in optimizing their size, morphology and dispersity. In recent years, a variety of chemical methods has been identified for generating 1-D nanostructures, offering different levels of control over their dimensional parameters. A summary of the 1-D nanostructures synthesised using a variety of techniques is presented in Table 2.2.

Table 2.2 One-dimensional nanostructures overview (Almeida, 2010)

Material	**Fabrication technique**	**Shape**	**Length**	**Diameter**	**Growth Mechanism**
MOS_2	Redox reactions in aqueous solution	NR	50-150 (nm)	20-40 (nm)	Growth via template
CNT	Fluid bed CVD	Multi-walled carbon tube	0.02-60 (μm)	3-11 (nm)	Surface diffusion and precipitation on a catalyst
$LnVO_4$	Hydrothermal synthesis	NR	50-200 (nm)	10-50 (nm)	Ostwald ripening
BN	Boron oxide CVD	NT	10 (μm)	50 (nm)	Catalytic growth parallel to {1010} plane
Eu_2O_3	Precipitation	NR	200 (nm)	10-30 (nm)	Crystalline nucleation anisotropic growth in {001} direction followed by calcination
CdS	Wet chemical method	NR	< 64 (nm)	< 25 (nm)	Oriented attachment
ZnO	Wet chemical method	NR array	1-5 (μm)	20-200 (nm)	Nucleation and anisotropic growth
TiO_2	Sol-gel processing	NW array	10 (μm)	180 (nm)	Nucleation
Si	Laser ablation	NW	>100 (μm)	3-43 (nm)	Laser ablated material from the Fe/Si target collides with inert gas molecules and condenses in the gas phase, resulting in Fe-Si nanodroplets, which act as seeds for vapour-liquid-solid Si NW growth
FePt	Solvothermal synthesis	NW	5 (μm)	30-50 (nm)	Coarsening (Ostwald ripening)
$W_{18}O_{49}$	Solvothermal synthesis	NW	5 (μm)	Bundles of 2-5 (nm)	Alignment of ultra-thin NWs that grow anistropically in the <010> direction
$PbCrO_4$	Facile aqueous solution	NR	< 2.5 (μm)	> 150 (nm)	$PbCrO_4$ NPs nucleate and grow up to 50 nm agglomerate and crystalline into NRs
CdS	Sonochemical synthesis	NR/NW	1.3 (μm)	80 (nm)	Ultrasound expels S^{2-} and Cd^{2+} and strong pentadentate ligand complexing action mediates CdS NR formation along the [001]

A schematic illustration of some growth mechanisms identified so far is presented in Figure 2.4.The formation mechanism of 1-D nanostructure is influenced by the material, production technique and environment, and may change radically with small variation in the processing parameters. Therefore, understanding the effect of each process variable on the structural evolution is required to fully control their size, shape, phase and by implication, their functional properties (Almeida, 2010).

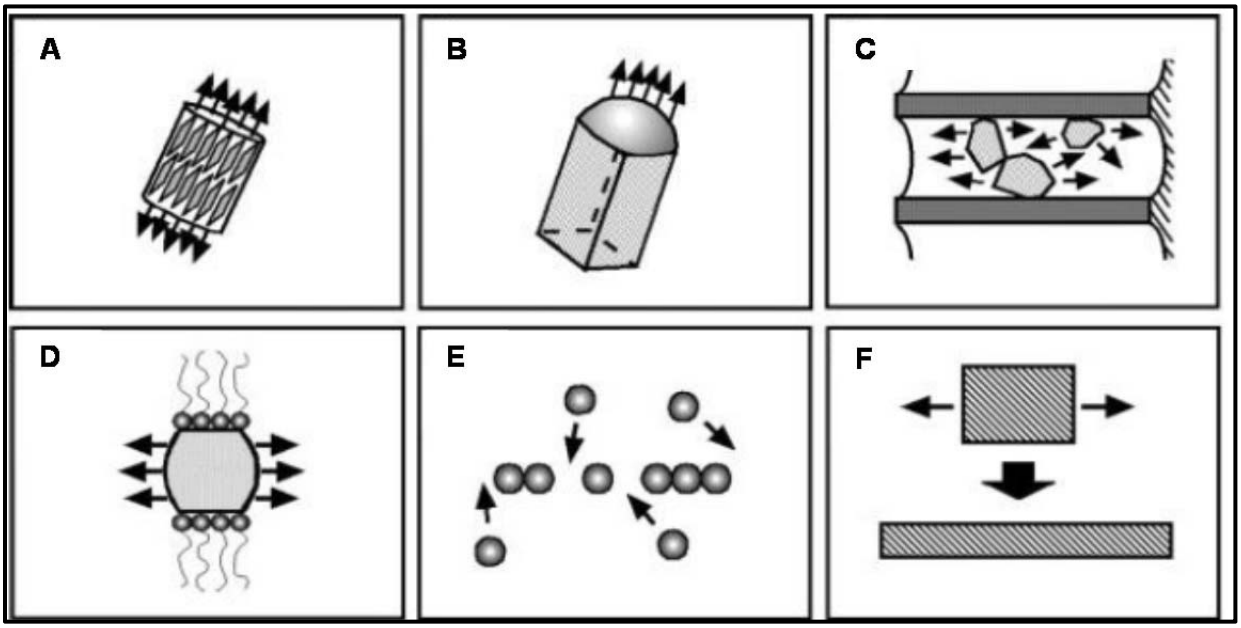

Figure 2.41-D nanostructure growth mechanism, A) controlled by the anisotropic crystallographic structure of a solid; B) confinement by a liquid droplet as in the vapour-liquid-solid process; C) direction as controlled through the use of a template; D) capping reagent provides kinetic control; E) self-assembly of the nanoparticles; and F) 1-D microstructure size reduction (Almeida, 2010).

A brief literature review of the techniques for the synthesis of nanoparticles is provided in the following section, together with their pros and cons.

2.4 Fabrication approaches and techniques

The ability to synthesise and process nanoparticles and nanostructures is the first step in nanotechnology to explore novel physical properties and phenomena and realise potential applications of nanostructures

and nanomaterials. Two techniques exist to fabricate nanoparticles (Figure 2.5), the top-down and bottom-up approach (Zheng, 2009). Slicing or successive cutting of a bulk material to obtain nanosized particles is referred to as the top-down approach. Milling is a typical example of a top-down approach. The building up of a material from the bottom, atom-by-atom, molecule-by-molecule or cluster-by-cluster, is referred to as the bottom-up approach. Colloidal dispersion is an example of the bottom-up approach.

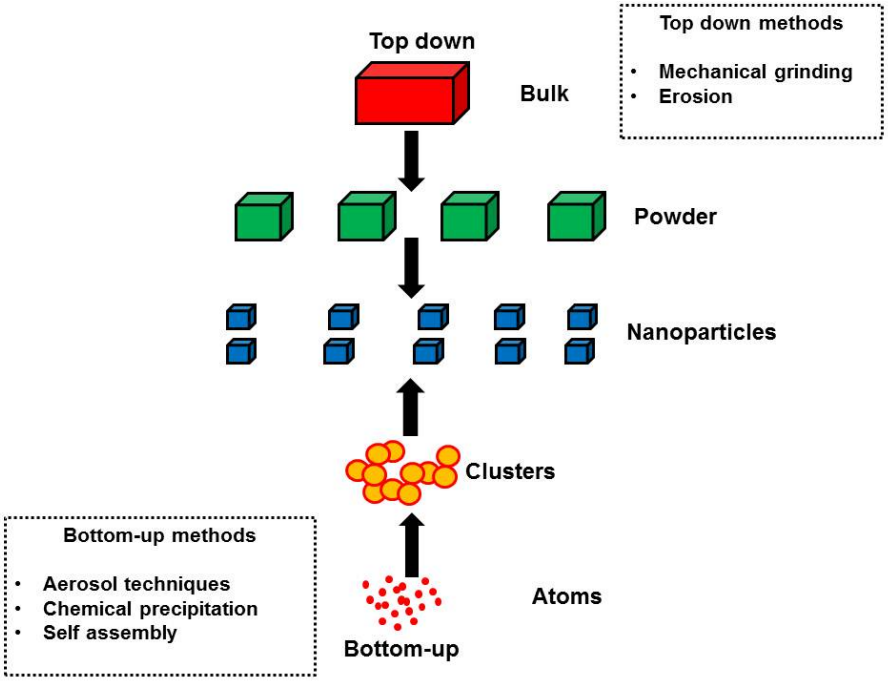

Figure 2.5 Schematic representation of two different approaches for fabricating nanomaterials (Zheng, 2009)

Different techniques have been established to date to synthesise nanoparticles. These are:

- Vapour-phase growth
- Liquid-phase growth
- Solid-phase formation
- Hybrid growth, i.e. (vapour-liquid-solid or VLS)

2.4.1 Hydrothermal / solvo-thermal synthesis

The concept "hydrothermal" is primarily a geological term, relating to the natural processes resulting from the joint action of heat and water under pressure (Mambote et al., 2000). Hydrothermal synthesis (HS) of inorganic materials has been carried out since the end of the 19th century (Byrappa & Yoshimura, 2001), and is defined as the precipitation of these materials from aqueous solutions at temperatures above boiling point and at pressures greater than ambient pressure (Dawson & Han, 1993). Hydrothermal synthesis technique is generally operated at around a temperature range of 100°C— 200°C (Arai et al., 2002).Figure 2.6 presents a pressure/temperature map of hydrothermal synthesis in relation to other material processing techniques.

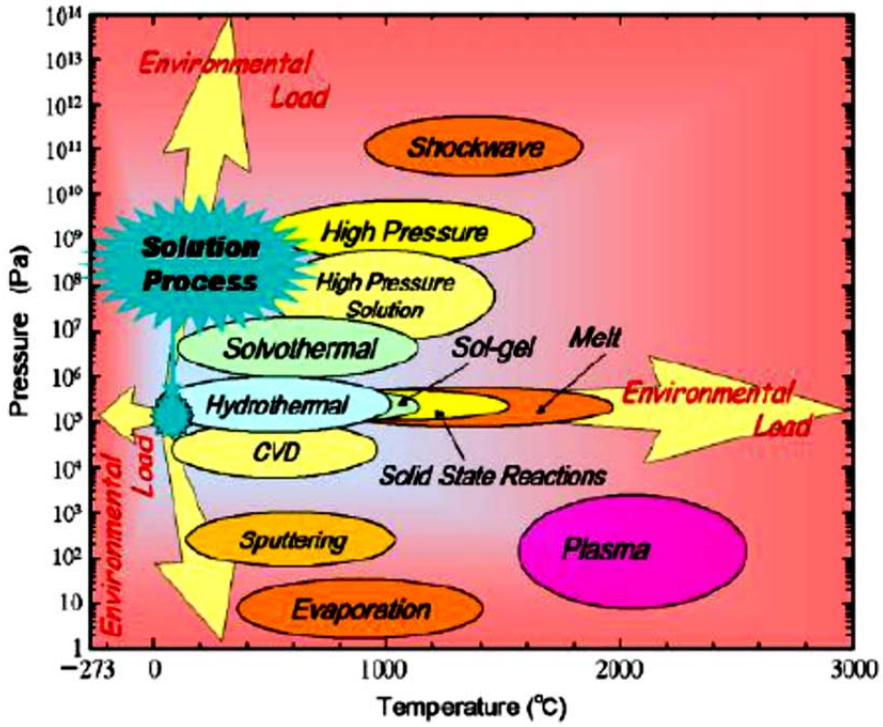

Figure 2.6 A pressure/temperature map for different material processing techniques (Yoshimura et al., 2000)

HS generally involves two reactions in the case of the formation of metal oxide particles. The reactions normally proceed as the hydrolysis of the metal salts first, then followed by dehydration (Matson et al., 1996). The reactions follow as:

$$M(NO_3)_x + xH_2O = M(OH)_x + xHNO_3 \longrightarrow \textbf{Hydrolysis}$$

$$M(OH)_x = MO\frac{x}{2} + \frac{x}{2}H_2O \longrightarrow \textbf{Dehydration}$$

The hydrolysis and dehydration reactions as shown above produce nuclei and eventually crystals during the pressurized heat-up period. Homogeneous nucleation and grain growth take place resulting in materials with desired microstructure and properties. Hydrothermal synthesis is one of the most widely used processes for the preparation of fine powders with controlled size, shape, crystallinity, and composition. A comparison between the different processes is presented in Table 2.3.

Table 2.3 Comparison between different techniques (Dawson, 1988)

Variable	Solid-state reactions	Sol-gel	Co-precipitation	Hydrothermal
Cost	Low - Moderate	High	Moderate	Moderate
Control over composition	Poor	Excellent	Good	Good-excellent
Control over morphology	Poor	Moderate	Moderate	Good
Purity (%)	< 99.5	> 99.99	> 99.5	> 99.5
Calcination step	Yes	Yes	Yes	No
Milling step	Yes	Yes	Yes	No

Both batch and continuous or flow systems can be used to carry out hydrothermal synthesis. The batch system is simple and easy and also allows one to control the oxidation states of the elements and to prepare systems with a desirable ratio of phases which contain one element in different oxidation states (Galkin et al., 2001). In the flow system a high reaction rate at short residence time is achievable. Particle

size, shape and size distribution can be controlled to some extent by independently varying the different process parameters (Xu, 2006).

2.4.1.1 Batch synthesis

Batch hydrothermal synthesis requires a vessel known as autoclave capable of handling highly corrosive solvent, operating under extreme pressure, temperature and processing conditions with adequate tolerance.Pressure vessels/ autoclaves are manufactured from thick glass or quartz cylinders and high-strength alloys, such as austenitic stainless steel, iron, nickel, cobalt-based superalloys or titanium and its alloys (Byrappa & Adschiri, 2007). Figure 2.7 presents pictorial representations of a typical pressure vessel or autoclave for illustration purpose.

Figure 2.7 A typical pressure vessel/autoclave (Byrappa, 2005)

Hydrothermal synthesis technique has been extensively used to synthesise a broad range of nanoparticles, especially metal oxides (Somiya & Roy, 2000), that is, hematite (Katsuki & Komarneni, 2001), quartz (Hosaka & Miyata, 1993), etc. Synthesis of quartz using the hydrothermal technique was conducted several decades ago and it is currently used commercially (Balaraman, 2005). High crystalline titanium oxide nanoparticles with large surface areas have been synthesised hydrothermally under supercritical conditions in a batch system (Hayashi & Torii, 2002). A new family of quaternary alkali tungsten tellurites, $A_2TeW_3O_{12}$ (A = K, Rb, or Cs) was also synthesised, demonstrating its versatility to control the

composition of targeted materials (Goodey et al., 2003). More recently, the use of the supercritical water approach in a batch reactor has been demonstrated for phosphate materials (Lee & Teja, 2006). Highly crystalline micro or nanoparticles of $LiFePO_4$ were obtained and higher electrochemical performance was reported compared with that synthesised at low temperatures, less than 200 °C (Yang et al., 2001). However, fundamental understanding of the kinetics during hydrothermal crystallisation is very limited. This is due to lack of data relating to the formation of intermediate phases and the inaccessibility of direct *in situ* investigative tools under conditions of high pressure and temperature (Almeida, 2010).

2.4.1.2 Continuous synthesis

In recent years, continuous hydrothermal synthesis (CHS) using near critical or supercritical water has attracted attention compared to the batch process (Adschiri et al., 1992; Hakuta et al., 1998). This technique has exhibited promise in the production of nano and submicron-sized fine particles (mainly metal oxides and oxyhydroxide), owing to the high reaction rates at short residence time and the ability to control particle characteristics to some extent. Various materials have been prepared using continuous process under NCW or SCW conditions. A summary is given in Table 2.4.

In a continuous process, pressurized water is preheated to near- critical or supercritical temperature and is then contacted with a metal salt solution pre-mixed if necessary with a hydroxide solution. Figure 2.8 presents a typical CHS setup. Due to high temperature and pressure use, the process control in the continuous hydrothermal synthesis becomes difficult in terms of mass production due to problems such as corrosion and blockage.

Table 2.4 Materials prepared from under NCW or SCW conditions (Xu, 2006)

Material synthesised	**Precursor solution used**	**Particle size (nm)**	**References**
AlOOH	$Al(NO_3)_3$	~100-600	Adschiri et al., 1992
$BaO.6Fe_2O_3$	$Ba(NO_3)_2$, $Fe(NO_3)_3 \cdot 9H_2O$,KOH	~100-200	Hakuta et al., 1998
CeO_2	$Ce(NO_3)_4$	~300	Hakuta et al., 1998
Co_3O_4	$Co(NO_3)_2 \cdot 6H_2O$, NaOH	~50	Adschiri et al., 1992
$\alpha - Fe_2O_3$	$Fe(NO_3)_3 \cdot 9H_2O$, $FeCl_2$, or $Fe(SO_4)_3$	~50	Adschiri et al., 1992
$\alpha - Fe_2O_3$	$Fe(NO3)_3 \cdot 9H_2O$ and PVA	Size changed with the experimental condition	Xu and Teja, 2007
$LiFePO_4$	$FeSO_4 \cdot 7H_2O$. LiOH, o - H_3PO_4	Size changed with the experimental condition	Xu et al., 2008
Fe_3O_4	$Fe(NH_4)_2H(C_6H_5O_7)_2$	~50	Adschiri et al., 1992
$LiCoO_2 + Co_3O_4$	LiOH and $Co(NO_3)_2 \cdot 6H_2O$	~1000	Kanamura et al., 2000
NiO	$Ni(NO_3)_2$	~100	Adschiri et al., 1992
TiO_2	$TiSO_4$ or $TiCl_4$	~20	Adschiri et al., 1992
ZrO_2	$ZrOCl_2$	~10	Adschiri et al., 1992
YAG:TB	$Al(NO_3)_3 \cdot 9H_2O$, $Y(NO_3)_3 \cdot 6H_2O$, $TbCl_3 \cdot nH_2O$	~100	Hakuta et al., 1999
$CoFe_2O_4$	$Co(NO_3)_2 \cdot 6H_2O$, $Fe(NO_3)_3 \cdot 9H_2O$, NaOH	~10	Cote et al., 2003
$BaZrO_3$	$ZrO(NO_3)_2$, $Ba(NO_3)_2$, NaOH	~74	Millot et al., 2005
Zno	$Zn(NO_3)_2$, $Zn(CH_3COO)_2$, $ZnSO_4$, KOH	~120-320	Viswanathan & Gupta, 2003
$BaTiO_3$	TiO_2, $Ba(OH)_2$	~10-60	Hakuta et al., 2005
Ag*, Fe_2O_3**, TiO_2***, and ZrO_2****	CH_3-COOAg, $Fe(NO_3)_3$, $Ti(SO_4)_2$, and $ZrO(NO_3)_2$	* ~ 9.6 ± 4.8 **~ 5.5± 3.3 ***~6.1±0.5 ****~3.9±1.3	Kawai-Nakamura et al., 2008

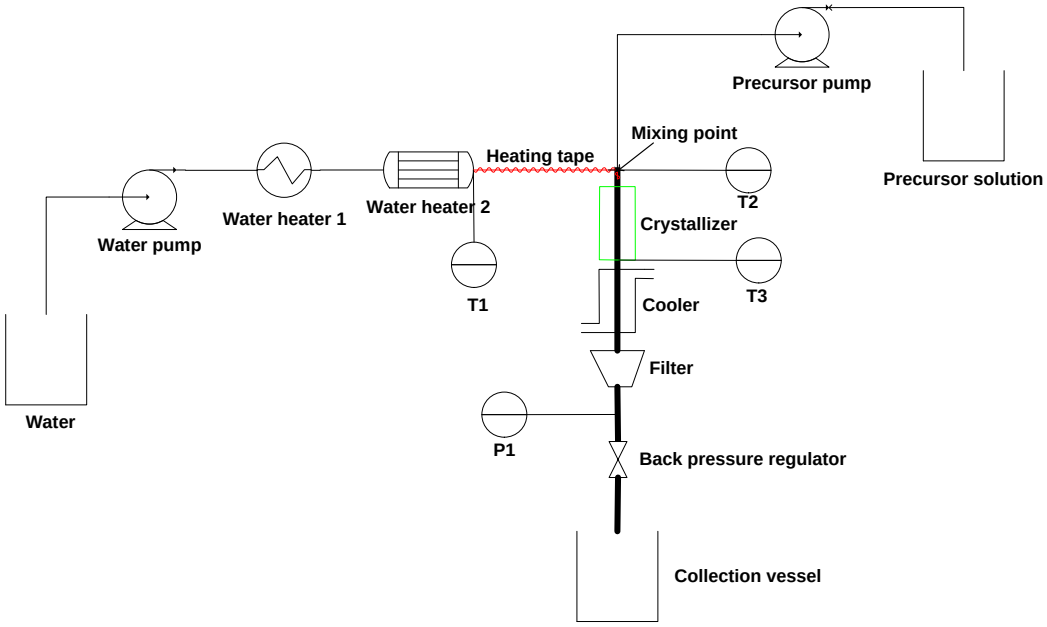

Figure 2.8 Continuous system to synthesise iron oxide nanoparticles (Xu & Teja, (2007)

The process control for the CHP technique is also very difficult, because of the high temperature and pressure. To realise the actual production of nanoparticles using the flow reaction system, there are still some problems in terms of engineering issues, namely, corrosion, blockage, and mass production.

2.5 Effect of nanoparticle size on physical properties

Nanoparticles act as an effective bridge between bulk materials and atomic or molecular structures. Constant physical properties are exhibited by bulk materials irrespective of their size and mass. NPs possess unique size-dependent properties due to the significant proportion of atoms existing on their surface in relation to the bulk, resulting in a large specific surface area (Almeida, 2010). The electronic, optical and magnetic properties of materials are found to change as their size decreases towards the nano-scale. The total free energy of a nanoparticle, $G_{Nanoparticle}$, is the sum of the free energy of the bulk, G_{Bulk}, and the surface, $G_{Surface}$, of the nanoparticles. This can be expressed as (Zhang & Banfield, 1999):

$$G_{Nanopartide} = G_{Surface} + G_{Bulk} \qquad \text{Equation 2. 1}$$

In the case of a nanoparticle, the surface-free energy becomes a large factor of the total free energy and an important element of its overall phase stability (Zhang & Banfield, 1998). The electronic properties of nanoparticles are size dependent. The electronic band gap, E_g, of a spherical semiconductor nanoparticle can be shown as:

$$E_g \approx \left(\frac{\pi^2 h^2}{2R^2}\frac{1}{\mu}\right) - \left(\frac{1.8e^2}{\varepsilon R}\right), \qquad \text{Equation 2. 2}$$

where, h, is Planck's constant, R, the particle radius, μ, the reduced mass of the electron-hole pair, e, the electric charge and ε, is the dielectric constant of the semiconductor. The optical properties of nanoparticles also vary greatly as a function of size. If a small spherical metallic nanoparticle is irradiated by light, the accompanying incident electric field causes the conduction electrons to oscillate coherently (Kelly et al., 2003). This electron oscillation is called the dipole plasmon resonance. Magnetic properties of nanoparticles are also size dependent. The magnetisation of a single-domain nanoparticle lies along an easy direction which is determined by the shape and the magnetocrystalline anisotropy of the nanoparticles. Before an external field is applied, the magnetisation of a single-domain nanorod lies along the easy direction which is presented in Figure 2.9 (a). After an external field is applied in the opposite direction, the nanorod is unable to respond by domain wall motion and instead the magnetisation must rotate through the hard direction (Figure 2.9b), to the new easy direction (Figure 2.9c). The anisotropy forces which hold the magnetisation in an easy direction in NRs are stronger than isotropic NPs, and thus the coercivity is large (Spaldin, 2003). For this reason, 1-D nanostructures are desirable for magnetic storage media applications.

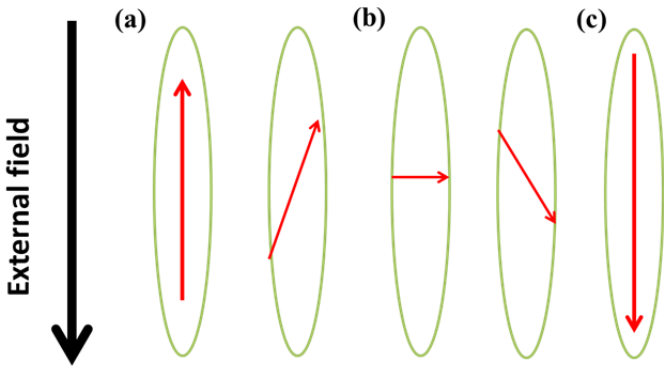

Figure 2.9 Single domain nanorods magnetisation rotations (Almeida, 2010)

2.6 Prediction of nanoparticle sizes under different experimental conditions

A mathematical relationship that describes the dependence of particle size on the processing conditions is important in production of uniform nanoparticles with specific sizes. However, there is a lack of a quantitative mathematical relationship between particle size and processing conditions.

Correlation to predict particle sizes under different experimental conditions was derived by Beach (2009) to predict spherical SnO_2 particle size under different temperatures. The correlation is presented below:

$$\varphi = 2.646 + \left(5.805X10^{-5}\right)\left(T\right)^{2.145} , \qquad \text{Equation 2. 3}$$

where, φ , is average particle diameter and, T , temperature.

Further work was done by Chiu et al. (2012). Their developed correlation predicts particle sizes of spherical hematite at different temperatures and reaction times. The correlation is presented below:

$$d_p = \left(0.49T - 26.4\right)t^{0.33} \qquad \text{Equation 2. 4}$$

where, d_p , is particle diameter, T , temperature, and t ,the time.

2.7 Surfactants

A surfactant is a surface-active compound used in practical applications (Scamehorn, 1986). Surfactants are usually organic compounds that are amphiphilic, meaning they contain both hydrophobic and hydrophilic groups. Surfactants are employed in a variety of technologies including detergent,

emulsification, dispersion, coating, wetting, flotation, petroleum recovery, lubrication, and adhesion (Rosen, 1989). Surfactants are also used to control the morphology, size and shape of the nanoparticles grown from chemical solution (Almeida, 2010).

2.7.1 Previous work reported on the effect of surfactants and alcohols on the iron oxide nanoparticle

Surfactant-assisted hydrothermal synthesis can be found in the literature. Liu et al. (2006) synthesised α-Fe_2O_3 nanorods and nanotubes in the presence of surfactant L113B and SPAN 80 in BuOH. They concluded that the surfactant plays an important role in determining the shape of the nanoparticle as only nanotubes were formed without the surfactants. Baruwati et al. (2006) produced various morphologies (tubes, rods and needles) of α-Fe_2O_3, utilising various hydrolysing agents in the presence of NaOH and CTAB. This was a two-stage process, hydroxylation followed by calcination of the as-prepared β-FeOOH. Only nanoparticles were obtained in the absence of NaOH, indicating that it is not only the effect of the surfactant that is important in the formation of nanorods. Fester et al. (2008) synthesised hematite nanorods in the presence of different alcohols and surfactant SPAN 80. They concluded that the surfactant plays no role in the formation of the nanorods. It was reported that the length of the nanorods increases with the increase in carbon chain in the alcohol solvent. Hematite nanoplates were synthesised by Chen et al. (2010). The authors used different alcohols as solvents. They concluded that the nanoplate diameter and thickness could be controlled by choosing alcoholsselectively. Rod, arrayed nanorods, bundled fibre and hexagram-like structures of β–FeOOH were obtained by Shao et al. (2005). The authors used a surfactant-free condition but ethanol was used as a solvent. Different shapes were obtained by varying the ethanol-water ratio. Aggregates of α–FeOOH and rod-like β–FeOOH particles were synthesised by Bashir et al. (2009). The authors used polyoxyethylene oxide as a surfactant and butan-2-ol (five times the amount of surfactant) to synthesise the particles. Precipitation of α- and β-FeOOH iron oxides in alcohol-surfactant medium was observed to be faster when compared with the precipitation in a free aqueous medium, though the reason for these phenomena is not clear. Liang et al. (2010) used isopropanol (IPA)

as a solvent to synthesise crystalline Fe_3O_4 nanoparticles in a CHS process. The IPA provided reducing atmosphere due to the conversion of IPA into acetone. It was suggested that the acetone molecules adsorbed on the Fe_3O_4 surfaces suppressed crystallite growth. In another work, Guo and Xiao (2006) reported that the addition of alcohol in the hydrothermal reaction largely affected the crystallisation process. The crystallite size and crystallinity of the particles decreased with increasing isopropanol (IPA) addition.

The above discussion clearly highlights the application of various alcohols in the synthesis of different iron oxide nanoparticles. No systematic study has been reported in the literature to the best of my knowledge despite the number of work has been carried out.

2.8 An overview on the effect of processing conditions on β-FeOOH particle characteristics reported in literature in the absence of alcohol

A brief review of literature, on the effect of processing conditions on β-FeOOH particle characteristics in the absence of alcohol is presented in this section.

2.8.1 Effect of temperature on the β-FeOOH particle characteristics

Cornell and Schwertmann (2000) synthesised β-FeOOH particles using a 0.1M $FeCl_3$ solution. The pH of the solution was kept at 1.7. A synthesis temperature of 40—90˚C was used to synthesise these particles. The authors reported that well crystalline somatoidal particles were formed in the temperature range of 40—70˚C. The particles were elongated in the c-direction and had a surface area of 30 m^2/g. Poorly crystalline particles were formed at higher temperature (90˚C). Hematite formed competitively with akaganeite at reaction temperatures above 90˚C.

2.8.2 Effect of $FeCl_3$ concentrations on the β-FeOOH particle characteristics

Yue et al. (2011) studied the effect of $FeCl_3$ concentrations on the physiognomies of β-FeOOH nanorods. A $FeCl_3$ concentration range of 0.05—0.75M was used. They reported that $FeCl_3$ concentrations affect the nucleation and growth of particles. However, at the same time, an increase in $FeCl_3$ concentration will

decrease the pH, leading to a slow hydrolysis process. However phase and morphology changes were not reported with change in $FeCl_3$ concentrations.

2.9 General synthesis theory

Nanocrystal formation is a two-stage process, firstly nucleation of an initial seed followed by subsequent growth (Yadong & Alivisatos, 2005). Transformation from solution to solid occurs when the free energy of the initial solution phase is greater than the sum of the free energies of the crystalline phase plus the final solution phase (Gibbs, 1876).

2.9.1 Nucleation

Nucleation is one of the two major mechanisms of the first order phase transition, the process of generating a new phase from an old phase whose free energy has become higher than that of the emerging new phase (Hohenberg & Halperin, 1977). Nucleation occurs via the formation of small embryos of the new phase inside the large volume of the old phase. The statement that the free energy per molecule of the new phase is less than that of the solvated phase only applies to the bulk of the new phase (De Yoreo & Vekilov, 2003). The difference between the free energy per molecule of the bulk and that of the surface is referred to as the interfacial free energy. The interfacial free energy is always a positive term and acts to destabilise the nucleus. As a consequence, at very small size when many of the molecules reside at the surface, the nucleus is unstable. The addition of more molecules just increases the free energy of the system. On average, such a nucleus will dissolve rather than grow. But once the nucleus gets large enough, the drop in free energy associated with formation of the bulk phase becomes sufficiently high that the surface-free energy is unimportant, and every addition of a molecule to the lattice lowers the free energy of the system. There is an intermediate size at which the free energy of the system is decreased, whether the nucleus grows or dissolves, and this is known as the critical size. A number of implications are associated with the existence of a critical size. Nucleation of the new phase is the result of fluctuations that bring together sufficient numbers of molecules to exceed the critical size; the probability of nucleation will be strongly affected by the value of the critical size. This implies that nucleation can be

controlled, to some extent, by modulating the critical size, which is in turn a function of the interfacial energy. The smaller the interfacial energy, the smaller the critical size and the more likely nucleation becomes for any given supersaturation. As a consequence, by varying either the solution composition or the supersaturation, the probability of nucleation can be manipulated (De Yoreo & Vekilov, 2003).

2.9.2 Growth mechanisms

Understanding of the dynamics that affect crystal growth kinetics and the microstructure development in nanocrystals is fundamental to tailor new types of nanostructures and control material properties (Zhang et al., 2009). Two types of growth mechanisms have been reported, 1) the classical Ostwald ripening, OR kinetics, and 2) Oriented attachment, OA kinetics.

2.9.2.1 Classical growth kinetics, OR kinetics

OR kinetics involves the growth of larger particles at the expense of smaller ones. The driving force for this process is the decrease in total surface free energy (Zhang et al., 2010). According to the Gibbs–Thomson equation (Campbell et al., 2002), the equilibrium solute concentration at the surface of larger particles is lower than that of smaller ones and the resultant concentration gradients lead to solute ions flowing from small particles to larger ones. The coarsening mechanism is often controlled by the diffusion, particle growth via addition of ions to the particle surface from solution (Zhang et al., 2010). An illustration of the OR kinetic is presented in Figure 2.10. The classical kinetic model for the OR mechanism is known as the LSW (Lifshitz-Slyozov-Wagner) model which is based on the Gibbs–Thomson equation (Kirchner, 1971). The general kinetic equation for these cases can be written as:

$$D = D_o + k(t)^{\frac{1}{n}}, \qquad \text{Equation 2. 5}$$

where, D, is the particle diameter, D_o, the initial diameter, K, material constant which is temperature dependent, t, time and, n, exponent which is relevant to coarsening mechanisms. An ‘n’ value of 2 dictatesa crystal growth that is controlled by the diffusion of ions along the matrix-particle boundary.

Crystal growth controlled by volume diffusion of ions in the matrix and dissolution kinetics is represented by an exponent, n, value of 3 and 4 respectively (Kirchner, 1971).

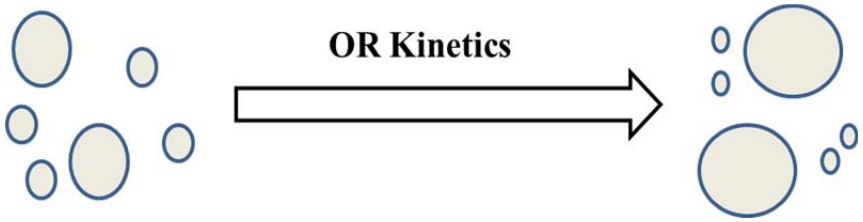

Figure 2.10Illustration of Ostwald ripening kinetics

Disagreements still remain between experimentally reported particle distribution and that predicted by OR kinetics despite the amount of work reported on OR growth kinetics. A few typical examples are presented below:

1) Huang et al. (2003) reported two-stage crystal growths of ZnS nanoparticles. The authors reported that the first stage of growth could not be fitted by OR kinetics. The fitting yielded an exponent ($n > 10$) with no physical meaning (Huang et al., 2003).
2) The Ostwald ripening mechanism cannot be used to explain and fit the crystal growth in solid phases, that is, coarsening in air (Zhang & Banfield, 1999).
3) Krill et al. (2001) reported a linear growth rate of nanosized Fe (<150 nm) with time.

All sorts of irregular shapes, such as, elongated chains, butterflies, horseshoes, etc. (Tang et al., 2002) can be obtained in solution based growth. Nanocrystal often exhibits defects, that is, dislocation and planar defects.These occur seldom in the crystal growth via the OR mechanism (Zhang et al., 2009).

2.9.2.2 Oriented attachment, OA, mechanism

Oriented attachment mechanism was discovered by Penn and Banfield in 1998. It involves spontaneous self-assembly of adjacent particles. Nanoparticles with irregular shapes are often caused due to this mechanism. Formation of irregular shape occurs by consuming primary nanoparticles as building blocks. The growth rate of particles is size dependent (Huang et al., 2003). Typical examples of the OA mechanism observed and reported in the synthesis of iron oxide nanoparticles are presented in Table 2.5.

Crystal growth via the OA mechanism is presented in Figure 2.11. The self-assembly of particles occurs in such a way that the joined particles share common crystallographic orientation, followed by joining of these particles at a planar interface. It can be seen from Figure 2.12 that the big ZnS single crystal is composed of five single units. The arrowhead mark indentations represent the interfaces between the assembly units.

Table 2.5 OA mechanism controlled growth of iron oxide nanoparticles

Author	**Iron oxide phase**	**Morphology**
Penn et al., 2001	Fe_2O_3 and FeOOH	Rounded hematite plate and irregular feroxyhite plates
Niederberger., et al., 2002	α-Fe_2O_3	Rounded hexagonal plate
Guyodo et al., 2003	α -FeOOH	Nanorods
Nesterova et al., 2003	FeOOH	Various
Frandsen et al., 2005	α-Fe_2O_3	Chains
Penn	α-FeOOH	Nanorods

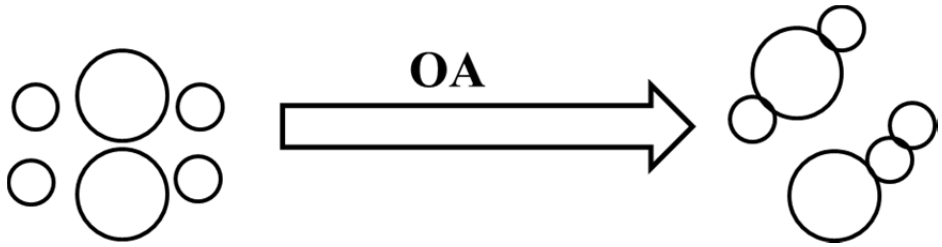

Figure 2.11Schematic illustration of OA mechanism

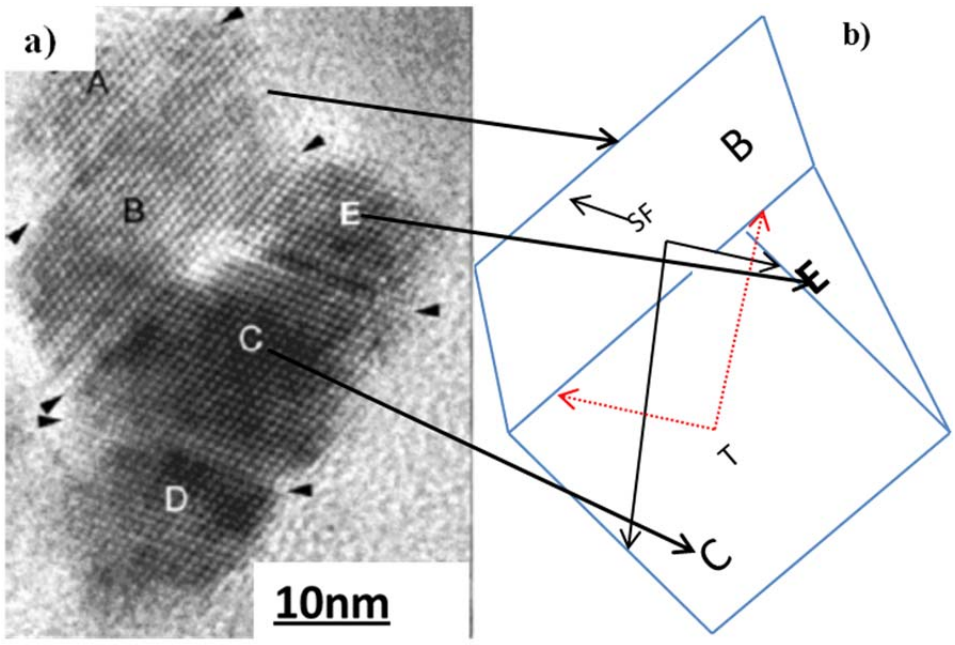

Figure 2.12 Growth of ZnS nanoparticle controlled by OA mechanism(Huang et al., 2003)

Two-stage growth kinetics was observed by Huang et al. (2003) in the synthesis of nanosized ZnS nanoparticles. The first stage could not be fitted by the OR kinetics but the second stage. The coarsening of nanosized ZnS in water was a combination of both OR and OA kinetics without the use capping agent. Co-existence of the OA and OR mechanism is a common phenomenon (Huang et al., 2003). Strong surface adsorption is a key factor in the growth of nanoparticles via a solo OA mechanism (Zhang et al., 2009).

2.9.2.3 OA based nanocrystal growth kinetic models

2.9.2.3.1 (A_1+A_1) model

The first Oriented growth kinetic model was developed to fit and explain the experimental growth curve of the ZnS nanoparticles (Huang et al., 2003). In the development of the kinetic model, the authors assumed that two primary nanoparticles, NP, attach and combine into a larger secondary particle according to the relation of volume between the primary and secondary particles. The Brownian motion of the nanoparticles is drastic under hydrothermal coarsening. When two adjacent particles collide, the

coalescence may occur on the premise and the two particles might share a common crystallographic orientation. The OA kinetic model can be described as the following reaction (Huang et al., 2003):

$$A_1 + A_1 \xrightarrow{K_1} B, \qquad \text{Equation 2. 6}$$

where, A_1 is the two primary particles and B, the product of the coalescence of two primary nanoparticles. K_1 is a kinetic constant for the reaction between two particles. Based on that, a growth model was derived (Huang et al., 2003):

$$d = \frac{d_o\left(\sqrt[3]{2}k_1 t + 1\right)}{\left(k_1 t + 1\right)}, \qquad \text{Equation 2. 7}$$

where, d, is particle diameter, d_o, initial particle diameter, k_1, growth rate constant dependent on temperature, and t, time.

Further studies were also initiated to attain a better understanding of the OA growth behaviour. Nanoparticle growth via OA mechanism was discussed from the degree of the electrostatic interaction and diffusion and coagulation of colloids (Penn, 2004 ; Riberio et al., 2005).

2.9.2.4 Two-step reaction during the OA growth

Oriented attachment-based nanocrystal growth often undergoes two reaction steps. The first is the diffusion of the nanocrystals followed by the coalescence and desorption of surface species. The motion of nanoparticles in a fluid is due to Brownian motion and fluid convection, which is much slower than the diffusion of molecules.

2.9.2.4.1 Rotation of nanoparticles before coalescence

After a collision of two or more particles in solution, the particles may not have any common crystallographic orientation. To achieve the structural accord at the interface, the primary particles would be free to rotate into an orientation (Zhang et al., 2009). This process is directly linked to the reduction of surface energy. It is also aimed at minimising the area of high-energy interfaces. The coarsening of nanocrystal via OA can be also named as the grain-rotation induced grain coalescence (GRIGC) mechanism (Figure 2.13) (Moldovan et al., 2002).

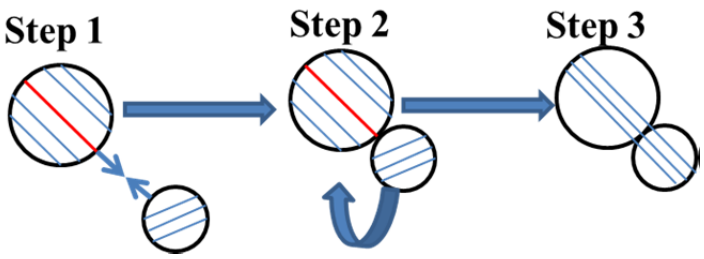

Figure 2.13 Particle rotation during OA mechanism (Zhang et al., 2009)

2.9.2.4.2 Self-recrystallisation of nanocrystal after coalescence

Often after coalescence of two individual nanoparticles, the as-produced nanoparticles undergo an adjustment of morphology named self-recrystallisation or self-integration. The state of the newly produced particle is not steady in view of energy, and that leads to the self-recrystallisation of the particle (Zhang et al., 2009). If two particles attach themselves without recrystallisation, the radius curvature at the joint is negative. This is according to the Gibbs-Thompson equation:

$$\mu = \frac{2\gamma\Omega}{R}$$ Equation 2. 8

where, μ is the chemical potential, γ, the surface free energy, Ω, the volume per atom and 1/R is the radius curvature at the joint. The chemical potential is negative at the joint. In self-recrystallisation the oriented attached nanoparticles go through three states (A, B and C) (Figure, 2.14). It is assumed that the self-recrystallisation from state A to B is very rapid and state B to C is slow (Zhang et al., 2009).

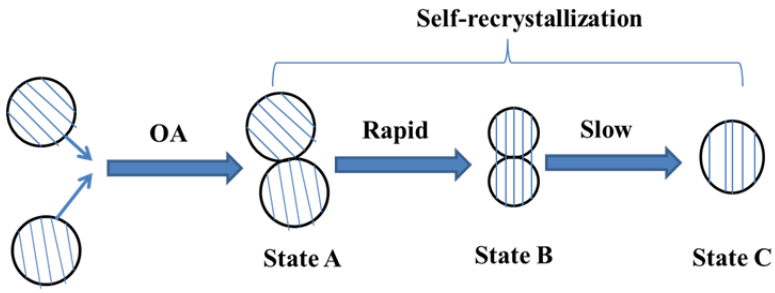

Figure 2.14 Self-recrystallisation in OA growth (Zhang et al., 2009)

2.10 Kinetic size control

The critical size of nanocrystals can be determined from the zero crossing point in Figure 2.15. Nanocrystals neither grow nor shrink at that point. The monomer concentration affects the critical size, with low monomer concentration favouring a larger critical size. On the other hand, a slow growth rate generates equilibrated and nearly round crystals. Slow growth rate is related to low monomer concentration.

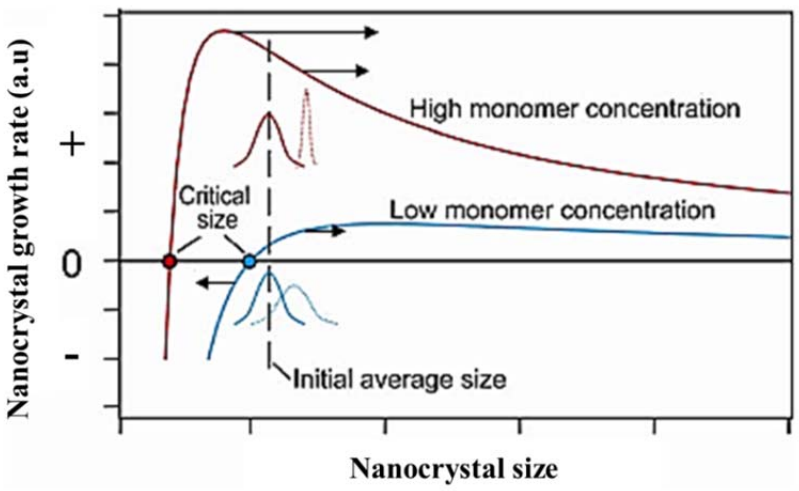

Figure 2.15 Relationship between growth rate and nanocrystal radius

2.11 Material characterisation techniques

There are several characterisation techniques available to understand the nanostructures grown during hydrothermal synthesis. A brief background on the analytical techniques that were used in this work is given in this section.

2.11.1 X-ray diffractometry

X-ray powder diffraction provides information regarding crystal size and disorder, structural parameters (unit cell edge lengths), degree of isomorphous substitution and surface area (Han, 2001). The ordered arrangement of a crystal atom is described by a number of symmetry elements. The position of any plane

of atoms within the crystal can be characterised by the intercepts the plane makes with the system axes. These intercepts are usually expressed as their reciprocal value, *hkl* (Miller indices), and thus converted into small integer numbers. The interaction of the electromagnetic waves with the atoms of the crystal is observed in the X-ray diffraction (Han, 2001).When a monochromatic beam of X-rays is directed towards a crystalline material, the incident X-ray photons interact with the electrons that surround the atoms. The electron clouds scatter the X-rays in all directions. However, at certain angles (θ), the distance travelled by the incident and scattered X-rays differs by a complete number (n) of wavelengths. These directions are related to the distances between atomic planes, the d-values, and the angle (θ) at which X-rays enter and leave a crystal. A schematic diagram is presented in Figure 2.16 to illustrate the constructive interference of scattered waves. This relationship can be described by the Bragg equation (Graef and Henry, 2012):

$$n\lambda = 2d_{hkl}\mathrm{Sin}\theta \qquad \text{Equation 2.9}$$

where, λ, is the wavelength of the X-rays used, θ , the angle at which the X-rays strike the crystal and for which the maximum interference intensity is observed, and d_{hkl}, the distance between the set of hkl planes in the crystal (lattice spacings).

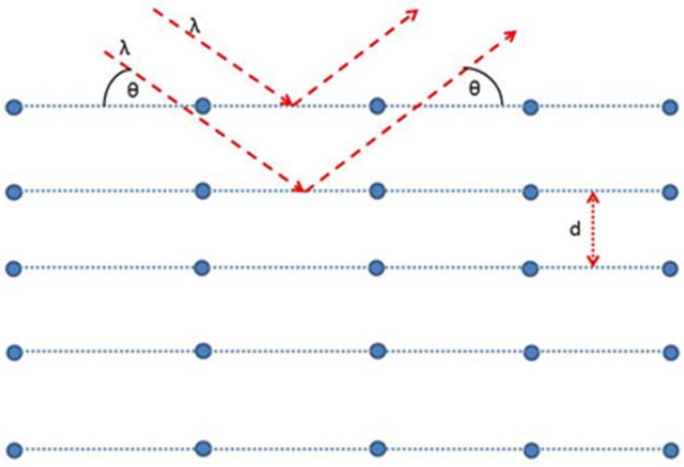

Figure 2.16 X-ray diffraction incident beam interaction with periodically aligned atoms (Almeida, 2010)

2.11.2 Electron microscopy

In an electron microscope a variety of signals can be detected when a high-energy electron beam interacts with a specimen (Figure 2.17). Many of these signals can be used for imaging. In a scanning electron microscope (SEM), mainly the secondary electrons (SE), backscattered electrons and characteristic X-rays (EDX) are analysed. The first two types of electrons provide visual information about the specimen. Information regarding specimen composition can be determined using EDX, Cathodoluminescence and Auger electron signals. Some of these signals are used in TEM (Williams, 1984).

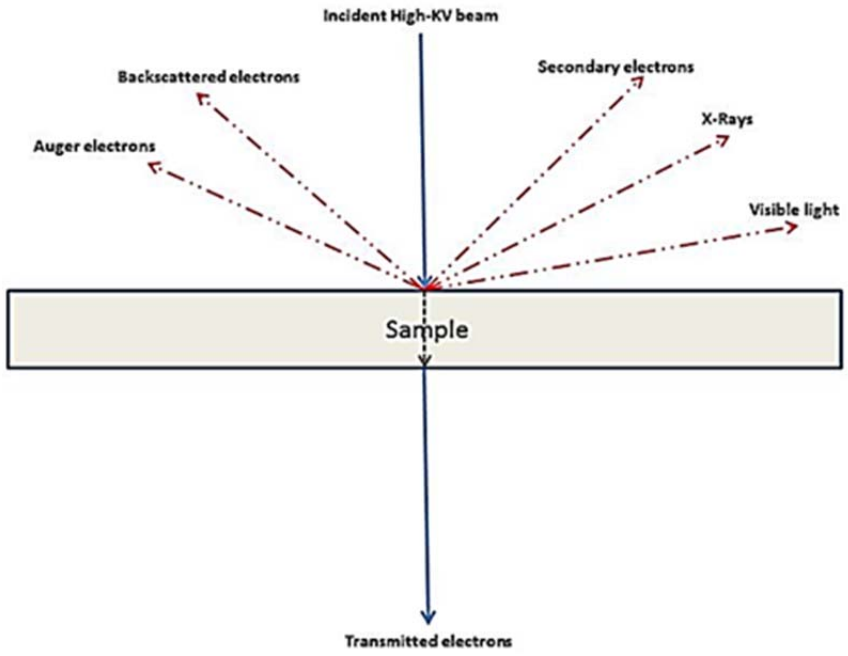

Figure 2.17 Different signals generated during the interaction of a high-electron beam with a thin specimen (Goodhew & Humphreys, 1988)

2.11.2.1 Transmission electron microscopy (TEM)

A beam of electrons is transmitted through an ultrathin specimen (<100 nm) in this technique. As the beam passes through the specimen it interacts with the specimen. An image is formed from the interaction of the electrons transmitted through the specimen. The formed image is magnified and focused onto an

imaging device, such as a fluorescent screen, on a layer of photographic film or detected by a sensor such as a CCD camera (Goodhew & Humphreys, 1988). Only the transmitted beams or some of the forward scattered beams are used in conventional TEM to form a diffraction contrast image.

High-resolution TEM (HRTEM) uses the transmitted and scattered beams to create an interference image. Preparation of TEM specimens is specific to the material under analysis and the desired information to obtain from the specimen.

2.11.2.2Scanning electron microscopy (SEM)

Bulk specimens are observed using Scanning Electron Microscopy (SEM). Scanning electron microscopy uses a fine electron probe (7~10 nm diameter) to illuminate the specimen (Williams, 1984). An image may be formed by scanning the probe across the specimen, and detecting the low- energy secondary or high-energy primary backscattered electrons returning from the surface (Han, 2001). All samples must be of an appropriate size to fit in the specimen chamber and are generally mounted rigidly on a specimen holder called a specimen stub. Several models of SEM can examine any part of a 6-inch (15cm) semiconductor wafer, and some can tilt an object of that size to 45 degrees. For conventional imaging in the SEM, specimens must be electrically conductive, at least at the surface, and electrically grounded to prevent the accumulation of electrostatic charge at the surface. Nonconductive specimens tend to charge when scanned by the electron beam, and especially in secondary electron imaging mode, which causes scanning faults and other image artefacts. The non-conducting materials are therefore usually coated with an ultrathin coating of electrically conducting material, such as gold, deposited on the sample either by low vacuum sputter coating or by high vacuum evaporation (Suzuki, 2002).

2.11.3 Thermogravimetric analysis

Thermogravimetric analysis (TGA) is an analytical method that has been used to determine a material's thermal stability and its fraction of volatile components. This is done by measuring the weight loss of a sample that occurs when the sample is heated. The measurement is normally carried out in air or in an inert atmosphere. Helium or nitrogen can be used to create inert atmosphere. The weight of the sample is

recorded as a function of increasing temperature. Sometimes lean oxygen atmosphere is used to perform the measurement if one wants to slow down oxidation. Differential thermal analysis or DTA is another thermo-analytical technique. Normally TGA and DTA measurement is done simultaneously with the same instrument. The temperature difference between sample and reference is recorded. This differential temperature is then plotted against time or temperature, which is represented as DTA curve or thermogram. A DTA curve provides data on the transformation that has occurred, such as glass transitions, crystallisation, melting, decomposition or sublimation, etc. The area under a DTA peak is the enthalpy change for the process under study (Gabbot, 2008).

2.11.4 Energy dispersive spectroscopy

A standard method for local identification of elements within a sample in an SEM or TEM is EDS analysis. The interaction with the innermost electron shell of an atom by the high-energy electron beam leads to the ejection of a photoelectron. Consequently, an electron from an outer orbiting shell jumps into the core level vacancy, and emits energy in the form of an X-ray photon. The energy of the X-rays arising from the difference in energy between the shells, is characteristic of the atomic number, and therefore can be used to ascertain the elemental composition of a sample (Almeida, 2010). The relationship between atomic number and energy for a given X-ray is given by Moseley's Law (Garratt-Reed and Bell, 2003):

$$\sqrt{E} = C_1(Z - C_2) \qquad \text{Equation 2.10}$$

where, E represents the energy of the emission line for a given X-ray series (e.g. Kα, Kβ etc.), Z is the atomic number and C_1, C_2 are constants.

2.12 Conclusion

Application and physical properties of iron oxide nanoparticles, more specifically for α-Fe_2O_3 and β-FeOOH, are given in this chapter. The dependency of the physical properties of various nanostructures, in particular one-dimensional nanostructures, on their size and morphology, has been discussed. A comprehensive overview of literature on the effect of alcohols on the particle size, shape and morphology

is presented, highlighting the necessity to conduct a systematic study. Effect of processing conditions on the particle characteristics without the presence of alcohol reported in the literature is also given. An in depth discussion on the intricate details related to different growth mechanisms are reported. Finally a brief background to the fundamental concepts underpinning the structural characterisation techniques of XRD, electron microscopy and thermogravimetric analysis is given.

Chapter 3

Experimental methodology

3.1 Introduction

A detailed description of the hydrothermal synthesis technique, including the equipment and chemical precursors used are presented in this section.

3.2 General synthesis scheme of β-FeOOH particles

β-FeOOH particles in both nano and micro sizes can be prepared via hydrolysis and / or forced hydrolysis of $[Fe(H_2O)_6]^{3+}$. Hydrolysis involves a stepwise elimination of protons from the six water molecules that surround the central hydrated ferric ion to form mono- and binuclear species (Cornell & Schwertmann, 2000), which in turn becomes multinuclear moieties. The latter finally precipitates as a more or less a crystalline product whose crystallinity depends on the rate and conditions of the reaction (Cornell & Schwertmann, 2000). Two main variables that cause hydrolysis are: 1) increasing the temperature and 2) addition of base. Due to the release of protons, the pH of the system falls during the early stages of the hydrolysis. At high temperature, the pH may become low enough to inhibit further hydrolysis resulting in incomplete hydrolysis that reduces the yield (Cornell & Schwertmann, 2000). Akaganeite particles form at pH 1.9. The formation of the particles is controlled by a variety of factors, including rate of hydrolysis, solution pH, temperature, Fe^{3+} concentrations and the nature of anions present in the system (Cornell & Schwertmann, 2000). In forced hydrolysis, precipitation is carried in aqueous solutions at higher temperatures (>100˚C) and pressure. Simple equations presenting the precipitation of β-FeOOH from $FeCl_3$ solution are presented below:

β - FeOOH precipitation

$$FeCl_3 + 3H_2O \rightarrow FeOOH + 3HCl + H_2O$$ Equation 3.1

3.3 Materials and processing conditions

Analytical grade $FeCl_3.6H_2O$ and NH_4OH (B & M Scientific, Cape Town, RSA) were used as it is without any further purification. An equal amount (volume wise) of distilled water and various alcohols (methanol, ethanol, propanol and butanol), one at a time, was mixed, unless other ratios were specified. Different alcohols were used to evaluate the effect of carbon chain length and solvent surface tension on the particle morphology and characteristics. Ammonium hydroxide, NH_4OH, was added drop wise until the mixture pH reached 10. 2.7g of $FeCl_3.6H_2O$ was added to the solution and the solution was stirred until the iron salt was dissolved. The final pH of the resulting solution was ~2 under the experimental condition used, unless stated otherwise. 400ml solution was placed in a 0.99L Teflon-lined stainless steel pressure vessel. A standard synthesis temperature of 100˚C was used. Reaction temperature was controlled by using heating jackets connected to a controlling unit (Figure 3.1). Generally reaction was conducted for 2h but other durations were also used to study their effect on the particle characteristics. The synthesis duration was calculated from the time the specified reaction temperature was reached, though the particle formation would have occurred even during the temperature ramp-up.A typical reaction temperature and pressure profile is presented in Figure 3.2 and 3.3 respectively. The fluctuation of pressure was observed owing to the switching on and off of the heating elements. In addition sulfate and nitrate precursors were also employed to study the effect of anions on the particle characteristics. The reaction vessel was allowed to cool naturally after completion of the reaction followed by decantation of the supernatant liquid, centrifugation, washing of the solid with ethanol severally to remove residual chloride ions and storage in a desiccator. The process variables for the synthesis of β-FeOOH are summarized in Table 3.1. Experiments were carried out in a chemical fume hood with exhaust, while wearing proper personal protective equipment.

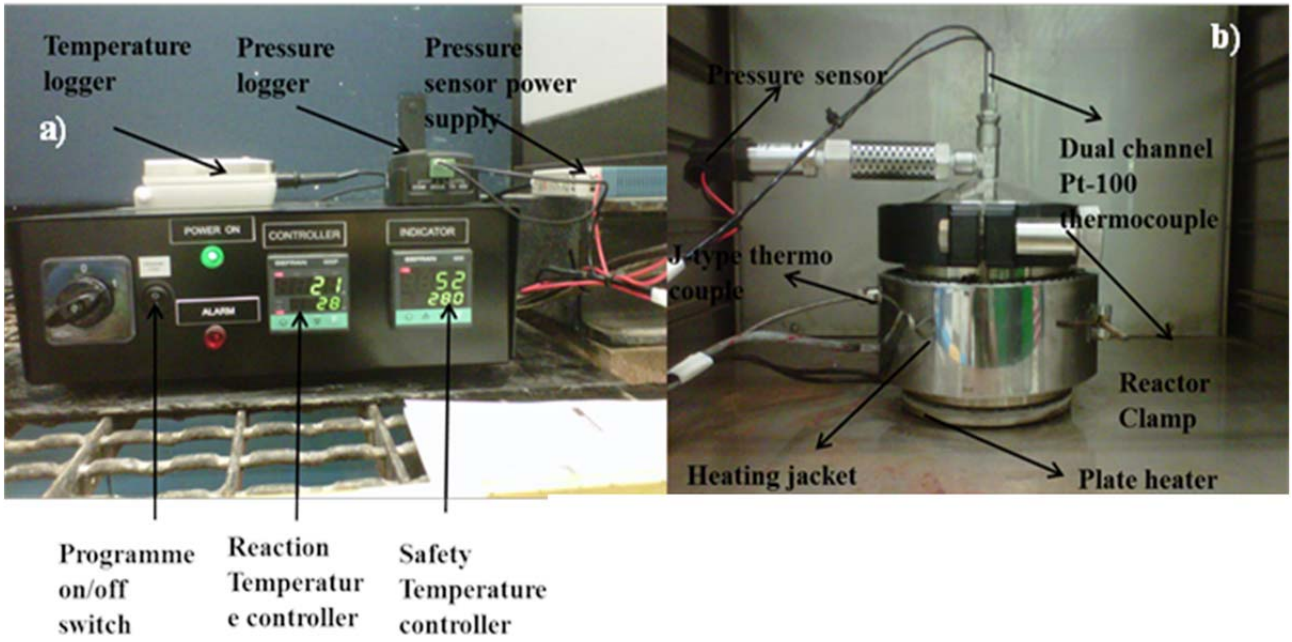

Figure 3.1 Experimental setup: a) controlling unit and b) autoclave / pressure vessel

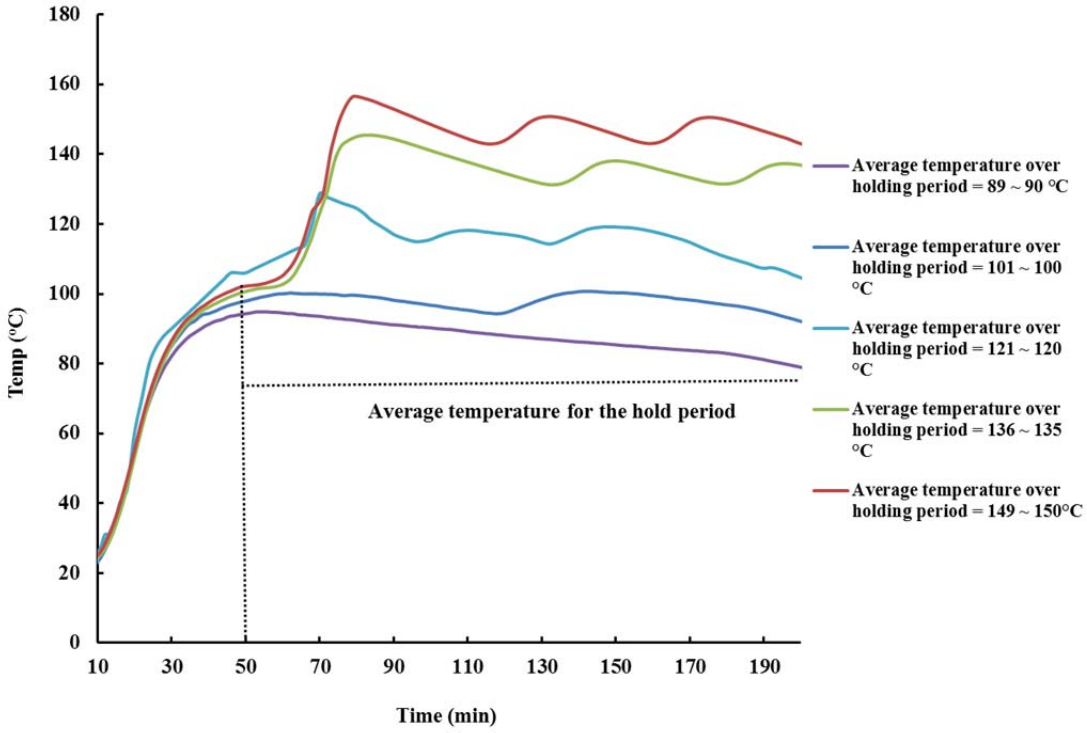

Figure 3.2 Temperature profile inside the reaction vessel

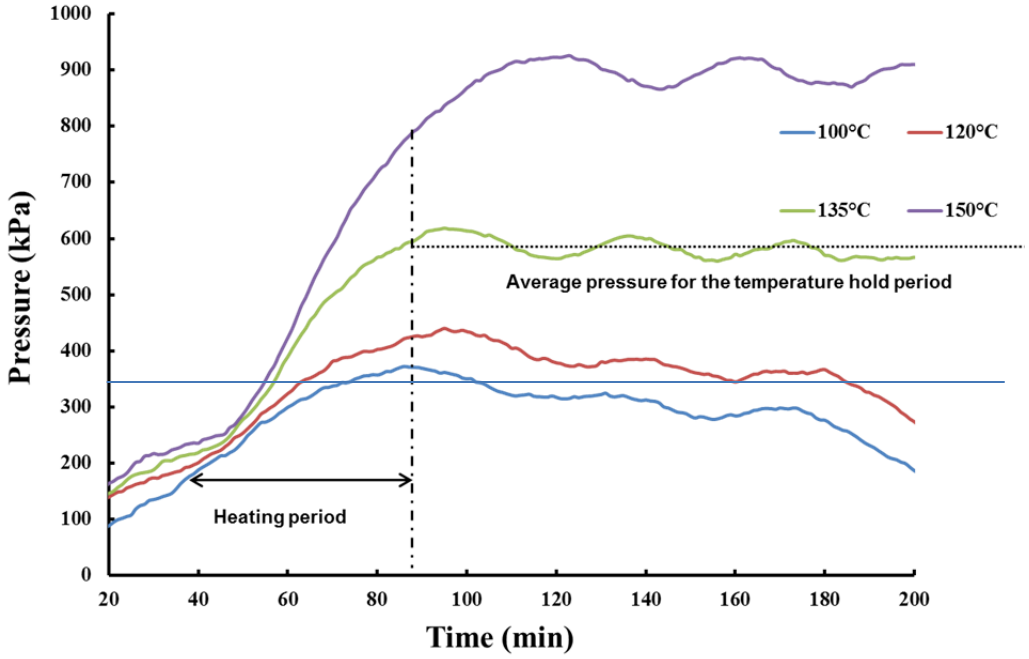

Figure 3.3 Pressure profile at different temperature inside the reaction vessel

Table 3.1 Process variable for the synthesis of β-FeOOH (bold text represents standard conditions)

Reaction variable	**Values**							
Reaction temperature (°C)	90	**100**	120	135	150	-	-	-
Synthesis time (minutes)	50	**120**	240	360	720	-	-	-
(%v/v) alcohol in the solution	0	10	30	**50**	70	95	98	100
$FeCl_3$ ratio	**0.05**	0.1	0.2	0.3	0.4	0.5	0.7	-

3.4 Factorial trial experiments

A two level, three factor, experimental design was used to identify the degree of interactions between process parameters statistically. Synthesis temperature and solution pH was omitted from the experimental design due to sensitive dependence of particle phase on these two variables. Butanol was used as solvent. Summary of the experimental design is presented in Table 3.2.

Table 3.2 Two level three factor experimental design

Experimental Run	**$FeCl_3$ concentration [M]**	**Solvent (ROH/H_2O) ratio (% v/v)**	**Time (h)**
1	0.05	30	12
2	0.50	30	12
3	0.05	30	2
4	0.05	90	12
5	0.50	90	12
6	0.50	30	2
7	0.05	90	2
8	0.50	90	2

Chapter 4

Hydrothermal precipitation of β-FeOOH particles in different solvent ratio (% v/v) and pH

4.1 Introduction

To evaluate the effect of alcohol-to-water ratio on the particle morphology and phase, four different alcohols at varying ratios (% v/v) ranging from 0 – 100% was used. A kinetic equation was evaluated to correlate particle size with solvent surface tension. The effect of solution pH on the particle phase and morphology was also evaluated.

4.2 Experimental methodology

A change in solvent ratio results in a change of solution pH. Simultaneous change of experimental variables may result in an outcome that is fallacious. In order to discern the effect of the variables individually on the particle morphology and phase, the study was conducted in two parts. In the first case, solvent ratio was varied at constant pH while in the second case, pH was changed keeping the alcohol-to-water ratio constant.

Accordingly, in the first case, a 0.05M $FeCl_3$ solution was prepared and mixed with different alcohols. The synthesis temperature was kept constant at 100°C for 2h. The solution pH was kept constant at ~2 by addition of NH_4OH. The temperature was maintained at 100˚C for 2h. Details of the experimental design are illustrated in Table 4.1.

To study the effect of the solution pH (prior to heating) on the particle characteristics, a 0.05M $FeCl_3$ solution was prepared and mixed with water and a given alcohol in 50/50 (v/v) ratio while changing the pH range from 2 - 2.5 - 3 by dropwise ammonia addition. The temperature was maintained at 100˚C for 2h. The details of this experimental design are shown in Table 4.2.

Table 4.1 Experiments with different solvent ratios

Solvent	**Solvent (ROH/H_2O) ratio (% v/v)**
BuOH	10,30,50,70,95,98,100
PrOH	10,30,50,70,95,98,100
EtOH	10,30,50,70,95,98,100
MeOH	10,30,50,70,95,98,100

Table 4.2 Experiments with different solution pH

Solvent	**Solvent (ROH/H_2O) ratio (% v/v)**	**Final solution pH**
BuOH	50	2, 2.5,3
PrOH	50	2, 2.5,3
EtOH	50	2, 2.5,3
MeOH	50	2, 2.5, 3

4.3 Results and discussion

4.3.1 Effect of BuOH-to-H_2O and PrOH – to-H_2O ratio on the akaganeite nanoparticle characteristics

Variation in alcohol-to-water ratio has a marked effect on the morphology of akaganeite particles. The morphologies evolved as a function of alcohol-to-water ratio variation are shown in Figure 4.1.

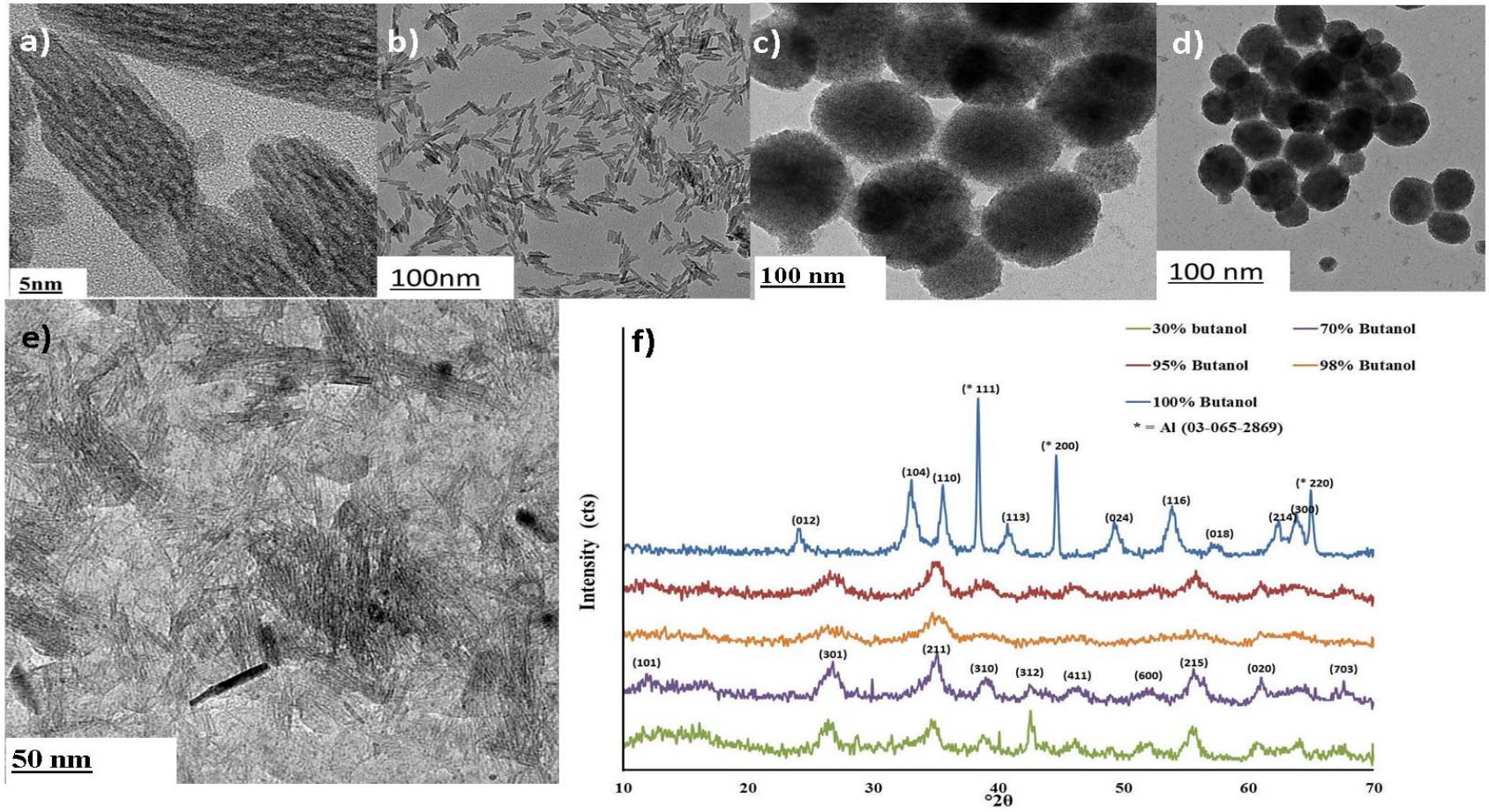

Figure 4.1 Dependence of morphological evolution as a function of variation on BuOH / H_2O and PrOH / H_2O ratio: (a) somatoids at 0% alcohol, (b) nanorods at 30% alcohol, (c) α-Fe_2O_3 spheres at 100% alcohol, (d) aggregation of spherical particles at 100% alcohol, (e) β-FeOOH nanofibers at 98% alcohol and, f) XRD patterns of the synthesised particles at different solvent ratios

About 75 nm long somatoidal (cigar-shaped) particles with ~20 nm diameter were formed in pure water (4.1a). No precipitate formed in solution containing 10 vol % BuOH or PrOH, while well-defined rod-shaped particles resulted in solution with 30 vol % BuOH or PrOH in water. In fact, crystalline β-FeOOH nanorods (aspect ratio ~10) could be synthesized in solvent mixtures containing BuOH or PrOH in 30-95 vol % concentration, as revealed by the XRD pattern in Figure 4.1f, that matches the JCPDS standard 42-1315. Crystalline β-FeOOH nanofibres (Figure 4.1 e) were obtained at 98 vol % BuOH or PrOH in water. It should be pointed out that presence of water facilitates the nucleation and growth of the nanorod-shaped β-FeOOH particle; in pure alcoholic solutions only spherical hematite (a-Fe_2O_3) particles could be seen, as shown in the TEM images (Figure 4.1c-d). Some of these are attached to one another, which imply growth via OA mechanism. Structurally, they are hematite (α-Fe_2O_3; JCPDS 33-0664) whose XRD pattern is shown in Figure 4.1 f. Similar observation was made by Chen et al (2010) who synthesized hematite nanoplates using different alcohols (BuOH, PrOH, EtOH and MeOH) as the solvent. It was theorized by them that trace amount of water could have facilitated nucleation and growth of hematite in nanoplate morphology which is contrary to the findings in the present work which demonstrates the formation of spherical hematite nanoparticles in the absence of water. It is believed that presence of water promotes the hydrolysis of ferric chloride and crystallization of β-FeOOH which is a hematite precursor as per the following reaction:

$$2\ \beta\text{-FeOOH} \longrightarrow \alpha\text{-}Fe_2O_3 + H_2O$$

Equation 4.1

No study has been reported to the best of our knowledge in the literature that uses 100% alcohol as solvent to synthesise akaganeite particles. For this reason a direct comparison could not be made regarding the nucleation and growth of akaganeite particles in solvent only.

Huang et al. (2003) reported that the presence of water around the nanoparticle surface induces the oriented attachment via Brownian motion-induced reorientation and thereby promoting growth by bulk diffusion. Diffusion, either via surface reorganisation or addition of ions from aqueous solution, eliminates the indentations at particle contacts, ultimately generating rounded crystals. This is

corroborated by the spherical hematite particles formed in the absence of water (Figure 4.1-D), which are seen attached to one another via oriented attachment mechanism. This observation contradicts with the findings of Huang et al. (2003). In addition to promoting nucleation of β-FeOOH, presence of water significantly impacts the growth of β-FeOOH nanorods; 2-5 vol % water transforms the nanofibres into high aspect ratio nanorods.

Though the formation of highly anisotropic particles using growth inhibitors, such as, surfactants or templates, has been reported in the literature, neither was used in the present study. It was shown that the addition of butanol and propanol confines the growth of the akaganeite nanorods in both diameter and length directions. For example, in a solvent mixture containing 30 vol % butanol, the diameter and the length of the particles was reduced by 70% and 50%, respectively, compared to when no butanol was used; reduction in diameter and length was 70 and 75%, respectively, in the case of 30 vol % propanol-water mixture. This clearly highlights the crucial role of alcohol as solvent in controlling particle dimensions. Figure 4.2 presents the % reduction in particle dimensions relative to those without alcohol. As can be seen, the particle size reduction is highest at 50% ROH/H_2O mixture (4.2a& b). Also, the effect of propanol is more pronounced than that of butanol on diameter and length. The results are summarized in Table 4.3.

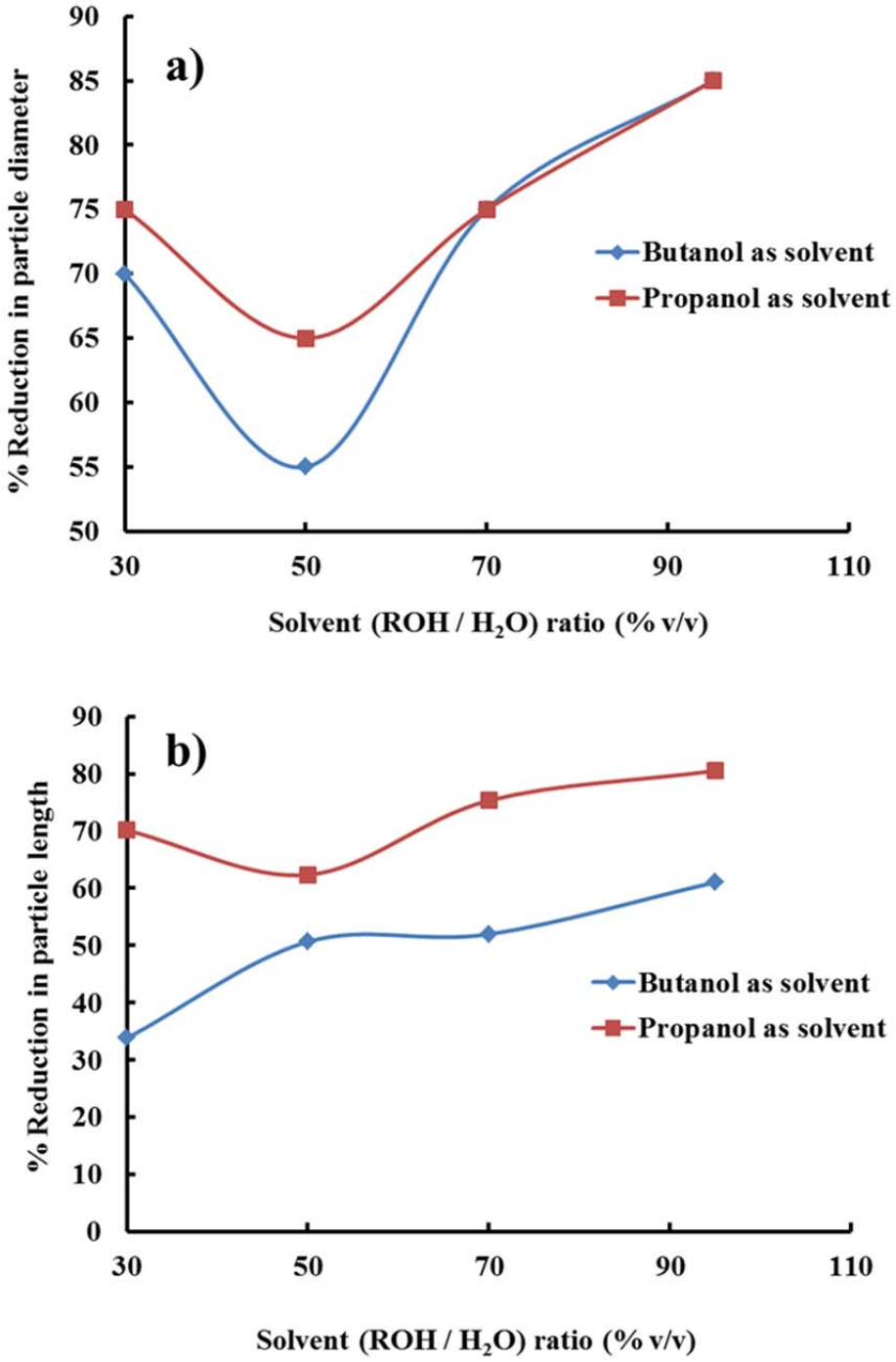

Figure 4.2 % Reduction in particle size using solvent compared to without solvent; a) particle diameter and b) particle length

Table 4.3 Effect of solvent ratio on the particle characteristics

Solvent	Solvent (ROH/H_2O) ratio (% v/v)	ϕ_{AV}(nm)	L_{AV} (nm)	Phase	Morphology	Average aspect ratio
BuOH	0	20 ± 6	77 ± 7	β-FeOOH	Somatoidal	4
	10	-	-	No precipitation	-	-
	30	6 ± 2	51 ± 5	β-FeOOH	Rods	9
	50	9 ± 2	38 ± 5	β-FeOOH	Rods	4
	70	5 ± 1	37 ± 5	β-FeOOH	Rods	7
	95	3 ± 1	30 ± 3	β-FeOOH	Rods	10
	98	n/a	n/a	β-FeOOH	Fibres	-
	100	130 ± 15		α-Fe_2O_3	Spheres	-
PrOH	0	20 ± 6	77 ± 7	β-FeOOH	Somatoidal	4
	10	-	-	No precipitation	-	-
	30	5 ± 2	26 ± 4	β-FeOOH	Rods	5
	50	7 ± 2	29 ± 3	β-FeOOH	Rods	4
	70	5 ± 1	50 ± 2	β-FeOOH	Rods	10
	95	3 ± 1	15 ± 1	β-FeOOH	Rods	5
	98	n/a	n/a	β-FeOOH	Fibres	-
	100	108 ± 15	n/a	α-Fe_2O_3	Spheres	-

4.3.2 Effect of EtOH - to - H_2O and MeOH – to - H_2O ratio on the akaganeite nanoparticle characteristics

The morphologies evolved as a function of alcohol-to-water ratio are illustrated in Figure 4.3.Somatoidal particles were formed in mixture containing 10 vol % MeOH or EtOH in water. In solvent mixtures containing up to 70 vol % EtOH in water, β-FeOOH nanorods were formed, while aggregates resulted at higher (98 vol %) EtOH-to - H_2O mixture. The particles assumed spindle-like shape in 30-70 vol % MeOH while fibres and nanoflakes were formed in 95-98 vol % MeOH to water mixtures. Fast Fourier Transform (FFT) algorithm was performed on the TEM images of the particles. The dots in the FFT (Figure 4.3 a) represent the crystallinity of the material. The XRD patterns (Figure 4.3 i) of the samples synthesized in 95-98% to EtOH / H_2O mixture tallied with those (JCPDS card no: 33-0664) of the α-Fe_2O_3 particles.

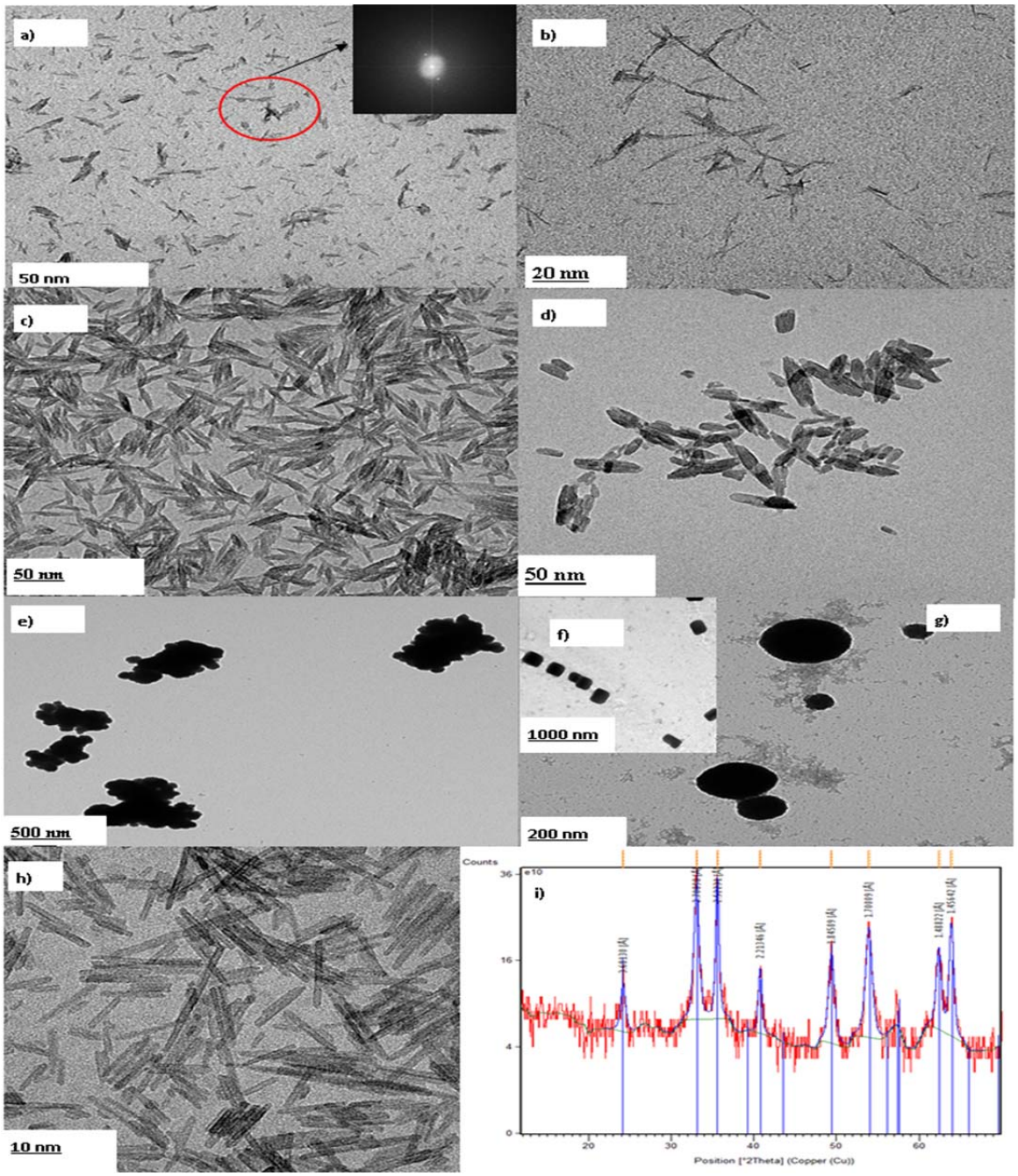

Figure 4.3 Dependence of morphological evolution as a function of variation on MeOH to H_2O and EtOH to H_2O ratio: (a& b) nanoflakes and stranded fibres at 95% MeOH to H_2O, (c) spindles at 30% MeOH to H_2O, (d) somatoids at 10% MeOH to H_2O, (e) aggregation at 98% MeOH to H_2O and, f & g) spherical and pseudo cubes at 95% EtOH to H_2O, h) Particles with high aspect ratios at 70% EtOH to H_2O and, i) XRD patterns of the synthesised particles at different ROH/H_2O ratio

From the foregoing discussion it appears that carbon chain length of the alcohol and the alcohol-to-water ratio control the nucleation and growth of particles. Particle length and diameter decrease with increase in the alcohol-to-water ratio; for example, a 50% ethanol-to-water mixture changes the particle diameter and length by 75 and 71% respectively, compared to when no alcohol was used. The percentage reduction in nanorod diameter and length was constant over the methanol-to-water ratio range of 10 – 50% compared to when no alcohol was used.These results are summarized in Table 4.4.

Table 4.4 Effect of solvent ratio on the particle characteristics

Solvent	Solvent (ROH/H_2O) ratio (% v/v)	ϕ_{AV} (nm)	L_{AV} (nm)	Phase	Morphology	Average aspect ratio
MeOH	10	3 ± 1	23 ± 9	β-FeOOH	Rods	8
	30	3 ± 1	24 ± 9	β-FeOOH	Rods	8
	50	5 ± 2	22 ± 5	β-FeOOH	Rods	4
	70	4 ± 2	35 ± 8	β-FeOOH	Rods	9
	95	n/a	n/a	α-Fe_2O_3	Aggregated	-
	98	n/a	n/a	α-Fe_2O_3	Aggregated	-
	100	n/a	n/a	α-Fe_2O_3	n/a	-
EtOH	10	3 ± 4	50 ± 4	β-FeOOH	Rods	13
	30	3 ± 4	55 ± 4	β-FeOOH	Rods	18
	50	3 ± 2	58 ± 3	β-FeOOH	Rods	19
	70	3 ± 2	60 ± 3	β-FeOOH	spindle	20
	95	n/a	n/a	β-FeOOH	Fibrous	
	98	n/a	n/a	β-FeOOH	Flakes and fibrous	-
	100	n/a	n/a	α-Fe_2O_3	n/a	-

4.3.3 Relationship between particle size and surface tension

According to classical electrostatic model, the chemical potential of two phases (when a solute precipitates from a supersaturated ideal solution) are equal in equilibrium and can be written as (Israelachvili, 1992):

$$\mu^{o}{}_{S} + KT\ln C_S = \mu^{o}{}_{L} + KT\ln C_L \qquad \text{Equation 4.2}$$

Where, μ^o is the standard chemical potential and C, concentration of solute. Solid and liquid phase are denoted by subscripts S and L respectively. T is the temperature expressed in Kelvin and K, Boltzmann constant. Equation 4.3 also known as Coulombs interaction and can be used to express the energy required to separate the charged ions from the solid state (Israelachvili, 1992):

$$\Delta\mu^o = \frac{Z_+ Z_- e^2}{4\pi\varepsilon_o\varepsilon(r_+ + r_-)} \qquad \text{Equation 4.3}$$

where, ε_o, represents the permittivity in vacuum and ε, dielectric constant of a given solution and r_+ and r_- the ionic radius of species with charge Z^+ and Z^-, respectively. By putting appropriate values and combining Equations 4.2 and 4.3, Equations 4.4 and 4.5 can be written as follows:

$$\frac{Z_+ Z_- e^2}{4\pi\varepsilon_o\varepsilon(r_+ + r_-)} + 0 = KT\ln C_L \qquad \text{Equation 4.4}$$

$$C_L = \exp\left(\frac{Z_+ Z_- e^2}{4\pi\varepsilon_o\varepsilon KT(r_+ + r_-)}\right) \qquad \text{Equation 4.5}$$

From the nucleation theory it is known that the formation of particles is dependent significantly on the supersaturation defined as:

$$S = \frac{C}{C_L} \qquad \text{Equation 4.6}$$

where, S is the supersaturation of solute, C and C_L the solute concentration and solvent concentration. Relationship between super-saturation and particle size can be expressed by Kelvin equation (Mullin, 2001):

$$\ln(S) = \frac{2m\gamma}{rKT\rho} \qquad \text{Equation 4.7}$$

where, m is the weight of the solute molecule, γ, the interfacial energy in terms of j/m^2. The term interfacial energy can also be written as Nm^{-1}. Combining Equation 4.2 – 4.6yields (Chen and Chang, 2004):

$$\frac{1}{r} = \frac{KT\rho}{2m\gamma}\ln C + \frac{\rho\left[Z + Z - e^2\right]}{8\pi m\varepsilon_0\gamma\varepsilon\left(r_+ + r_-\right)} \qquad \text{Equation 4.8}$$

The Coulomb interaction is very strong in long range but weaker in water and other media of high dielectric constant (Israelachvili, 1992). In the case of mixtures of water with alcohols of the kind used in this thesis, the Coulomb interaction can be assumed very weak. For the sake of simplicity therefore, the second term can be treated as a constant and, Equation 4.8 can be rewritten as:

$$r = \frac{2m\gamma}{KT\rho\ln C} + \frac{1}{A} \qquad \text{Equation 4.9}$$

where,

$$A = \frac{\rho\left[Z + Z - e^2\right]}{8\pi m\varepsilon_0\gamma\varepsilon\left(r_+ + r_-\right)} \qquad \text{Equation 4.10}$$

Equation 4.9 is valid for spherical particles, whereas those synthesized in this work are rod-shaped. In that case, equivalent diameter, d_e, was used as calculated using Huebscher formula (Yuan et al., 2009):

$$d_e = 1.30\left[\frac{(ab)^{0.625}}{(a+b)^{0.25}}\right] \qquad \text{Equation 4.10}$$

where, a and bare the measured diameter and length of the particles.

The correlation between surface tension of the solvent-water mixtures and the theoretically computed equivalent diameter is linear and independent of the nature of alcohol, as can be seen from Figure 4.4.This illustration proves the point that particle nucleation and growth can be related to solvent surface tension which was discarded previously.

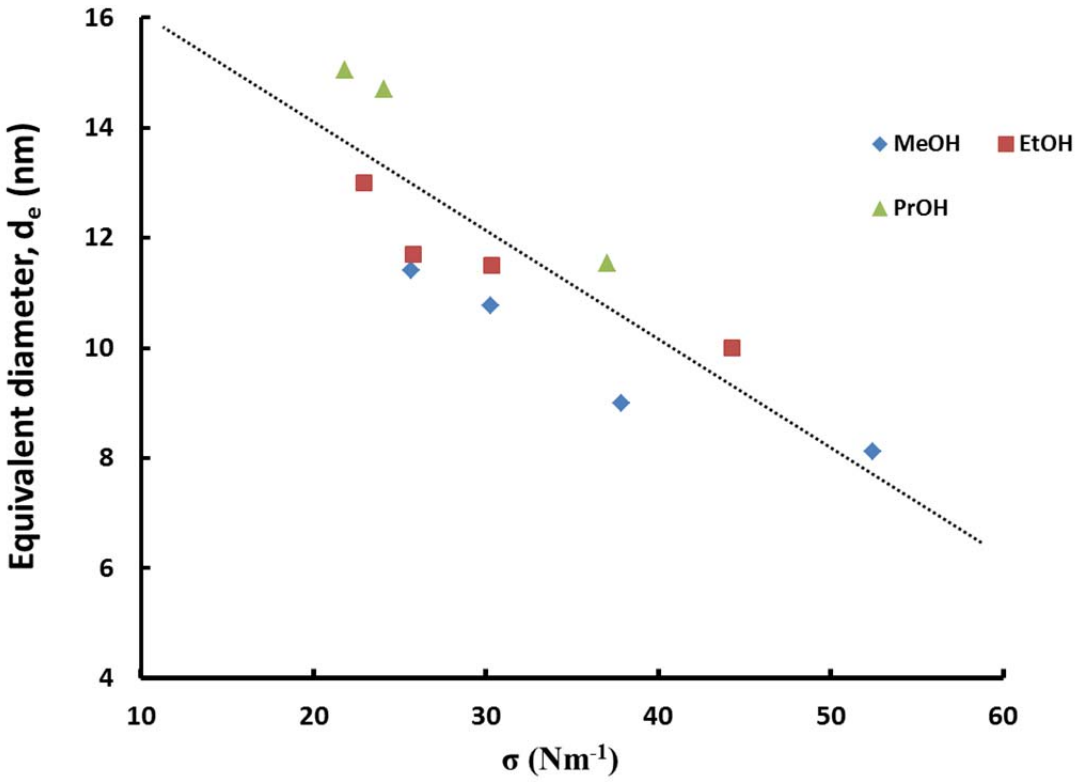

Figure 4.4 Correlation between particle size and solvent surface tension

4.3.4 Effect of pH on the growth of β-FeOOH nanoparticles

pH greatly affects the particle morphology. According to Vayssieres et al. (2001), Fe^{3+} is easy to hydrolyse in solution forming $Fe(OH)_3$;hence, the formation of β-FeOOH nanorods is facilitated in low pH solutions. The morphologies evolved as a function of alcohol-to-water ratio variation are shown in Figure 4.5.

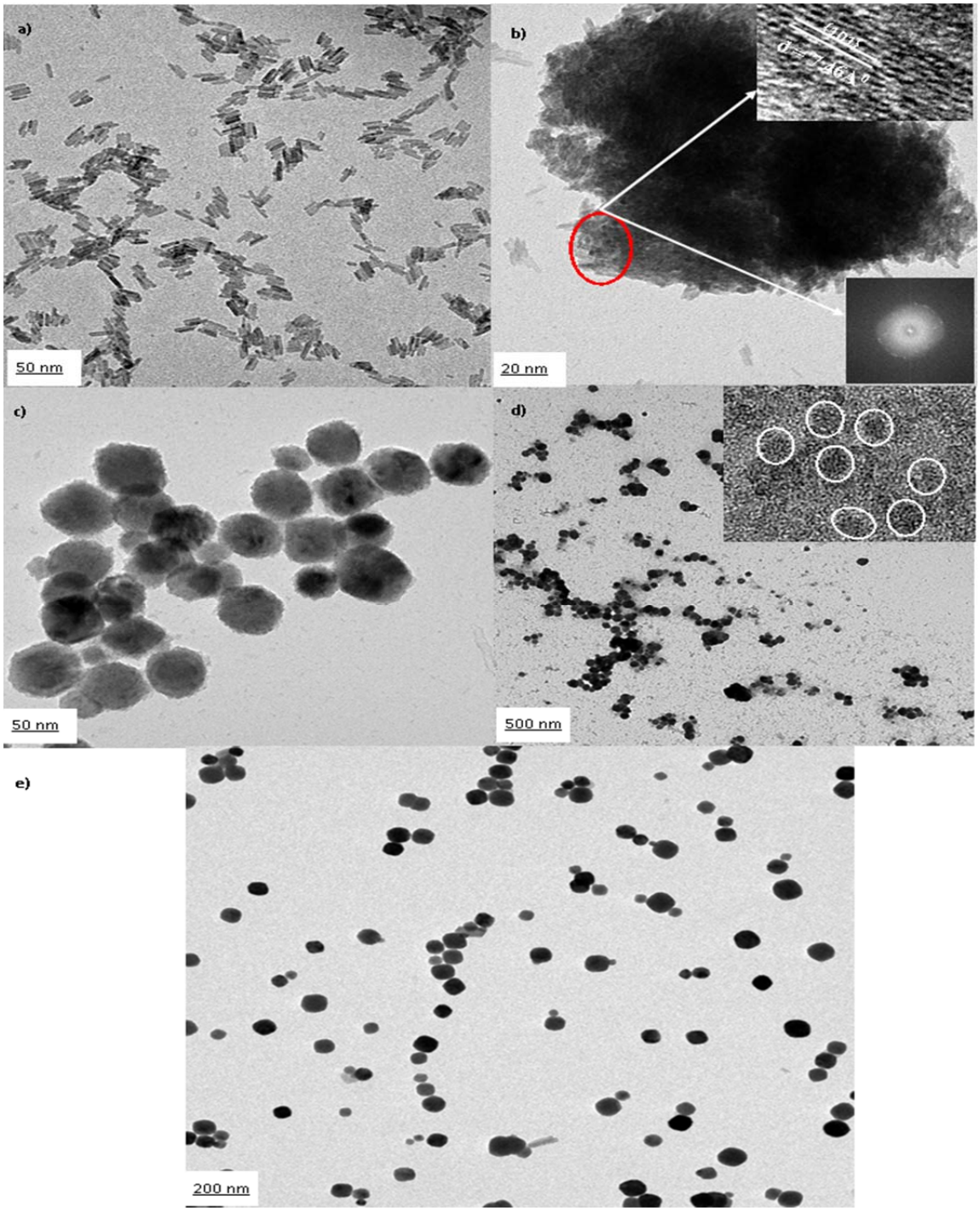

Figure 4.5 Dependence of morphological evolution as a function of pH: a) nanorods at pH 2, b) aggregation of nanorods at pH 2.5 in butanol and propanol, c) spherical α-Fe_2O_3 particles at pH 3 in butanol and propanol, d) clustered α-Fe_2O_3 particles at pH 2.5 in ethanol and e) dispersed α-Fe_2O_3 particles at pH 2.5 in methanol

β-FeOOH nanorods were obtained at pH 2 in all cases (Figure 4.5 a). With increase in pH to 2.5, aggregation of the β-FeOOH rods (Figure 4.5 b) was observed in both butanol and propanol. Spherical nanosized α-Fe_2O_3 particles were obtained when the precursor pH was adjusted to pH~3 (Figure 4.5c). The spherical nanoparticles have an average diameter of ~95 ± 19nm.

Clustered α-Fe_2O_3 nanoparticles (Figure 4.5 d) were obtained at pH ~2.5 in ethanol contrary to butanol and propanol. From the TEM image it was observed that the particle clusters were formed from small spherical particles. The spherical particles are marked with white circles and presented as a subset in Figure 4.5d.

Dispersed crystalline α-Fe_2O_3 (Figure 4.5 e) particles with an average diameter of ~112 ± 38 were obtained at pH~2.5 in methanol contrary to other three solvent used. Khan et al. (2011) synthesised spherical α-Fe_2O_3 nanoparticle with and without surfactant Tween 80 at 200˚C for a total duration of 5h. Irregular-shaped α-Fe_2O_3 nanoparticles with a wide range of size distribution in the range of 150 – 300nm were obtained without the surfactant. Moreover, the surfactant was effective in controlling the particle shape and restricting particle growth to a narrow range of 40 – 60nm.

It was shown that dispersed α-Fe_2O_3nanoparticles with controlled particle sizes could be synthesised without the use of surfactant under mild conditions just by altering the pH of the solution. XRD patterns of the synthesised β-FeOOH and α-Fe_2O_3 particles are presented in Figure 4.6.

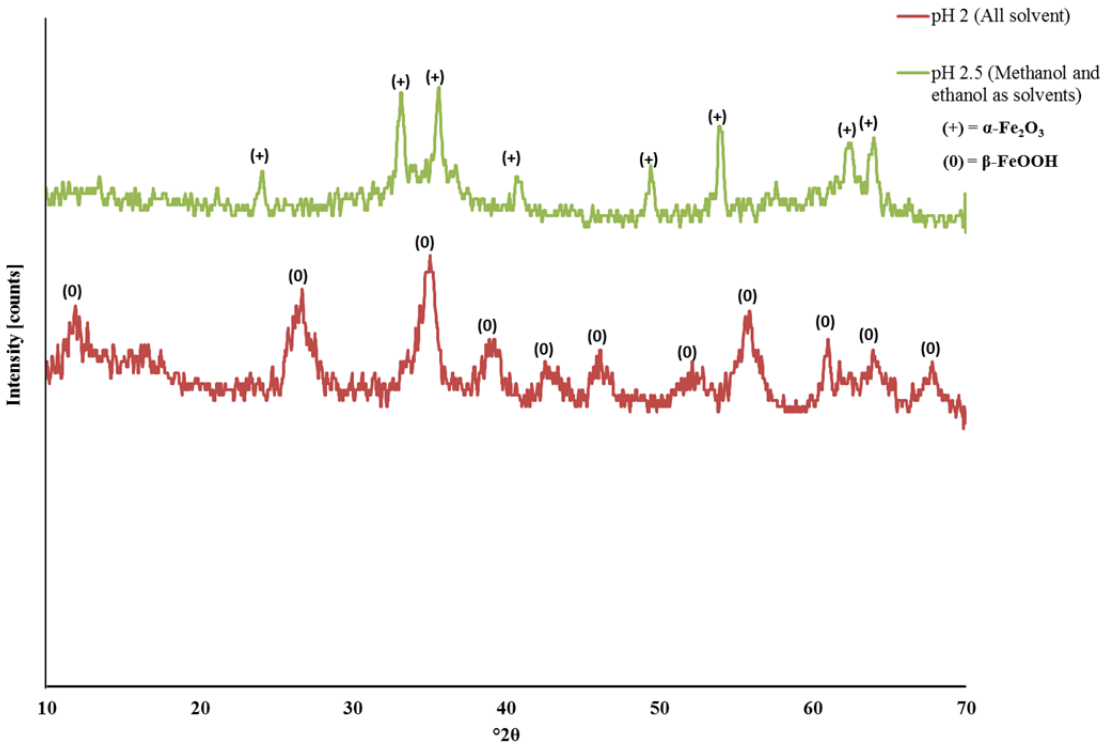

Figure 4.6 XRD patterns of the particles synthesised at different pH

4.3.5 Effect of alcohol on the Raman spectra of the synthesised particles

Raman spectroscopy was performed to evaluate the effect of alcohols on the particle morphology and chemistry, using Horiba Jobin Yvon spectroscope (Model LabRAM HR 800). The spectra were collected using a 532nm laser (250 muW), a 5x objective and a grating of 600 lines/mm. The spectra were identical in all the cases, as seen from Figure 4.7, from which the presence of β-FeOOH and α-Fe_2O_3 could be discerned. The spectrum of bright flakes (region 1) is characteristic of akaganeite with peaks at 308, 391, 486, 537, 718 and 3500 cm^{-1}(Réguer et al., 2007). The spectrum of region3 is characteristic of hematite with large, broad peaks at 1315 and 2440 cm^{-1}, and narrow peaks at 224, 291, 408 and 486 cm^{-1} (region 3). This is consistent with the literature. Region 2 contains a mixture of akaganeite and hematite. The inset shows slight stretching of the OH peak at ~3500 cm^{-1}, which is ascribed to the presence of Cl^{-1} in the sample (as an impurity) that originates from the chloride precursor for iron.

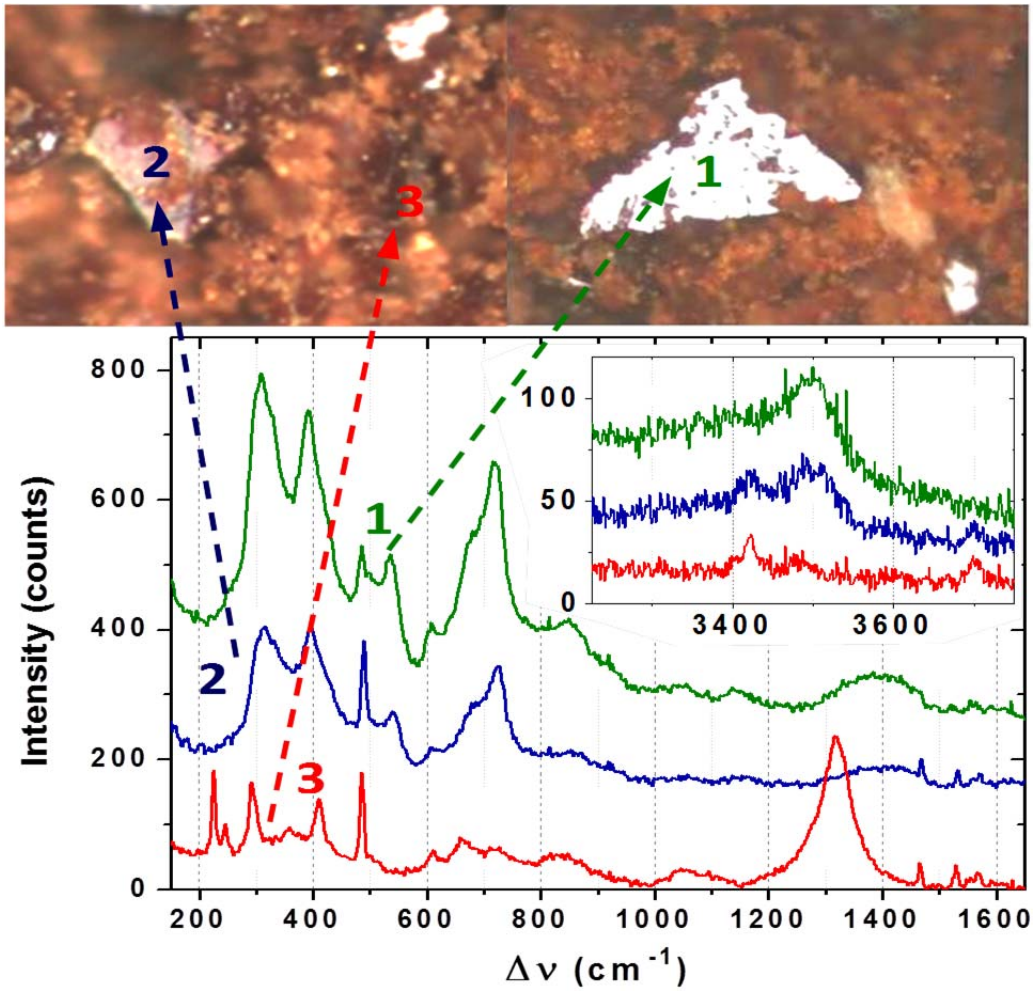

Figure 4.7 Raman spectra of the sample prepared in the presence of alcohol: akaganeite (region 1), akaganeite + hematite (region 2) and hematite (region 3).

4.4 Conclusion

The effect of alcohol-to-water ratio using four analogous aliphatic alcohols as well as the effect of solution pH (prior to heating) on the nature of particles was examined. In the absence of alcohols, somatoidal β-FeOOH particles of ~20 nm diameter and ~77 nm length were formed; same morphology resulted in the case of 10% (v/v) $MeOH/H_2O$ and $EtOH/H_2O$ mixtures. No precipitation occurred, however, in the case of 10% (v/v) $BuOH/H_2O$ and $PrOH/H_2O$ mixtures. Well-defined rod-shaped particles with a clear framework and diameter and length of ~6 nm and length ~37 nm were formed in 30% (v/v) $BuOH/H_2O$ mixture, which corresponds to 70% and 50% reduction is diameter and length,

respectively, of the nanorods. The dimensional reduction was 70% and 75% in 30% (v/v) PrOH/H_2O mixture. Nanofibrillar and aggregated nanoparticles of β-FeOOH were formed in 98%PrOH/H_2O and EtOH / H_2O mixture, respectively; flakes and fibres resulted in 95% MeOH / H_2O mixture. The presence of water plays an important role in the formation of β-FeOOH particles. Only spherical α-Fe_2O_3 particles were formed in pure alcohols implying nucleation and growth of particles was dependent on the length of the carbon chain in these alcohols as well as on the alcohol-to-water ratio. Kinetic equation was tested to fit the experimental data as a function of solution pH at constant $FeCl_3$ concentration and reaction time. Surfactant free synthesis of spherical α-Fe_2O_3 nanoparticles is not reported widely in the literature and therefore, their synthesis under conditions of controlled pH might be an alternative approach. β-FeOOH structure was not particularly affected by the choice of solvent as revealed by Raman data.

Chapter 5

Role of solvent on the growth kinetics of β-FeOOH nanorods

5.1 Introduction

The effect of four different alcohols on the growth kinetics of the β-FeOOH nanorods has been assessed. Relationship between surface tension and growth rate constants are also demonstrated in this chapter.

5.2 Experimental methodology

To conduct time evolution study, a 0.05M $FeCl_3$ solution was prepared and mixed with water and a given alcohol in 50/50 (% v/v) ratio. Reaction temperature and solution pH was maintained at 100˚C and 2 respectively. Synthesis time was varied in the range of 2 – 12h. Details of this experimental design are presented in Table 5.1.

Table 5.1 Experiments with different synthesis time

Solvent	Solvent (ROH/H_2O) ratio (% v/v)	Time (minutes)
BuOH	50	50, 60, 120, 240, 280, 300, 360 and 720
PrOH	50	50, 60, 120, 240, 280, 300, 360 and 720
EtOH	50	50, 60, 120, 240, 280, 300, 360 and 720
MeOH	50	50, 60, 120, 240, 280, 300, 360 and 720

Synthesis time had no effect on the particle phase over a synthesis time range of 1 – 12h in BuOH, PrOH and EtOH. A mixture of particles (β-FeOOH + α-Fe_2O_3) and pure α-Fe_2O_3 particles was formed at 360 and 720 minutes respectively in MeOH as shown by the XRD patterns in Figure 5.1.

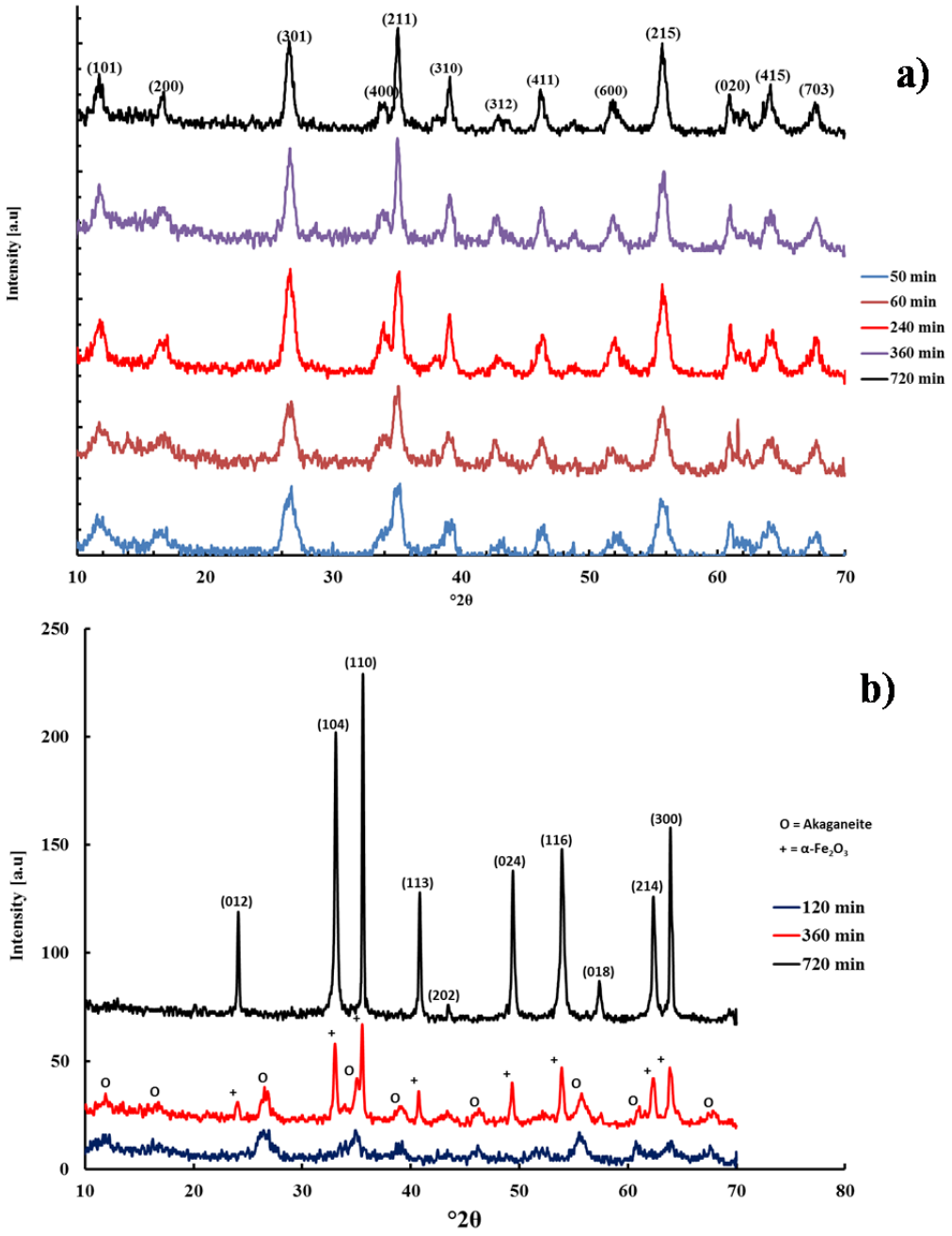

Figure 5.1 XRD patterns a) β-FeOOH particles synthesised in butanol, propanol and ethanol, b) particles synthesised in methanol

5.3 Results and discussion

5.3.1 Evaluation of growth mechanism via HRTEM

5.3.1.1 Investigation of β-FeOOH growth in BuOH and PrOH

Structural evolution of β-FeOOH particles as a function of synthesis time variations are shown in Figure 5.2.

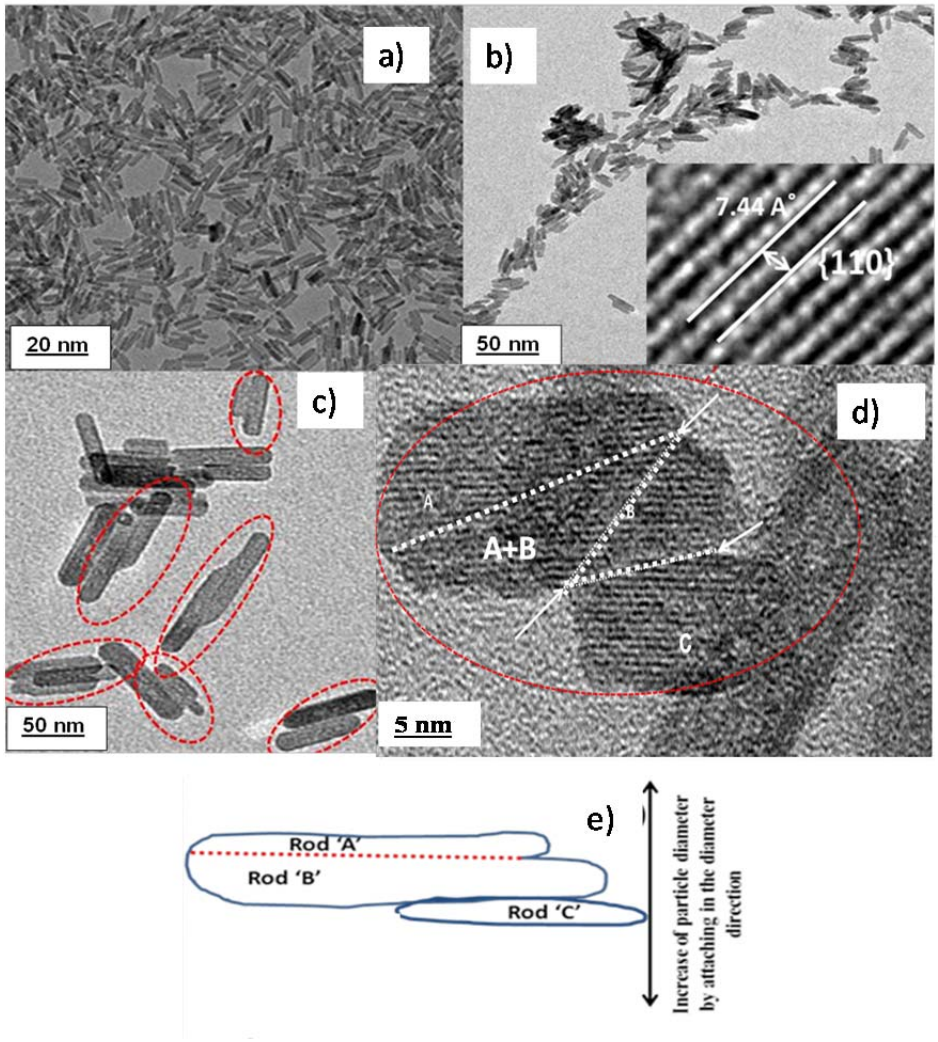

Figure 5.2 Structural evolution over time, a) mono-disperse particles after 60 minutes, b) aggregation after 240 minutes, c & d) twinning and crystallographic oriented attachment observed after 360 minutes and e) schematic illustration of the crystallographic oriented attachment mechanism

Uniform akaganeite nanorods are formed after 60 minutes (Figure 5.2 a). Aggregation of particles occurs with increase in synthesis time (Figure 5.2b). It was suggested by Huang et al. (2003) that for spherical particles, once a particle pair is formed via the OA mechanism, the radius of the new larger particles is smaller than twice the radius of the two primary particles. Hence, the distance between the new particles and other adjacent particles increases. Aggregation ensures small distances between the nanoparticles as can be seen from Figure 5.2 b, providing the possibility of coarsening via oriented attachment. Twinning of rods is observed after a synthesis time of 360 minutes (Figure 5.2c). Twin rods and stacking faults are common signs of the OA mechanism. Side by side crystallographically oriented growth of akaganeite nanorods are shown in Figure 5.2 d and a schematic outline is presented in Figure 5.2 e. The arrowhead (Figure 5.2 d) marks indentations, interpreted to be the interfaces between assembly units. Once formed, it is possible to preserve the structure in the following growth process (Deng et al., 2007).

Growth by OA mechanism as illustrated in Figure 5.3 will result in a broader and unsymmetrical particle size distribution (Figure 5.4) due to random attachment symmetry. However Particle growth via OR mechanism will normally result in an undisturbed size distribution curve due to systematic growth of the particles. It can be seen from Figure 5.4 (a & b) that particle size distribution at 50 minutes represents a bell-shaped curve (variance, $\sigma^2 = 6.7$ and standard deviation, $\sigma = 2.58$). As the time increases, the shape of the curve deviates from ideal Gaussian distribution. The standard deviation, σ and variance, σ^2 for the particles synthesised at 720 minutes were found to be 4.32 and 19 respectively, implying that inconsistent distribution occurs over time, confirming the presence of OA growth. A similar observation was reported by Zhang and Benfield (2002) during the heating of amorphous TiO_2in air, to form nanocrystalline anatase. The findings are summarized in Table 5.2 and 5.3.

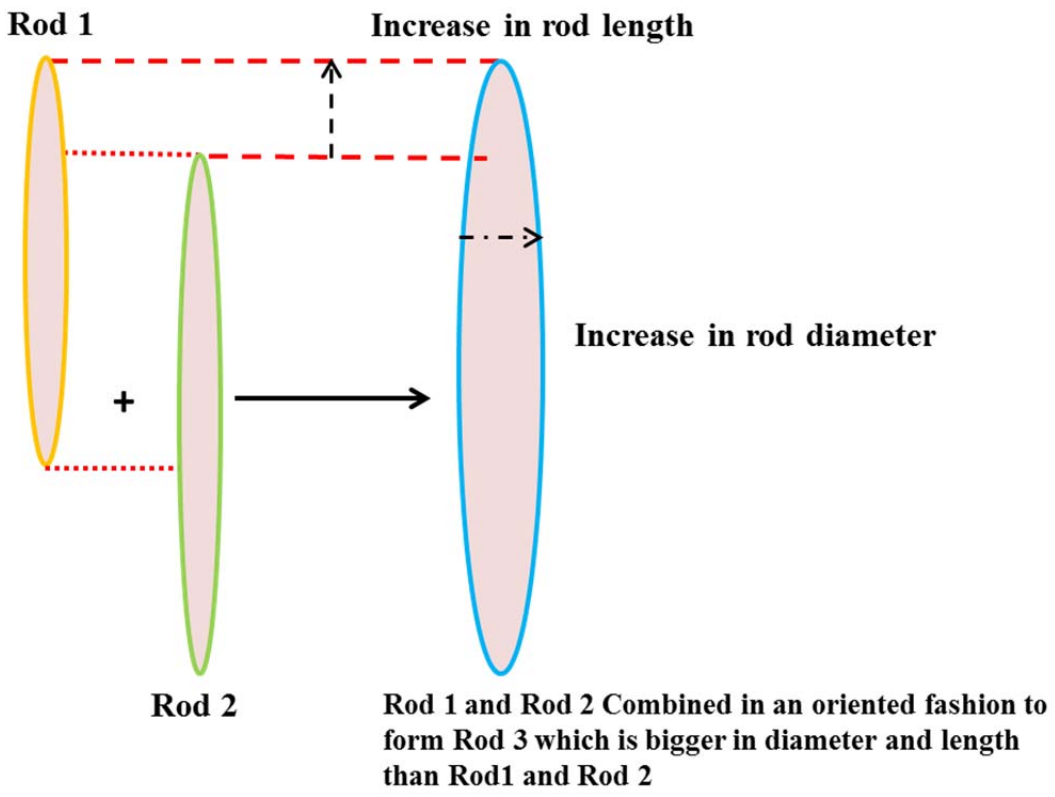

Figure 5.3 Illustration of particle growth via OA mechanism

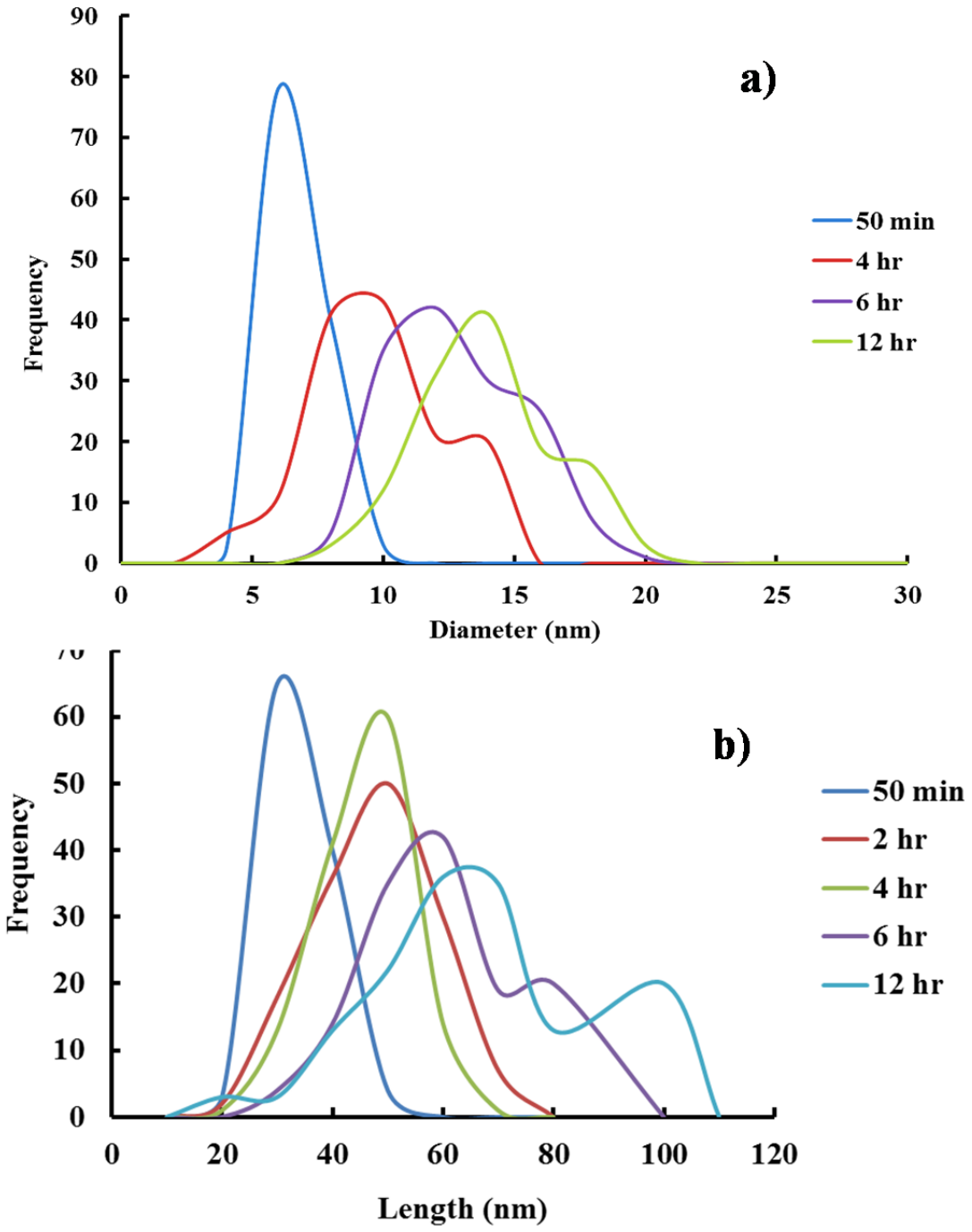

Figure 5.4 Particle size distribution of β-FeOOH nanorods in, a) transversal & b) longitudinal directions

Table 5.2 Effect of time on the particle characteristics in BuOH

Time (min)	Φ_{AV}(nm)	L_{AV} (nm)	Morphology	Phase	Average aspect ratio
50	6±1	30±6	Rods	β-FeOOH	5
60	7±1	32±7	Rods	β-FeOOH	5
120	7±2	36±10	Rods	β-FeOOH	5
240	8±2	39±11	Rods	β-FeOOH	5
280	9±5	39±11	Rods	β-FeOOH	4
300	10±9	44±12	Rods	β-FeOOH	4
360	12±7	50±13	Rods	β-FeOOH	4
720	13±8	58±14	Rods	β-FeOOH	4

Table 5.3 Effect of time on the particle characteristics in PrOH

Time (min)	Φ_{AV}(nm)	L_{AV} (nm)	Morphology	Average aspect ratio
50	5±1	27±6	Rods	5
60	6±2	29±7	Rods	5
120	6±1	32±7	Rods	5
240	7±3	35±8	Rods	5
280	7±2	35±8	Rods	5
300	7±1	39±9	Rods	6
360	10±2	44±8	Rods	4
720	11±3	52±9	Rods	5

5.3.1.2 Investigation of β-FeOOH growth in EtOH

Only rod-shaped particles were obtained in ethanol over the time range. Particle size distribution given in Figure 5.5, highlights that the distribution curves are symmetrical and become broader as the time progresses. A diffusion-based growth such as OR would normally result in symmetrical distribution curve, postulating that particle growth in ethanol is controlled by OR mechanism. The results are summarised in Table 5.4.

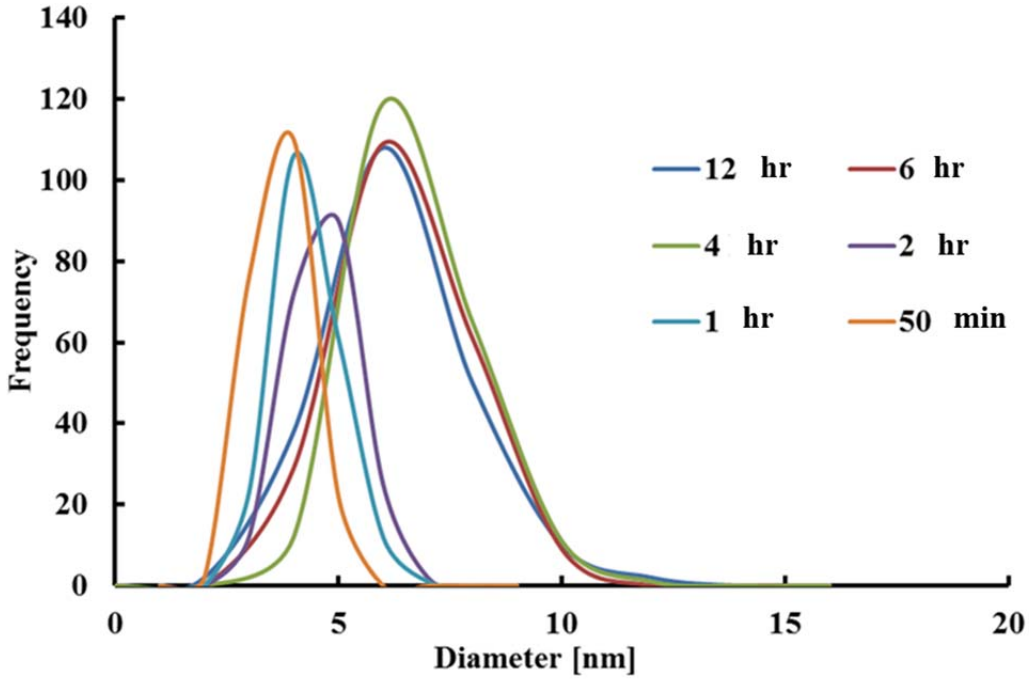

Figure 5.5 Particle size distribution of β-FeOOH nanorods synthesised in ethanol

Table 5.4 Effect of time on the particle characteristics in EtOH

Time (min)	ϕ_{AV}(nm)	L_{AV} (nm)	Phase	Morphology	Average aspect ratio
50	4±1	14±5	β-FeOOH	Rods	4
60	5±1	20±7	β-FeOOH	Rods	4
120	5±2	24±10	β-FeOOH	Rods	5
240	6±4	25±11	β-FeOOH	Rods	4
360	7±1	27±13	β-FeOOH	Rods	4
720	7±5	30±17	β-FeOOH	Rods	4

5.3.1.3 Investigation of β-FeOOH growth in MeOH

Effect of methanol on the progressive growth β-FeOOH nanoparticles is illustrated in Figure 5.6.

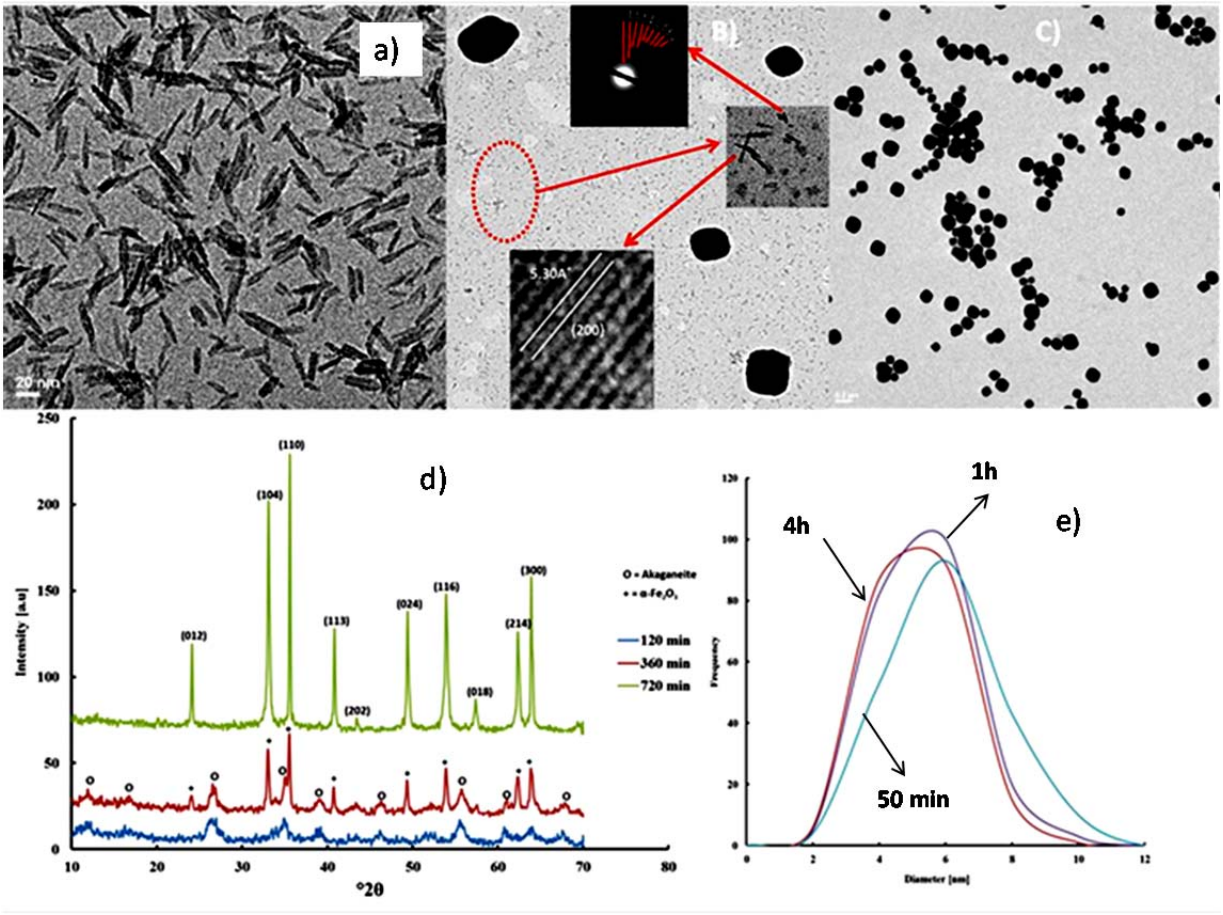

Figure 5.6 Structural evolution of particles as a function of time in methanol. In a) somatoidal particles over time range of 50 – 120 minutes, b) pseudo cubes with somatoidal particles after 360 minutes, c) spherical α-Fe_2O_3particles after 720 minutes, d) XRD patterns of particles, and e) particle size distribution

Somatoidal / ellipsoidal particles are formed in the synthesis time range of 50 – 240 minutes (Figure 5.6 a), followed by pseudo cubes and spherical particles in the range of 240 – 720 minute (Figure 5.6 b). Particle size distribution curves (5.6 e) at different synthesis time represent an approximate bell-shaped curve, which becomes broader over time, postulating OR mechanism. The results are summarised in Table 5.5.

Table 5.5 Effect of time on the particle characteristics in MeOH

Time (min)	ϕ_{AV}(nm)	L_{AV} (nm)	Phase	Morphology	Average aspect ratio
50	4±1	14±5	β-FeOOH	Somatoidal	4
60	5±1	20±7	β-FeOOH	Somatoidal	4
120	5±2	24±10	β-FeOOH	Somatoidal	5
240	6±4	25±11	β-FeOOH	Somatoidal	4
360	6±1	27±13	β-FeOOH+ α-Fe_2O_3	Somatoidal+Cubes	4
720	390±90	30±17	α-Fe_2O_3	Cubes	4

5.3.2 Relationship between particle size and carbon number present in the linear alkyl chain of the solvent

The variation of the full width at half maxima (FWHM) of {101}, {300} and {211} diffractions (Figure 5.7) for particles synthesised shows a monotonic decrease of FWHM with increasing carbon number in the linear alkyl chain of the solvent, confirming an increase in particle sizes with the increase in carbon number.

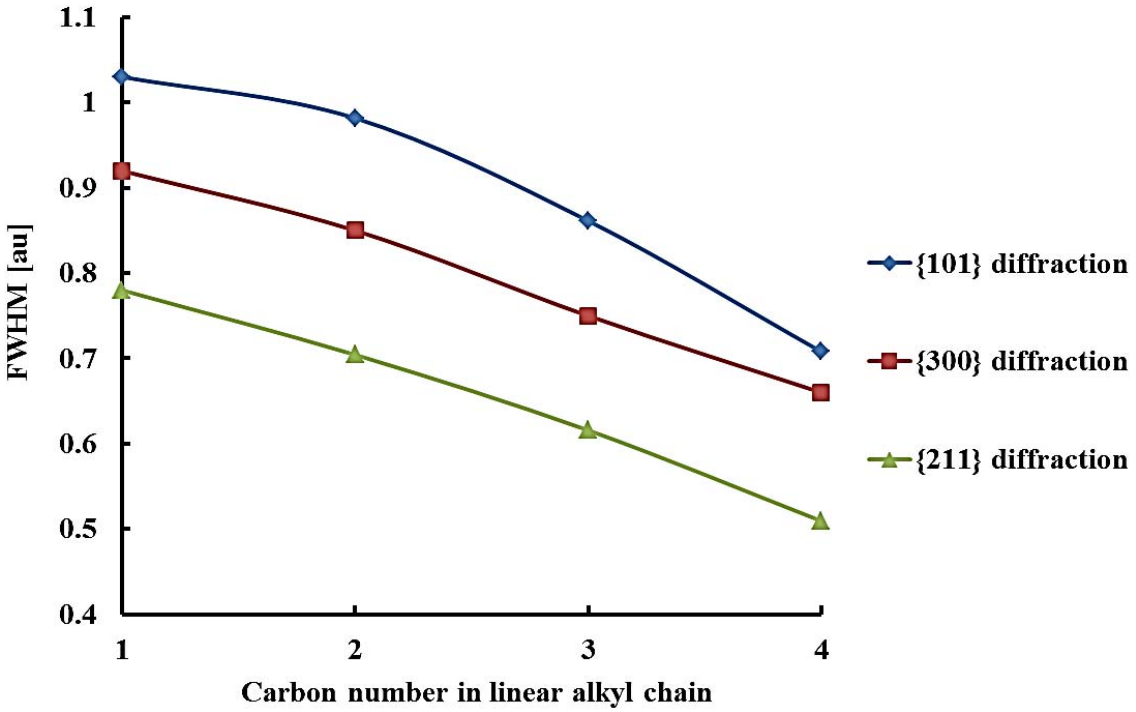

Figure 5.7Relationship between particle size and carbon number present in the linear alkyl chain of the solvent

5.3.3 Growth kinetic evaluation of akaganeite nanorods

5.3.3.1 Effect of BuOH and PrOH on the growth kinetics of akaganeite nanorods

Evidence for OA based growth comes both from interpretation of microstructure and the deviation of the growth kinetics from the OR model. OA growth does not follow Ostwald Ripening kinetics (Gilbert et al., 2003). Figure 5.8presents two stage hydrothermal coarsening of akaganeite nanorods in BuOH and PrOH. In both cases the stages start to occur around ~250 minutes. Two stage crystal growth for β-FeOOH particles has not been reported previously to the best of our knowledge.

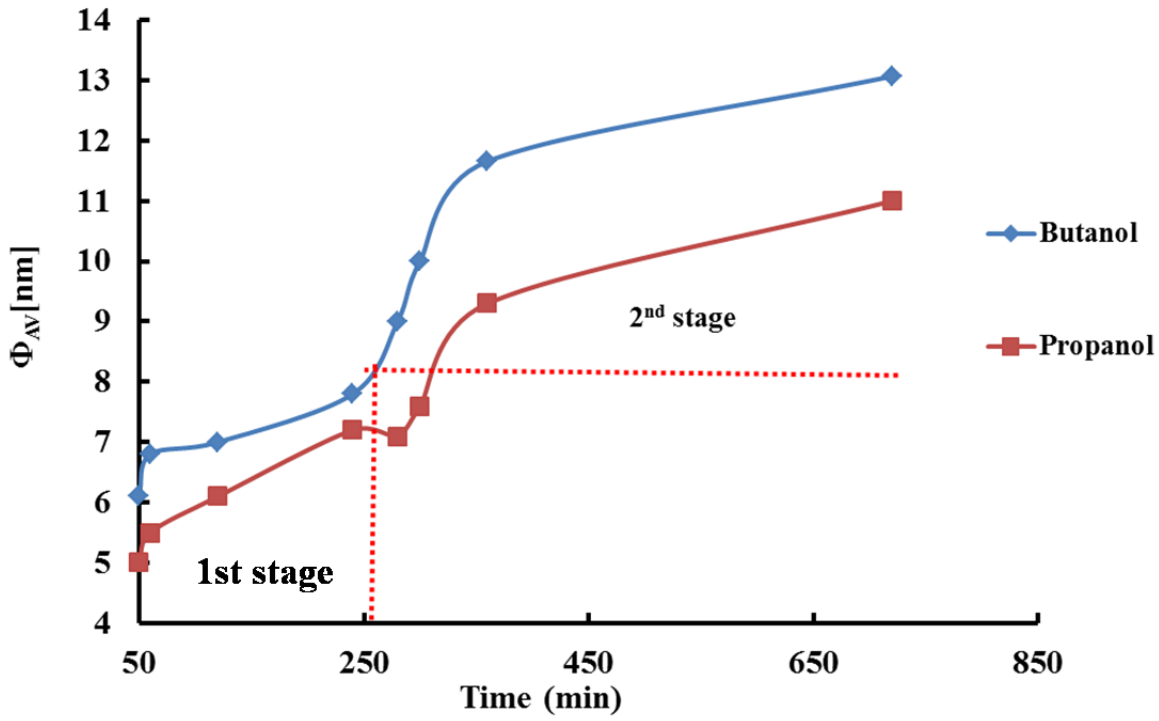

Figure 5.8 Two stage growth of β-FeOOH nanorods

Both OR kinetics and OA kinetics were evaluated in attempt to identify the controlling growth mechanism. A parabolic growth curve both in longitudinal and transversal direction represents the initial growth stage, followed by an asymptotic curve (Figure 5.9& 5.10). The existence of the OA mechanism can be seen throughout the time evolution study. However, the OR kinetic is dominant over the OA kinetic in the early growth stage. Simultaneous existence of OR and OA growth was reported by Huang et al. (2003) in the case of uncapped ZnS nanoparticles. Liang et al. (2012) also proposed a similar growth pathway in the synthesis of silver nanorice where the nanorice grows initially via OR kinetics, and then via OA kinetics.

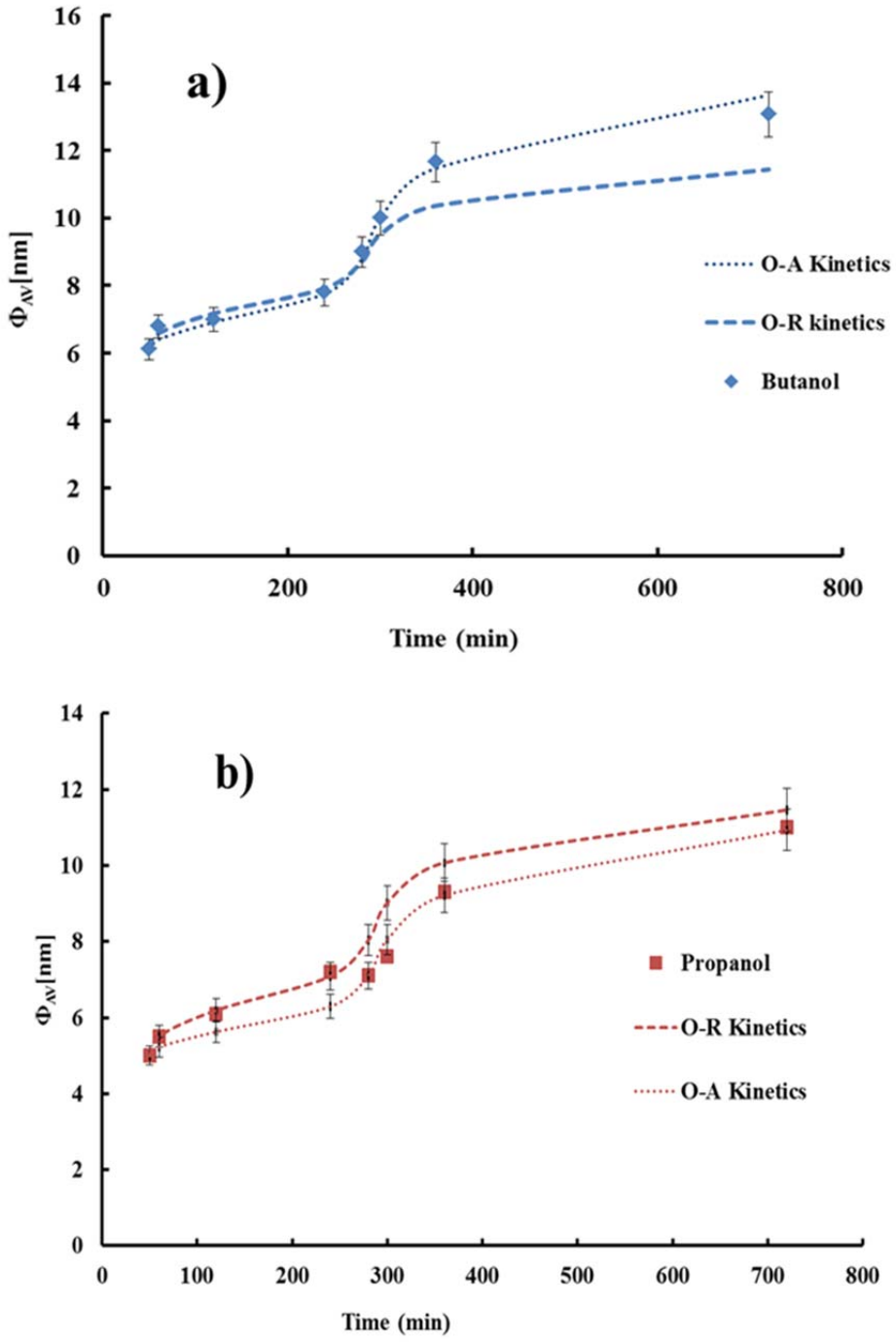

Figure 5.9 β-FeOOH growth kinetic (transversal growth), in a) BuOH and b) PrOH

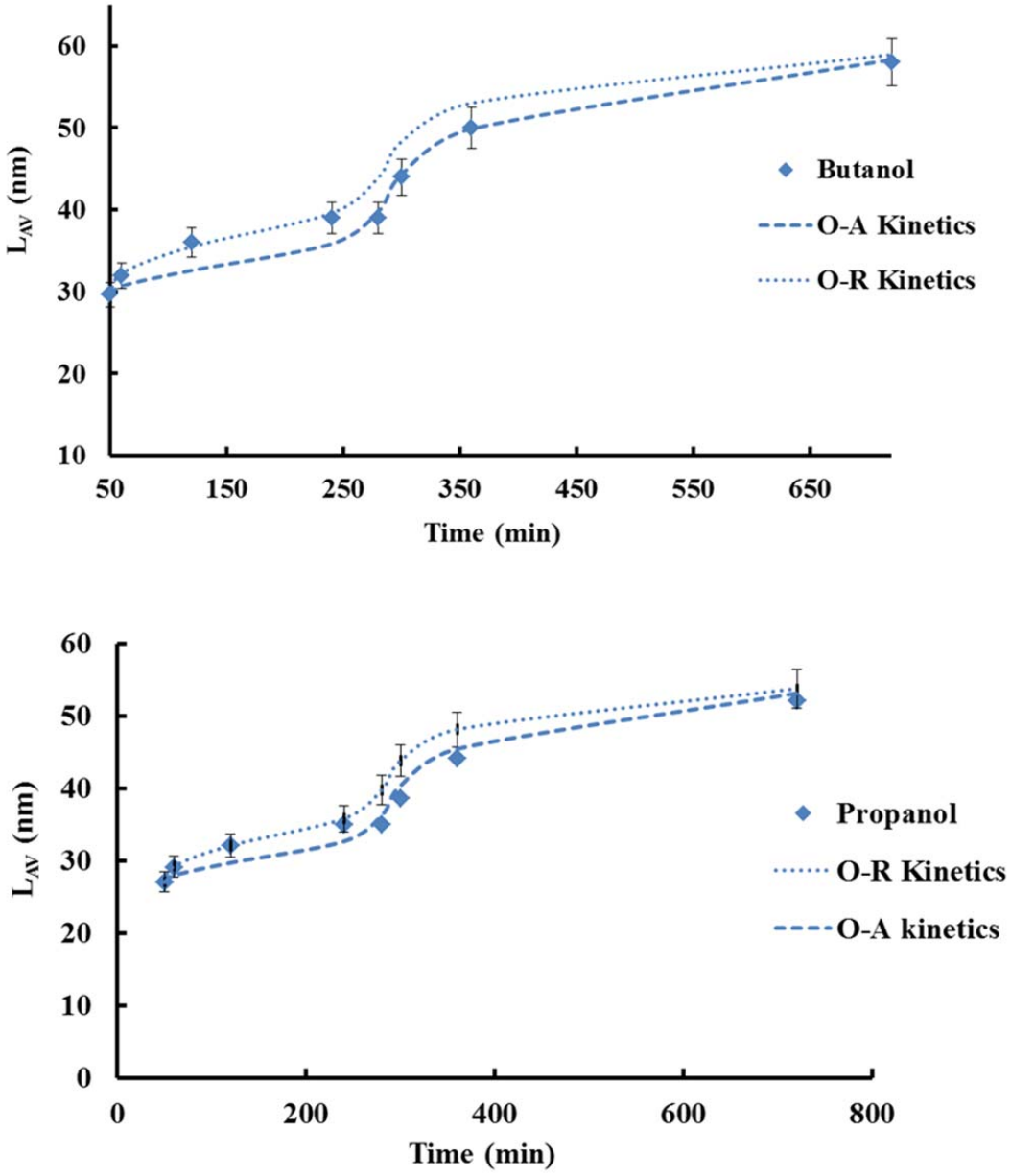

Figure 5.10 β-FeOOH growth kinetic (longitudinal growth), in a) BuOH and b) PrOH

Kinetic evaluation confirms the existence of OA growth, further validating the relationship between growth mechanism and particle size distribution curve as discussed earlier in this chapter.

The rate constants, K, for both OR and OA kinetic together with the exponent, n, for OR kinetic were obtained using multivariable regression and summarised in Table 5.6. The exponent, n for OR kinetics was found to be ~3 in all cases. A similar method was used by Kang and Yoon (1983). They concluded that this method gives accurate analysis. It was found that the rate constant for longitudinal growth is significantly higher than transversal growth for BuOH compared to PrOH as shown Table 5.6.

Table 5.6 Rate constants for both growth mechanisms

Solvent	**K_{OR} (min^{-1}) (Transversal direction)**	**K_{OR} (min^{-1}) (Longitudinal direction)**	**K_{OA} ($min^{-1/3}$) (Transversal direction)**	**K_{OA} ($min^{-1/3}$) (Longitudinal direction)**
BuOH	0.12	0.66	0.0036	0.0026
PrOH	0.10	0.47	0.0035	0.0024

5.3.3.2 Effect of EtOH and MeOH on the growth kinetics of β-FeOOH nanorods

No distinctive growth stages were observed in EtOH and MeOH contrary to the observation in both BuOH and PrOH. It can be seen from Figure 5.11 and 5.12 that both growth kinetics can be fitted to the data. The goodness of fit was found to be R^2>0.98 in all cases, postulating that both OR and OA kinetics occur simultaneously. However OR kinetics was dominant over OA kinetics. The exponent, n for OR kinetics was found to be ~3 for both cases implying precipitation/dissolution growth. The results are summarised in Table 5.7.

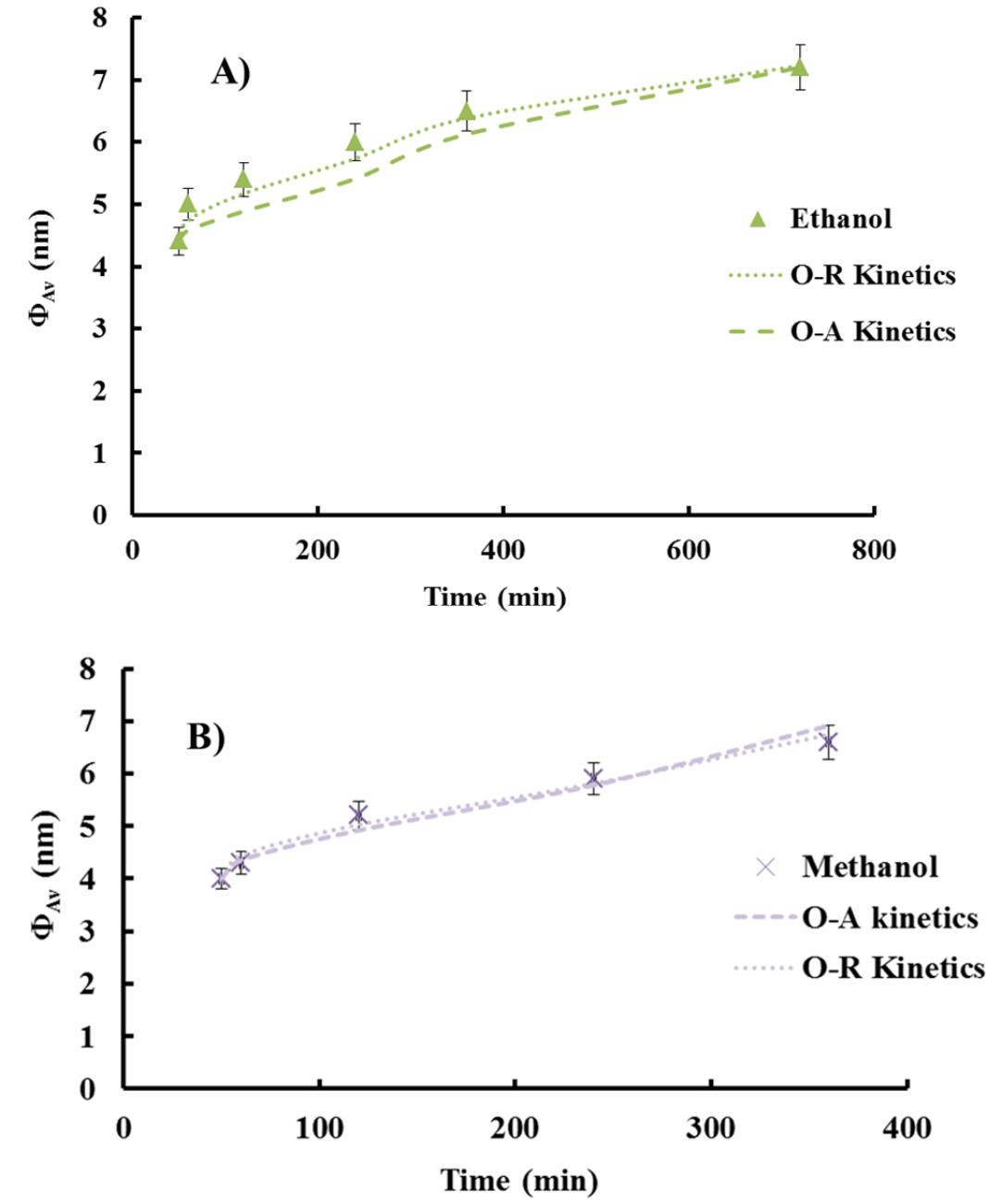

Figure 5.11 β-FeOOH growth kinetic (transversal growth), in a) EtOH and b) MeOH

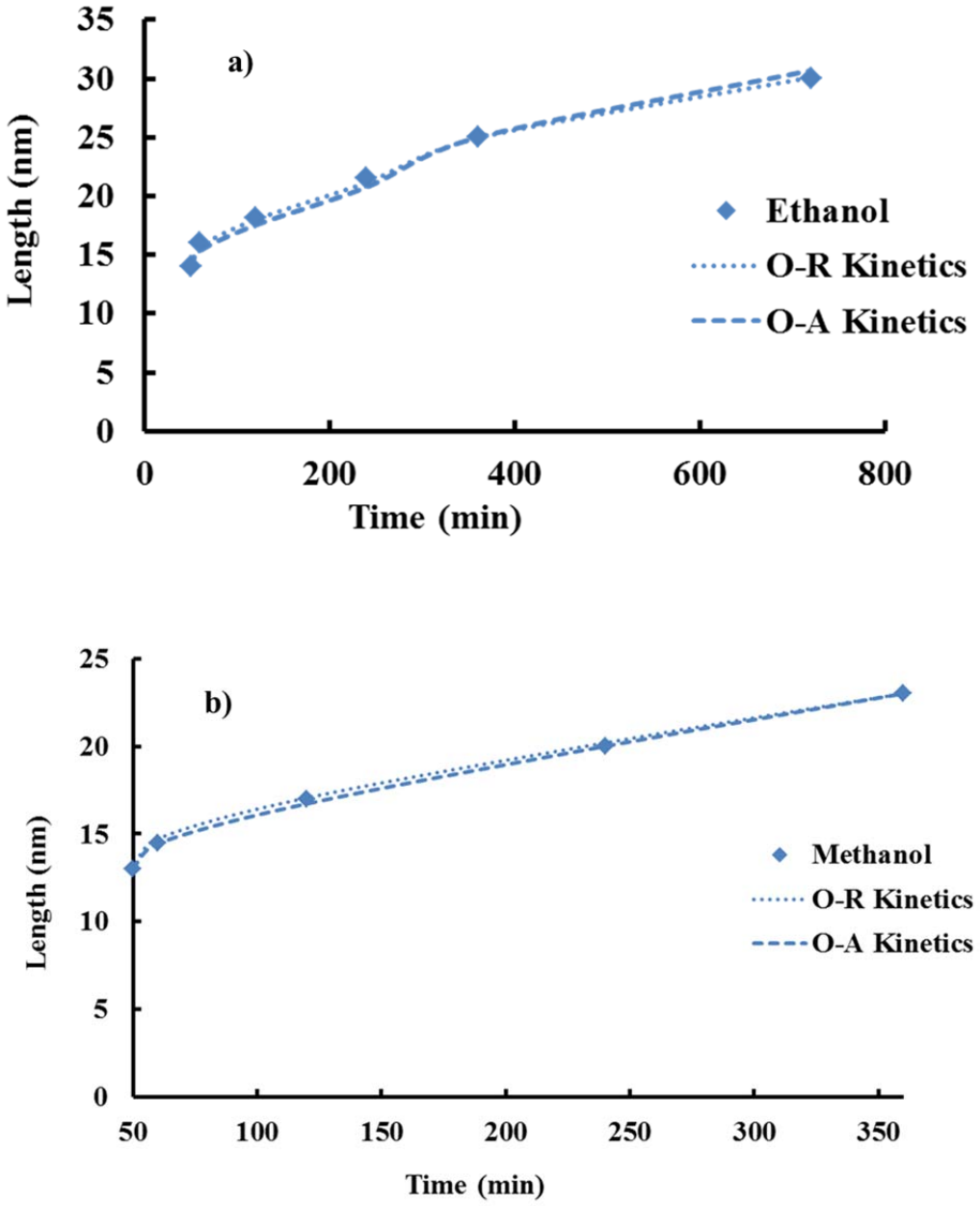

Figure 5.12 β-FeOOH growth kinetic (longitudinal growth), in a) EtOH and b) MeOH

Table 5.7 Rate constants for both growth mechanisms

Solvent	**K_{OR} (min^{-1})**	**K_{OR} (min^{-1})**	**K_{OA} ($min^{-1/3}$)**	**K_{OA} ($min^{-1/3}$)**
	(Transversal direction)	**(Longitudinal direction)**	**(Transversal direction)**	**(Longitudinal direction)**
EtOH	0.071	0.27	0.0032	0.013
MeOH	0.080	0.30	0.0033	0.010

5.3.4 Relationship between solvent surface tension and growth rate constants

The hydrothermal reactor can be considered as a closed system. If any changes occur in the total property of the system inside the reactor, this will be the result of the changes of that property in the liquid phase plus the changes of the property in the gas phase. Figure 5.13 presents a schematic representation of liquid and vapour phase inside a typical closed vessel.

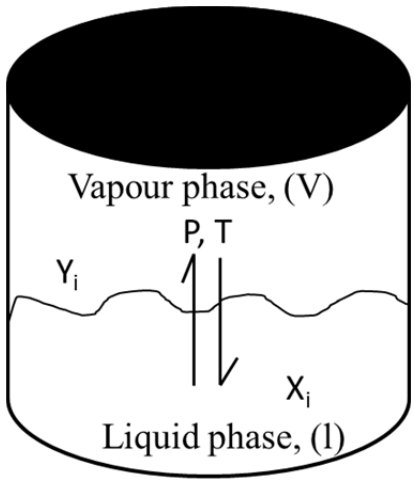

Figure 5.13 Vapour liquid equilibrium

In a closed system the vapour and liquid themselves are open systems as there is constant mass transfer occurring between liquid and vapour. However, to establish vapour-liquid equilibrium inside the closed system the system must be under constant temperature and pressure. This criterion creates a problem when one wants to

evaluate the actual liquid ratio of each component present in the mixture inside the reactor at a specific temperature and time. This is due to the fluctuation of pressure inside the vessel. The physical properties of four different alcohols and water are presented in Table 5.8. Vapour pressure values presented were calculated using Antoine equation.

Table 5.8 Physical properties of alcohol and water at 100˚C

Compound	**Boiling point**	**Pressure at 100˚C**
MeOH	64.70 ˚C	258.00 kPa
EtOH	78.37 ˚C	225.90 kPa
PrOH	97.00 ˚C	110.46
BuOH	118.00 ˚C	52.30 kPa

Butanol has a higher boiling point than water, implying the presence of a higher concentration of butanol in liquid phase (at 100˚C) compared to vapour phase inside the reactor at any given time. For MeOH – H_2O, EtOH – H_2O and PrOH – H_2O mixture systems H_2O is the less volatile component. If a MeOH – H_2O system is considered, the following occurred inside the reactor:

- As the temperature was raised to 64.7˚C, MeOH started to boil, slowly increasing the vapour pressure inside the reactor. At this point the concentration of MeOH in liquid phase starts to drop.
- The temperature rises quickly to 100˚C and at an intermediate temperature the concentration of water in the vapour phase would also start to increase, further increasing the vapour pressure to ~377kPa.
- At 377 kPa methanol vapour starts to condensate, hence increasing the concentration of methanol in liquid phase. Typical pressure profile and the schematics of thermodynamic behaviour of the methanol water system inside the reactor is presented in Figure 5.14 and 5.15 respectively.

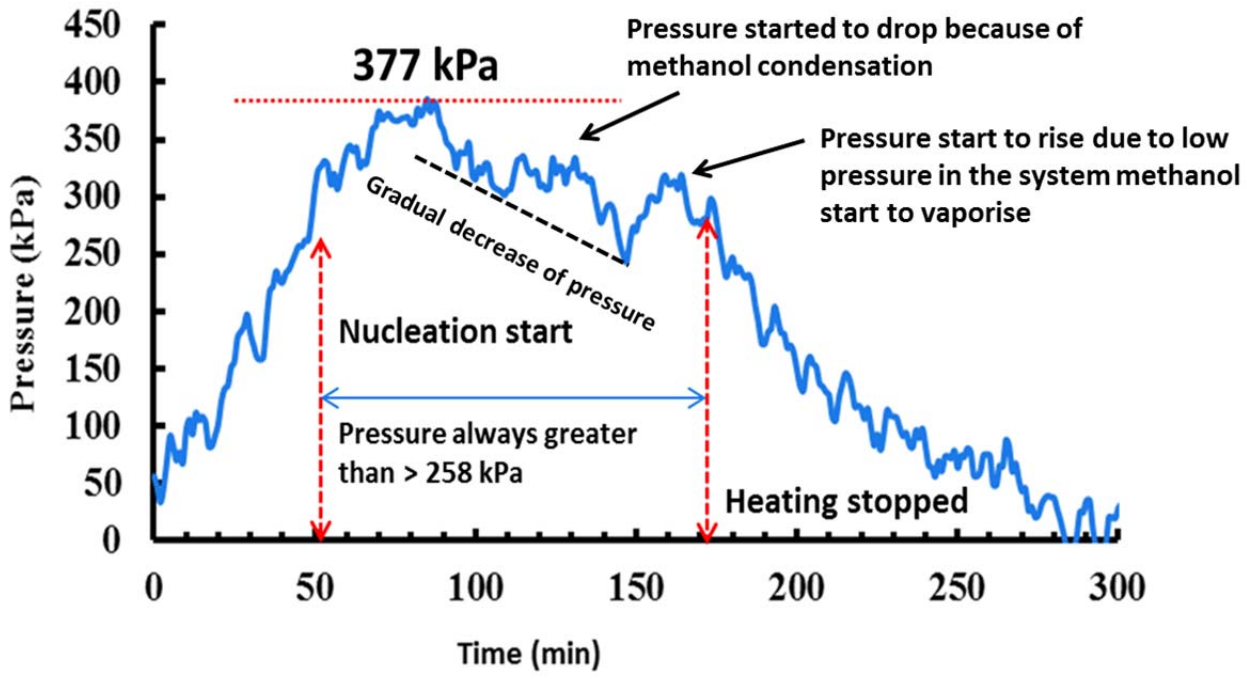

Figure 5.14 Pressure profile of MeOH + H_2O system inside the reactor at 100˚C

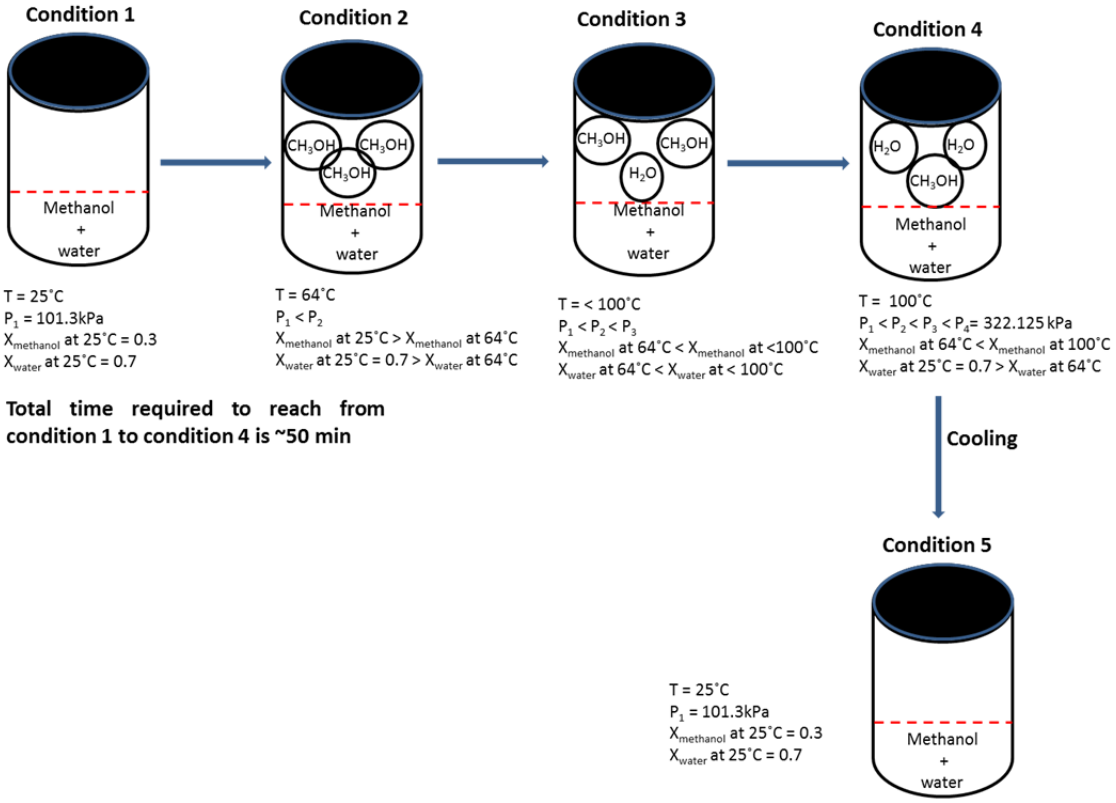

Figure 5.15 Schematic of assumed thermodynamic behaviour at 100˚C for MeOH + H_2O system

Similar observation was found for EtOH+ H_2O and PrOH + H_2Osystems. So, it was assumed that during the synthesis time, the concentration of alcohol in the liquid phase will be larger than that of water at any given time under the reported conditions.

Alcohol itself does not take part in the formation of β-FeOOH particle, water does. It is well known that OH^- ions from alcohol can form a bridge between two Fe^{3+} ions in acidic solutions containing $Fe^{3+}$and slows down the hydrolysis process (Shao et al., 2005). This phenomenon makes the surface tension of pure alcohol more important than water. Surface tension values of pure alcohol (at 25˚C) were used to evaluate the growth kinetic data in an attempt to relate the particle growth directly with surface tension. Table 5.9 presents the solvent surface tension and growth rate constants.

Table 5.9 Surface tension values of alcohol

Solvent	**σ (mnm^{-1}) (100% alcohol at 25˚C)**	**σ (mnm^{-1}) (50% alcohol water at 50˚C)**
Methanol	22.75	30.28
Ethanol	22.27	25.78
Propanol	23.70	22.30
Butanol	24.70	20.00

The relationship between solvent surface tension and growth rate constants are exponential and independent of the direction of growth, as can be seen from Figure 5.16, approving of the initial hypothesis. The validity of the relationship was checked further by conducting an independent study under identical conditions using octanol as solvent and presented in Figure 5.17.It can be seen from Figure 5.17 that the data generated by independent study follows the similar trend as reported in this work, thus further highlighting the validity of the relationship between surface tension and particle growth. Only K_{OR} was used to evaluate the relationship between surface tension and particle growth due to the higher significance of K_{OR} than K_{OA}.

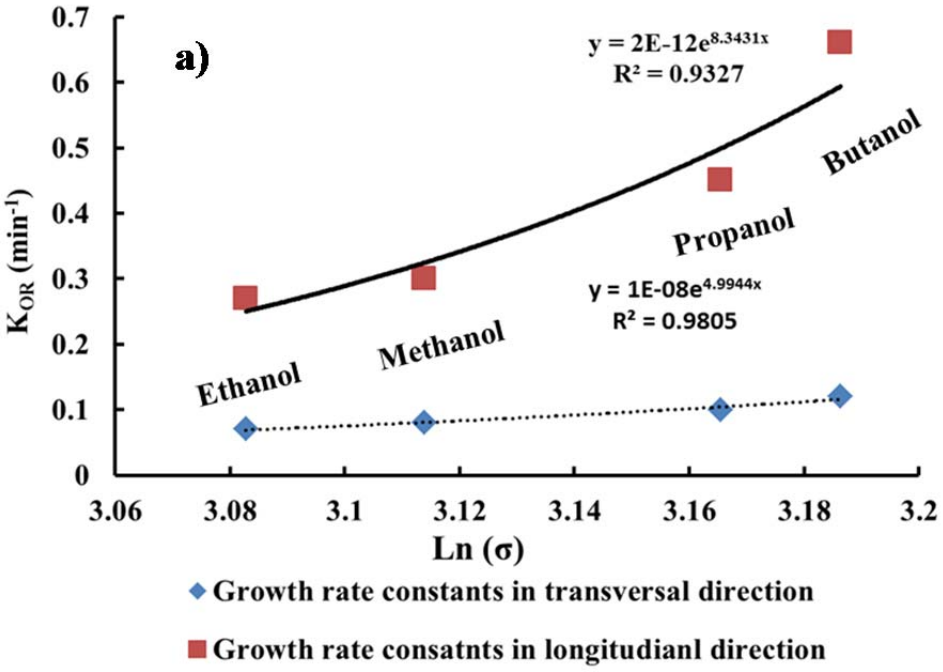

Figure 5.16 Relationship between surface tension and growth rate constants

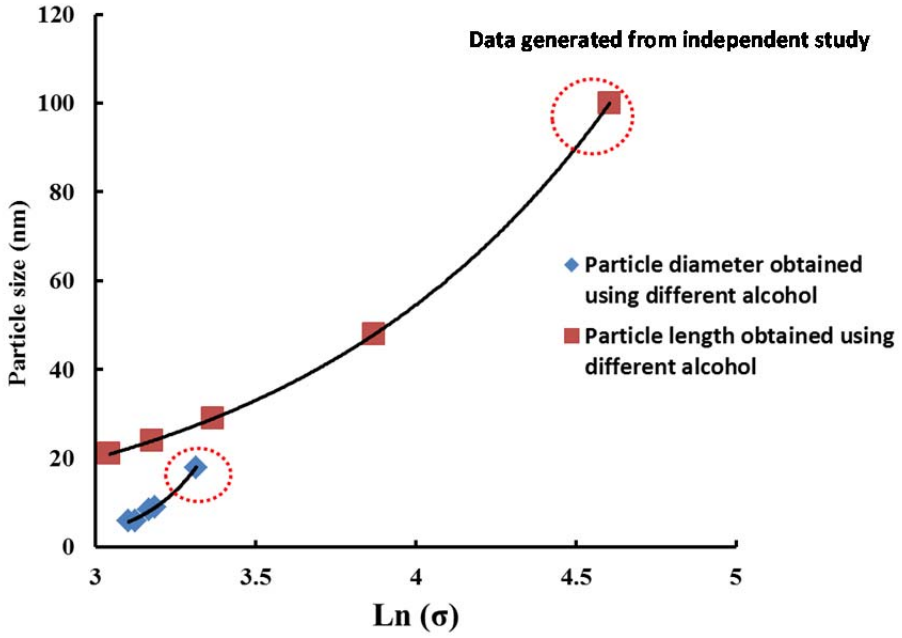

Figure 5.17 Relationship between particle size and surface tension

5.5 Conclusion

Solvent dependent growth kinetics of β-FeOOH nanorods was reported. Shape of the particle size distribution curve was evaluated to identify the growth mechanism of the particles. Two stage growth curve was reported for the first time for β-FeOOH particles. A quantitative relationship between growth rate constants and alcohol solvent surface tension was established and later validated. Although the relationship between the alcohol surface tension and rate constants was established at room temperature a clear dependence is demonstrated in this work.

Chapter 6

Prediction of hydrothermally synthesised solvent-dependent β-FeOOH nanorod sizes

6.1 Introduction

A wide range of hydrothermal synthesis process parameters were evaluated to determine the boundaries for β-FeOOH precipitation in order to develop a generalized correlation for nanorod size prediction.

6.2 Experimental methodology

The effect of alcoholic solvents, as a function of (a) $FeCl_3$ concentration, (b) nature of anion in the iron precursor and (c) reaction temperature, on the particle morphology is reported in this section. The process parameters are summarised in Table 6.1.

Table 6.1 HS processing variables

Sample	Solvent	Solvent (ROH / H_2O) ratio (% v/v)	$[Fe^{3+}]$ [M]	Anion	Temperature (°C)
S1	BuOH	50	0.05	Cl^-	100
S2			0.1		
S3			0.2		
S4			0.3		
S5			0.5		
S6			0.7		
S7	PrOH	50	0.05	Cl^-	100
S8			0.1		
S9			0.2		
S10			0.3		
S11			0.5		
S12			0.7		
S13	EtOH	50	0.05	Cl^-	100
S14			0.1		
S15			0.2		
S16			0.3		
S17			0.5		
S18			0.7		
S19	MeOH	50	0.05	Cl^-	100
S20			0.1		
S21			0.2		
S22			0.3		
S23			0.5		
S24			0.7		
S25	BuOH	50	0.05	Cl^-	90
S26					100
S27					120
S28					135
S29					150
S30	PrOH	50	0.05	Cl^-	90
S31					100
S32					120
S33					135
S34					150
S35	EtOH	50	0.05	Cl^-	90
S36					100
S37					120
S38					135
S39					150
S40	MeOH	50	0.05	Cl^-	90
S41					100
S42					120
S43					135
S44					150
S45	BuOH	50	0.05	NO^{3-}	100
S46	PrOH				
S47	EtOH				
S48	MeOH				
S49	BuOH	50	0.05	SO_4^{2-}	100
S50	PrOH				
S51	EtOH				
S52	MeOH				

6.3 Results and discussion

6.3.1 Effect of $FeCl_3$ concentration

6.3.1.1 Structural evolution of particles

Pure crystalline β-FeOOH particles were synthesised regardless of the nature of solvent used over an $FeCl_3$ concentration range of 0.05 — 0.7M as shown in Figure 6.1.

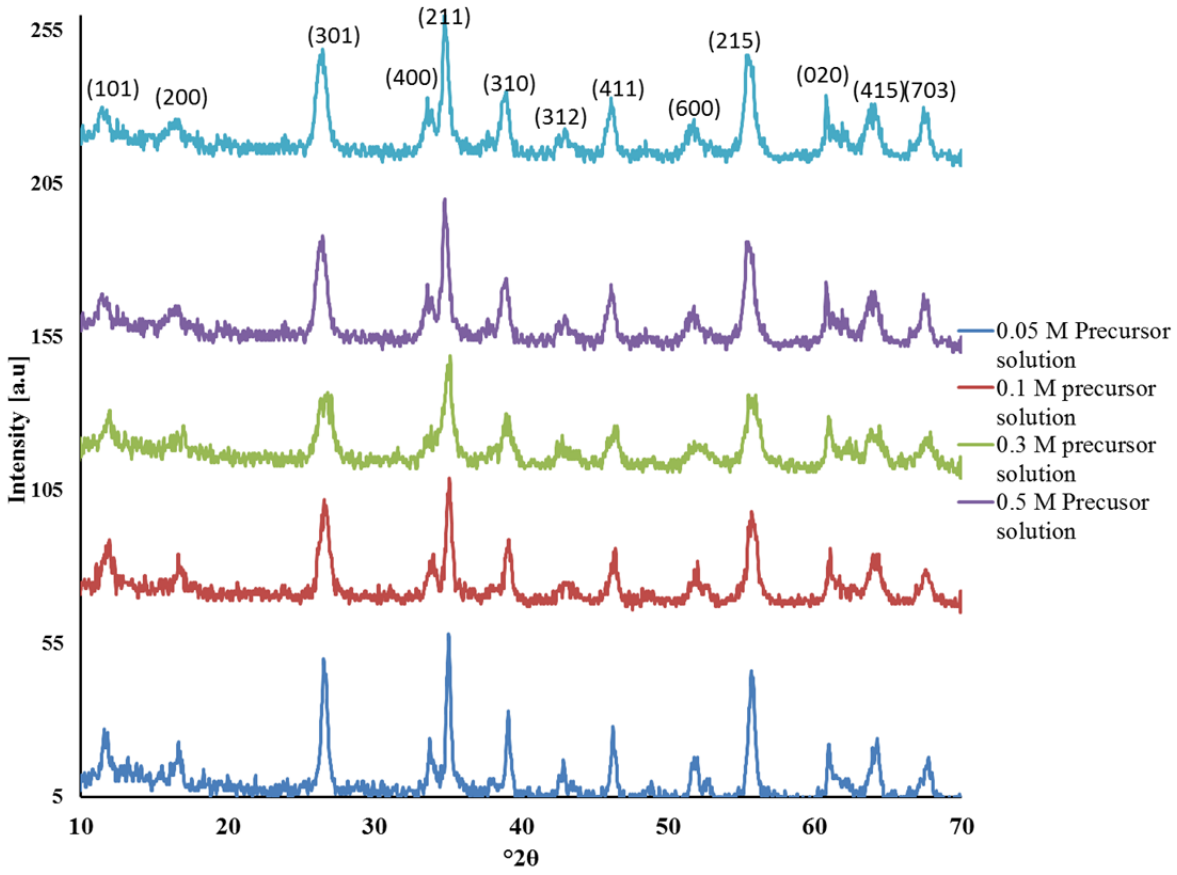

Figure 6.1 XRD patterns of the particles synthesised

6.3.1.2 Morphological evolution of particles in BuOH

Variation of $FeCl_3$ concentrations in BuOH has a marked effect on the morphology of akaganeite particles as shown in Figure 6.2.

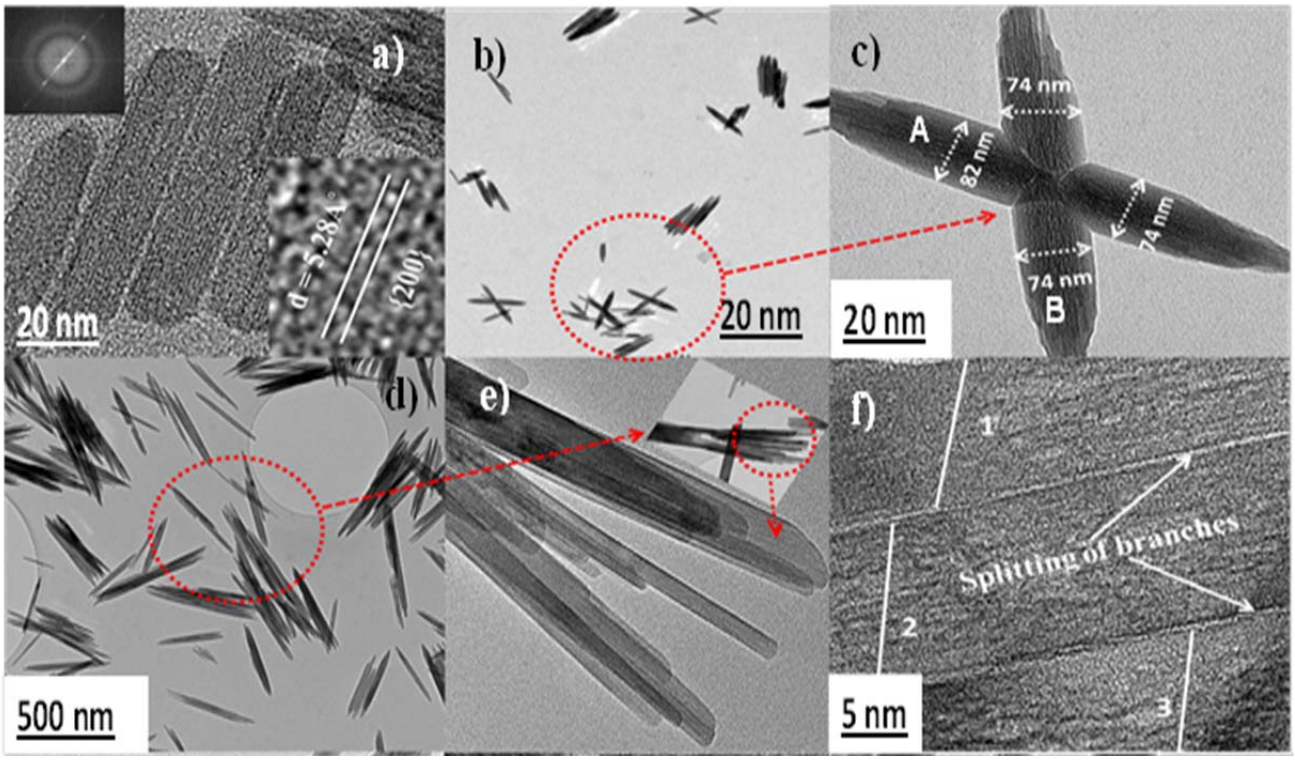

Figure 6.2 Dependence of morphological evolution as a function of $FeCl_3$ concentration: a) nanorods in 0.1M, b) cross shaped + spindle in 0.5M C) magnified image of the cross structure, d) splitting in 0.7M, e) magnified image of a branched crystal and f) schematic of splitting

Well-aligned rod-shaped β-FeOOH particles with smooth ends were obtained over a concentration range of 0.05-0.2M (Figure 6.2a). Spindle and cross shaped particles were observed over a concentration range of 0.30-0.5M (Figure 6.2b). The attachment of Spindle 'A' and 'B" (Figure 6.2 C) occurs through self-assembly and the ends of the cross structures were coarse, reflecting possibility of particles to grow in one-dimensional orientation. Chen et al. (2008) reported synthesis of β-FeOOH cross structures using urea under a synthesis temperature 95°C and time of 8h. Similar structures were obtained in 2h, highlighting the role of solvent in reducing synthesis time. Branched β-FeOOH (Figure 6.2 e) obtained in 0.7M contrary to the observation in 0.5M. A number of filamentary single crystals were split from a solid rod as can be seen from Figure 6.2 f. Manna, et al. (2003) exploited polyptism between hexagonal and cubic structures to create branch points in semiconducting nanocrystal. Changes in the relative growth rates of two facets of nanocrystals are responsible

for splitting (Tang & Alivisatos, 2006). Controlling precursor solution in BuOH resulted in artificial crystal splitting in β-FeOOH particles, which has not been reported before to our best knowledge. Split β-FeOOH might find applications where a larger surface area is required, owing to the fact that each filament possesses a different surface area. This makes the total surface area per single crystal very large compared to a solid single crystal only. Splitting is only possible if the oversaturation exceeds a certain 'critical' level (Tang & Alivisatos, 2006). 0.7M was found to be the critical limit in this study. Tang and Alivisatos (2006) reported that the splitting of crystal is favoured in situations where the organic surfactant is a very potent surface stabiliser and where at equilibrium the balance of bulk and surface energies dictates a particular crystal size. At lower temperature, when few nuclei form, fast growth can lead to a situation of metastability, where crystals grow beyond this size. It is then thermodynamically favourable for a large crystal to split, because of the strong adhesion of the surfactant to the newly created surface. Surface adsorption was shown as an important factor in controlling crystal growth stages (Huang et al., 2003). However, no surfactant was used in this study. So it can be postulated that the morphological evolution were merely due to the presence of butanol. A summary of the findings are presented in Table 6.2.

Table 6.2 Effect $FeCl_3$ concentrations on β-FeOOH particle characteristics in BuOH

$FeCl_3$ Conc. (M)	**Φ_{AV}(nm)**	**L_{AV} (nm)**	**Phase**	**Morphology**	**Average aspect ratio**
0.05	9 ± 1	42 ± 5	β-FeOOH	Rods	5
0.01	10 ± 1	50 ± 7	β-FeOOH	Rods	5
0.2	14 ± 2	68 ± 10	β-FeOOH	Rods	5
0.3	22 ± 4	194 ± 11	β-FeOOH	Spindle	9
*0.5	40 ± 1	406 ± 13	β-FeOOH	Coarse spindle + cross structure	10
*0.7	93 ± 90	780 ± 17	β-FeOOH	Branched spindle+cross structure	8

*Φ_{AV} and L_{AV} presented are for spindle shaped particles only

6.3.1.3 Morphological evolution of β-FeOOH particles in PrOH

The effect of $FeCl_3$ concentration in propanol is illustrated in Figure 6.3.

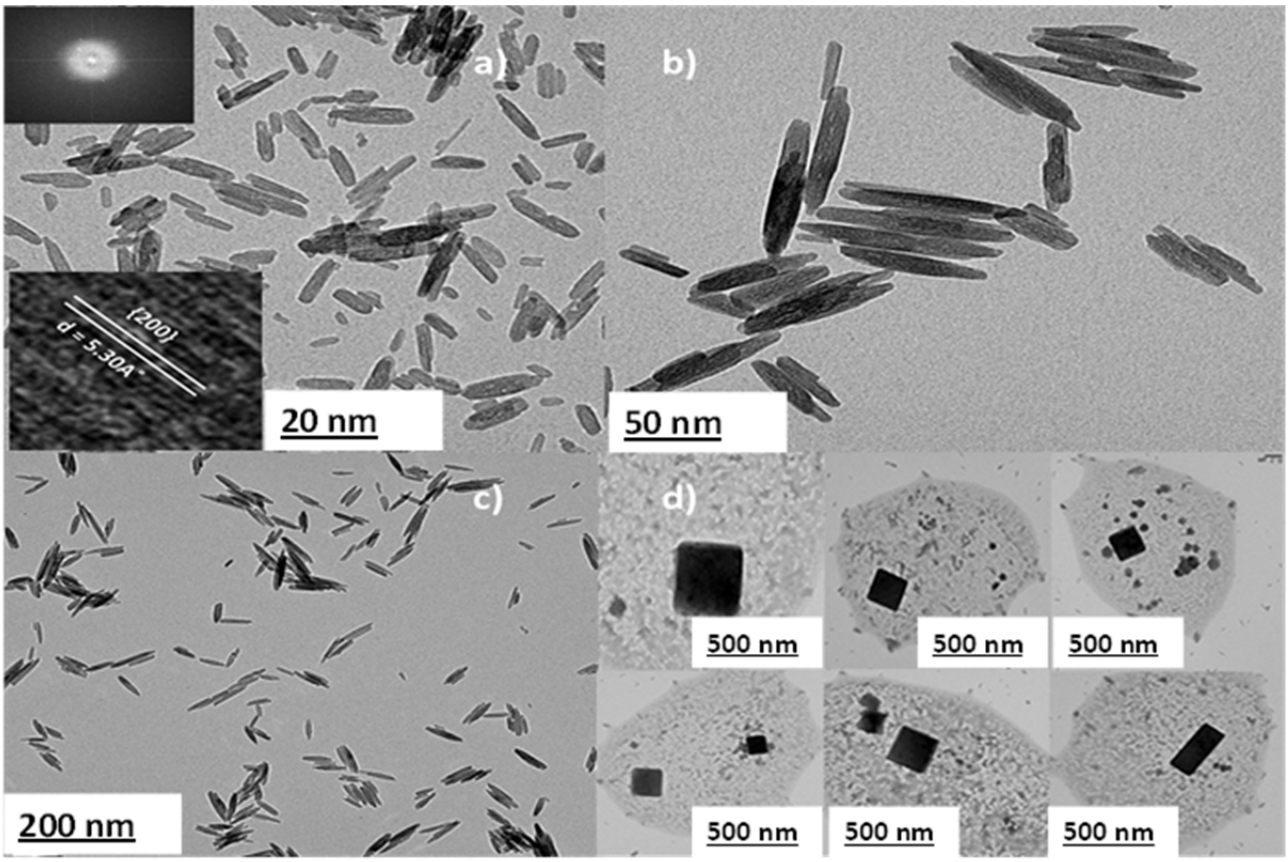

Figure 6.3 Dependence of morphological evolution as s function of $FeCl_3$ concentration: a) nanorods in 0.1M, b) spindle in 0.5M, C) no sign of splitting in 0.7M, d) rectangular particles in 0.7M.

Rod-like particles (Figure 6.3 a) were obtained at concentration ranging from 0.1 – 0.3M,which evolved into a mixture of spindle (Figure 6.3 b), somatoidal (Figure 6.3 c)and rectangular particles (Figure 6.3 d) at high concentrations. To our best knowledge, no studies have previously reported on the observation of rectangular β-FeOOH. A summary of the findings are presented in Table 6.3.

Table 6.3 Effect $FeCl_3$ concentrations on β-FeOOH particle characteristics in PrOH

[$FeCl_3$] Conc. (M)	**Φ_{AV}(nm)**	**L_{AV} (nm)**	**Phase**	**Morphology**	**Average aspect ratio**
0.05	9±1	29±5	β-FeOOH	Rods	3
0.01	10±2	35±7	β-FeOOH	Rods	4
0.2	12±2	50±11	β-FeOOH	Rods	4
0.3	15±3	74±12	β-FeOOH	Spindle+somatoidal	5
*0.5	30±5	121±13	β-FeOOH	Spindle+somatoidal	6
*0.7	65±9	350±17	β-FeOOH	Spindle+somatoidal+rectangular	5

*Φ_{AV} and L_{AV} presented are for spindle shaped particles only

6.3.1.4 Morphological evolution of β-FeOOH particles in EtoH and MeOH

The morphologies obtained as a function of $FeCl_3$ concentrations in EtOH and MeOH are shown in Figure 6.4.

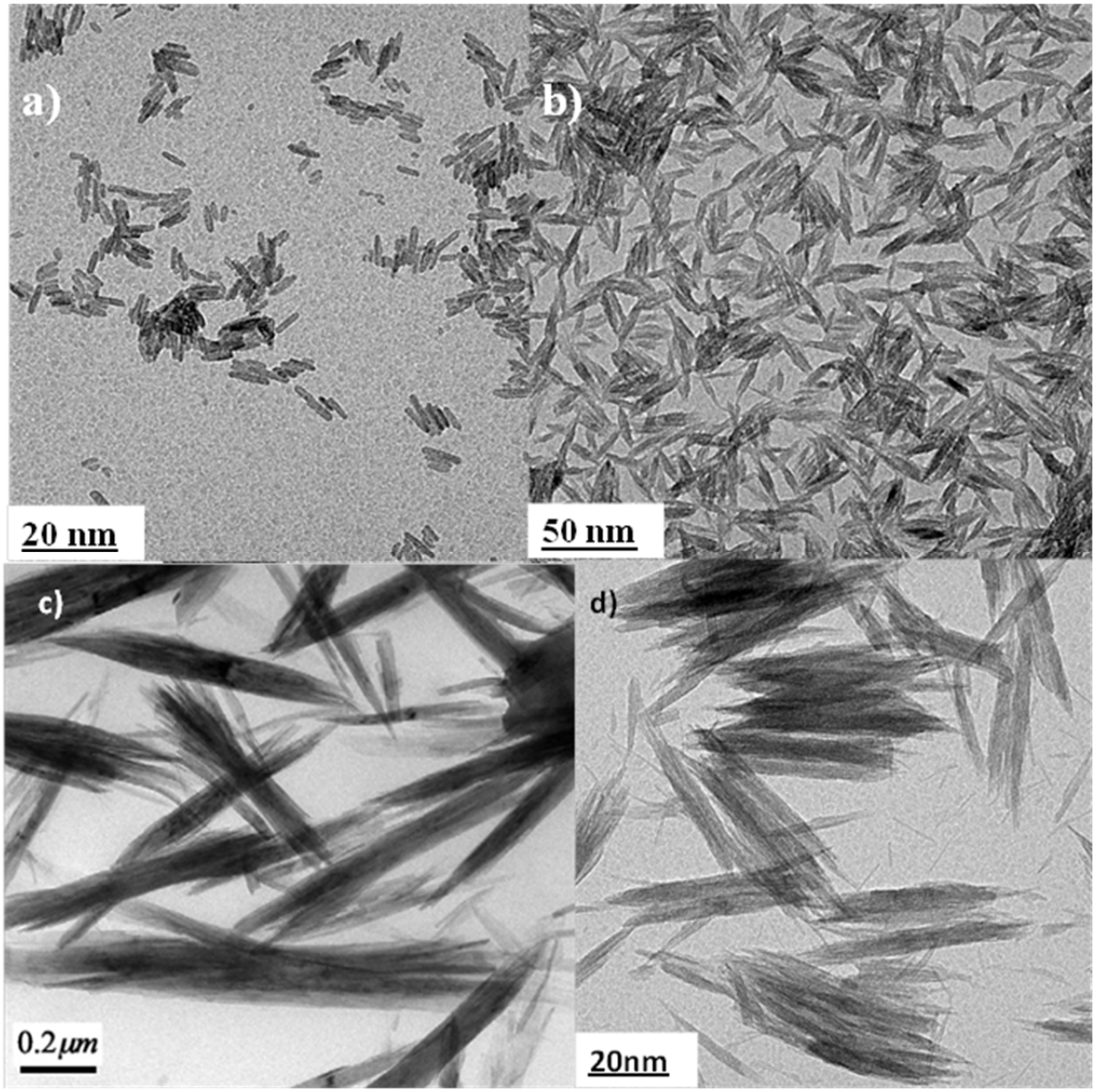

Figure 6.4a) β-FeOOH rod particles over the range 0.05-0.5M in EtOH, b) ellipsoidal particles over the range of 0.05-0.3M in MeOH, c) β-FeOOH nanoribbons synthesised by Wei and Nan (2011), d) β-FeOOH nanoribbon at 0.7M in MeOH

Rod particles (Figure 6.4a) were obtained over the concentration range of 0.05 – 0.5M and particles with no definite structures were formed at 0.7M in ethanol. Ellipsoidal / spindle shaped particles were synthesised over the range of 0.05 – 0.5M,which evolved into β-FeOOH nanoribbons (Figure 6.4 d) at 0.7M in methanol. Surfactant-assisted synthesis of β-FeOOH nanoribbons (Figure 6.4 c) was reported in the literature (Wei & Nan, 2011).Surfactant free synthesis of β-FeOOH nanoribbons have not been reported before to our best knowledge. However, the formation mechanism needs to be further evaluated. A summary of the findings are presented in Table 6.4 and 6.5.

Table 6.4 Effect $FeCl_3$ concentrations on β-FeOOH particle characteristics in EtOH

[$FeCl_3$] Conc. (M)	**ϕ_{AV}nm)**	**Length$_{AV}$ (nm)**	**Phase**	**Morphology**	**Average aspect ratio**
0.05	6 ± 2	24 ± 8	β-FeOOH	Rods	4
0.01	7 ± 2	29 ± 8	β-FeOOH	Rods	4
0.2	8 ± 2	35 ± 11	β-FeOOH	Rods	4
0.3	10 ±2	52 ± 18	β-FeOOH	Rods	5
0.5	13 ± 2	75 ± 12	β-FeOOH	Rods	3
0.7	-	-	β-FeOOH	-	-

Table 6.5 Effect $FeCl_3$ concentrations on β-FeOOH particle characteristics in MeOH

[$FeCl_3$] Conc. (M)	**Φ_{Av}(nm)**	**$Length_{AV}$(nm)**	**Phase**	**Morphology**	**Average aspect ratio**
0.05	6 ± 1	21 ± 8	β-FeOOH	Ellipsoidal / spindle	4
0.01	6 ± 2	23 ± 8	β-FeOOH	Ellipsoidal / spindle	4
0.2	7 ± 2	35 ± 11	β-FeOOH	Ellipsoidal / spindle	5
0.3	9 ± 3	42 ± 18	β-FeOOH	Ellipsoidal / spindle	5
0.5	12 ± 4	50 ± 12	β-FeOOH	Ellipsoidal / spindle	4
0.7	-	-	β-FeOOH	Nanoribbon	-

6.3.2 Effect of anions on the particle characteristics

Dependency of particle morphology and phase as a function of anions is presented in Figure 6.5.

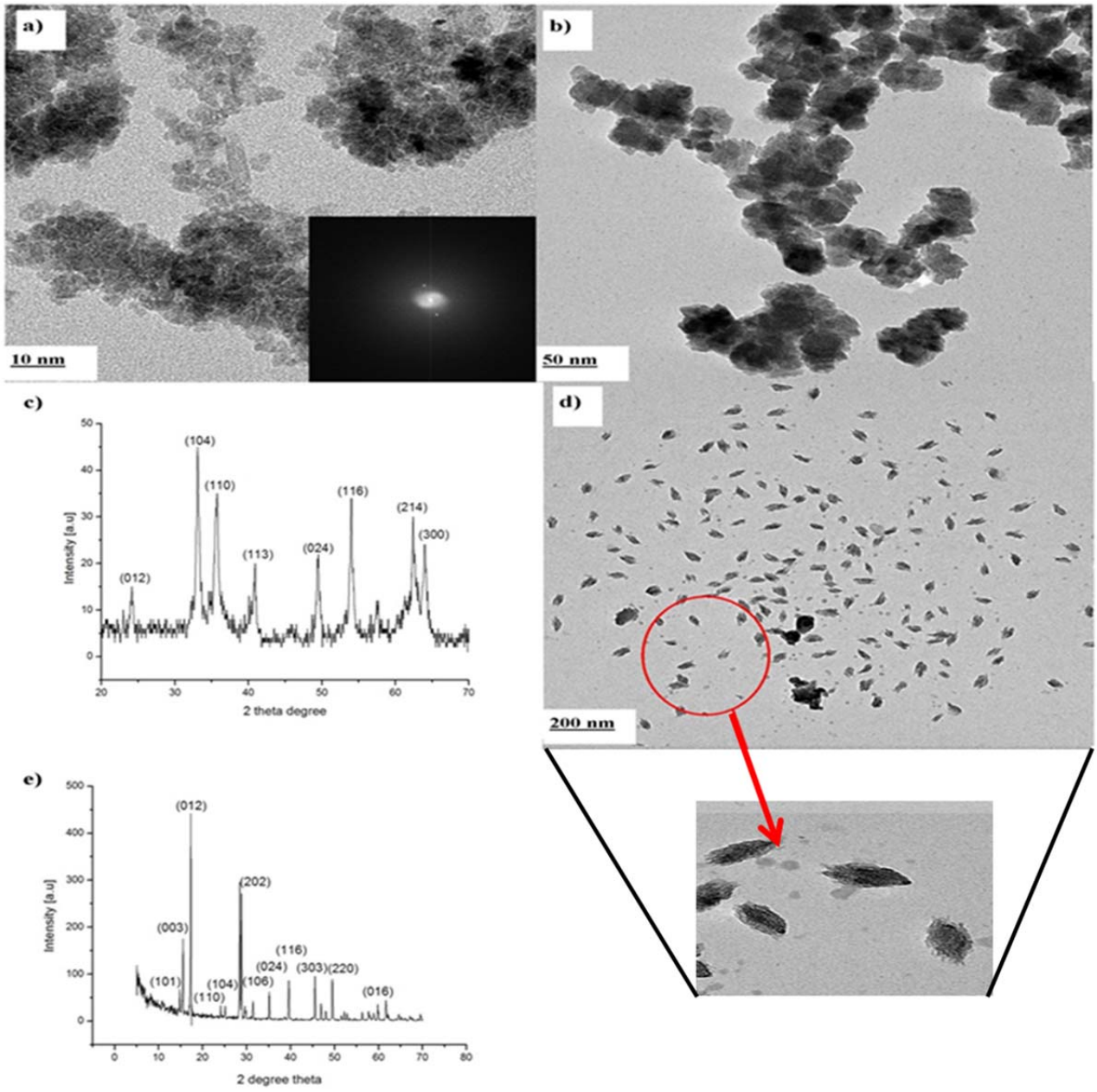

Figure 6.5 Structural evolution of particles as a function of anions, a & b) irregular shaped hematite using NO^{3-} in butanol and methanol, b) XRD of particles synthesised using NO_3^- anions, d) irregular shaped hydronium iron jarosite using SO_4^{2-} and e) XRD for hydronium iron jarosite

Irregularly shaped aggregated particles, independent of the nature of the solvent used, were produced when $Fe(NO_3)_3$ was used as a precursor salt (Figure 6.5 a & b).The XRD pattern (Figure 6.5 c) of the synthesised sample matches the standard diffraction patterns of α-Fe_2O_3 (JCPDS card no. 33-0664) in contradiction to the finding by Yue et al., 2011. They reported formation of spherical α-FeOOH particles (JCPDS card no: 81 - 0464) under atmospheric pressure.

Replacing the NO_3^- with SO_4^{2-}anions resulted in dispersed particles with no defined structure (Figure 6.5d). The XRD patterns (Figure 6.5 e) could be assigned to the rhombohedral single phase of hydronium iron jarosite, $H_3O.Fe_3(SO_4)_2(OH)_6$, (JCPDS card no. (021 – 0932) with lattice constants of a = b = 7.3559A˚, c = 17.0100 A˚ , α = β = 90^o and γ = 120˚. The colour of the powder is golden yellow, which is the typical colour of hydronium jarosite. High intensity peaks in the XRD patterns indicate that the synthesised hydronium iron jarosite is well crystalline. HS of hydronium iron jarosite reported by Earle et al. (1999) used 3days compared to 2h reported in this study. It is reported that hydronium iron jarosite forms in an acidic medium (pH ~2). The only modification done in the synthesis was dropwise addition of NH_4OH to keep the precursor solution at pH ~2 prior to heating, resulted in a 98% reduction of synthesis time.

Figure 6.6 shows particles (due to phase change) obtained when $FeCl_3$, $Fe(NO_3)_3$ and $Fe_2(SO_4)_3$ were used respectively. Single phase hydronium iron jarosite could not be synthesised without the presence of alcohol.

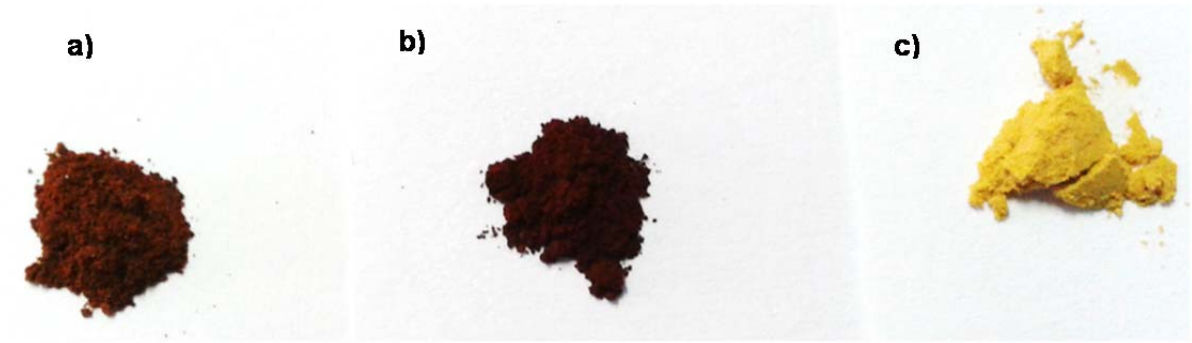

Figure 6.6 Colour of different iron oxides produced using different iron anions, in a) β-FeOOH particles from Cl^-, b) α-Fe_2O_3 from NO^{3-} and C) $H_3O.Fe_3(SO_4)_2(OH)_6$ from SO_4^{2-}

6.3.3 Effect of reaction temperature on the particle characteristics

6.3.3.1 Transformation of β-FeOOH to α-Fe_2O_3 in BuOH and PrOH

Temperature has a significant effect on the formation and transformation of β-FeOOH particles as shown in Figure 6.7.

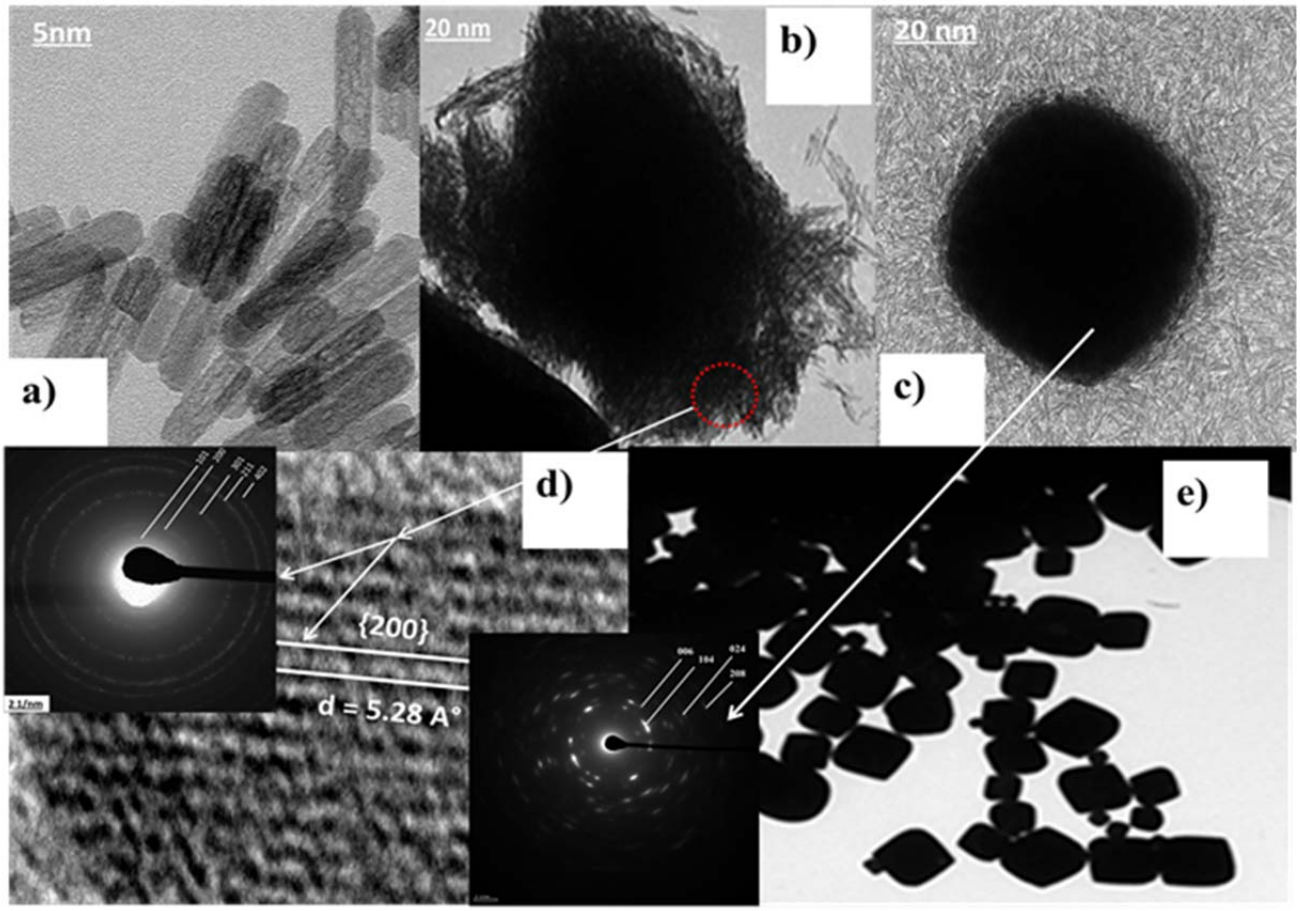

Figure 6.7 Reaction products obtained at different temperatures: a) β-FeOOH nanorods at 100°C, b) self-assembly of nanorods at 135°C, c) formation of α-Fe_2O_3 and pseudo cube at 135°C, d) d-spacing and SAED patterns of the nanorods at 135°C and e) α-Fe_2O_3 pseudo cubes and rhombohedral particles at 150°C.

Well crystalline β-FeOOH nanorods were synthesised in a temperature range of 90 – 120°C (Figure 6.7 a). The average crystal diameters and lengths increases with increasing temperature. Figures 6.7 (b – e) chart the transformation from an intermediate phase of β-FeOOH to a well-defined phase of α-Fe_2O_3. At 135°C there is enough surface energy available for the nanorods to initiate fusing, resulting in the self-assembly of the β-FeOOH nanorods. The d-spacing and the SAED patterns of the nanorods and pseudo cubes observed at 135°C are presented in Figure 6.7d, which matches well with the standard akaganeite and α-Fe_2O_3 patterns. Both β-FeOOH and α-Fe_2O_3 peaks were observed in the XRD pattern as presented in Figure 6.8,

complimenting the observations in TEM. Quantification of the two phases (Figure 6.9) shows that 60% of the peaks in the XRD pattern represent α-Fe_2O_3 and the rest is β-FeOOH. Pure α-Fe_2O_3 particles were obtained at 150˚C. The results are summarised in Table 6.6.

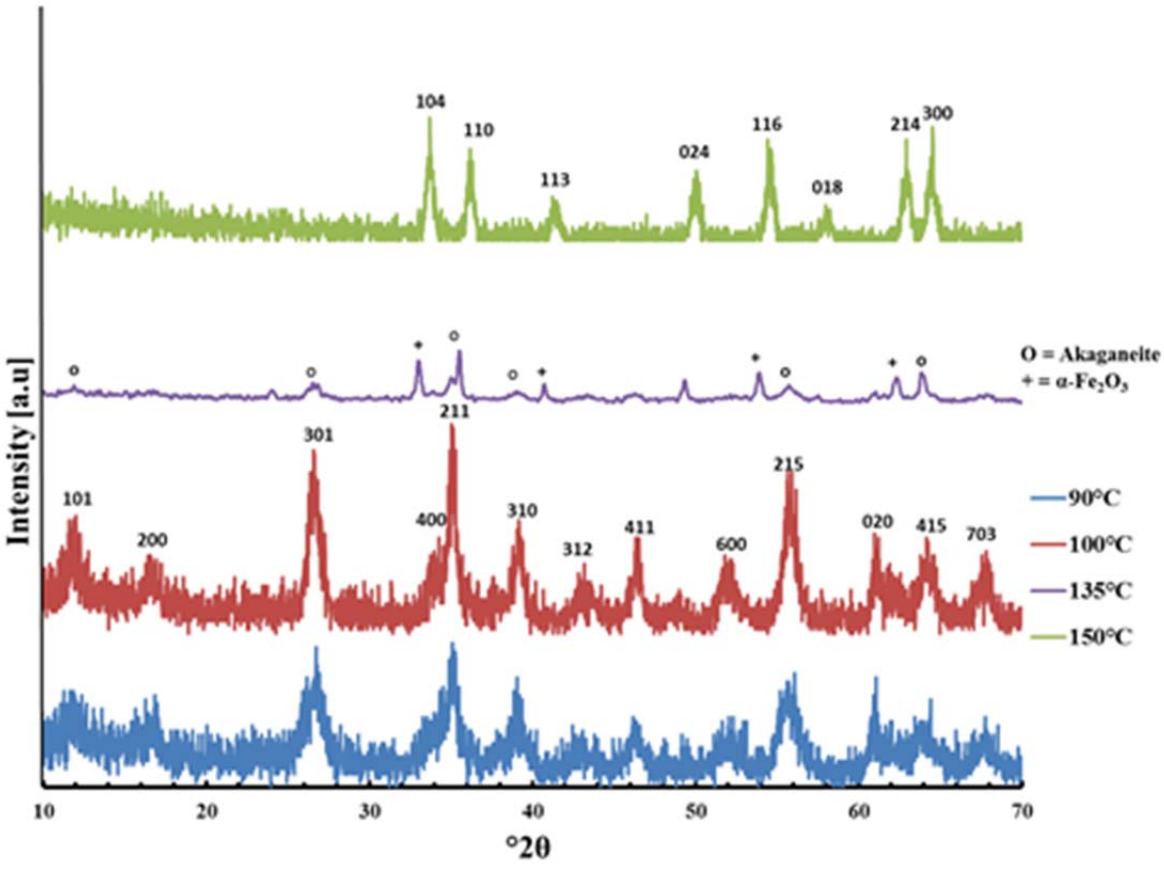

Figure 6.8 XRD patterns of the particles

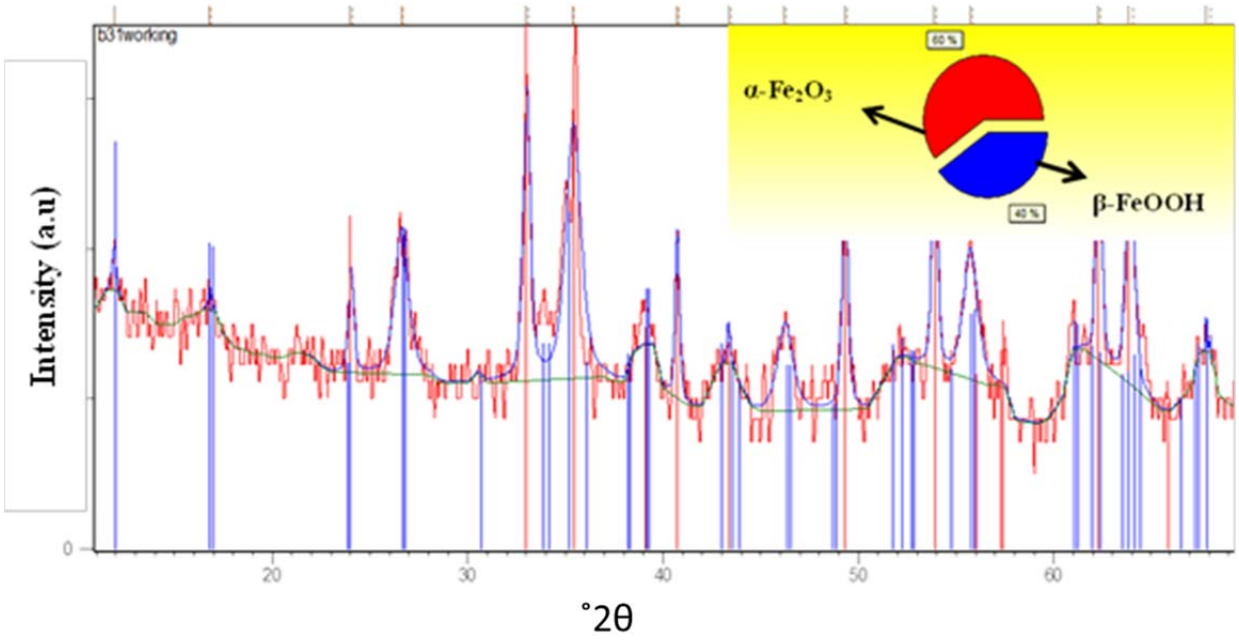

Figure 6.9 Phase quantification of the particles at 135°C

Table 6.6 Effect of temperature on the particle characteristics

Solvent	Temperature	Φ_{AV}(nm)	L_{AV} (nm)	Phase	Morphology	Average aspect ratio
BuOH	90	5 ±3	25 ± 5	β-FeOOH	Rods	5
	100	9 ± 5	38± 8	β-FeOOH	Rods	4
	120	12± 5	53 ± 8	β-FeOOH	Rods	4
	135	10± 8	71 ± 10	β-FeOOH	Rods + pseudo cube	7
	150	1200 ± 70	-	α-Fe_2O_3	Pseudo cube	-
PrOH	90	4 ± 3	19 ± 3	β-FeOOH	Rods	5
	100	7 ±5	29 ± 5	β-FeOOH	Rods	4
	120	10 ± 5	46 ± 6	β-FeOOH	Rods	5
	135	8±6	58 ± 10	β-FeOOH	Rods + pseudo cube	7
	150	1168±90	-	α-Fe_2O_3	Pseudo cube	-

6.3.3.2 Transformation of β-FeOOH to α-Fe_2O_3 in EtOH and MeOH

Structural evolution of particles as a function of temperature in EtOH and MeOH is illustrated in Figure 6.10.

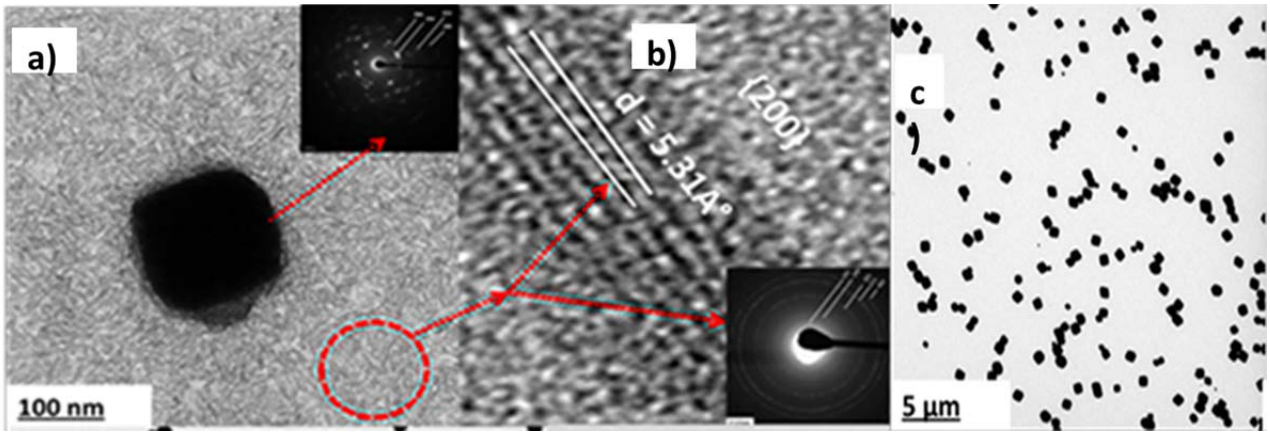

Figure 6.10 Morphological evolution of particles as a function of temperature, in a) self-assembly of the β-FeOOH at 120°C in ethanol, b) d-spacing and SAED of nanorods at 120°C, c) pseudo cubes at 135˚C

Pure β-FeOOH rod shaped particles could not be obtained at temperature higher than 100°C in EtOH and MeOH contrary to particles synthesised in BuOH and PrOH. Fusing of nanoparticles (Figure 6.10 a) followed by subsequent transformation of β-FeOOH to α-Fe_2O_3 starts at 120˚C in EtOH oppose to 135˚C in BuOH and PrOH. The β-FeOOH rods present at this temperature are well crystalline as can be seen from the d-spacing and SAED of the nanorods. Figure 6.11 presents phase quantification of the particles, indicating that at 120˚C 41% of β-FeOOH has already been converted to α-Fe_2O_3. All the akaganeite particles were converted to large α-Fe_2O_3 particles at 150°C. A 100% conversion of β-FeOOH to α-$Fe_2O_3$was obtained at temperatures higher than 100˚C in MeOH. A summary of the findings are presented in Table 6.7.

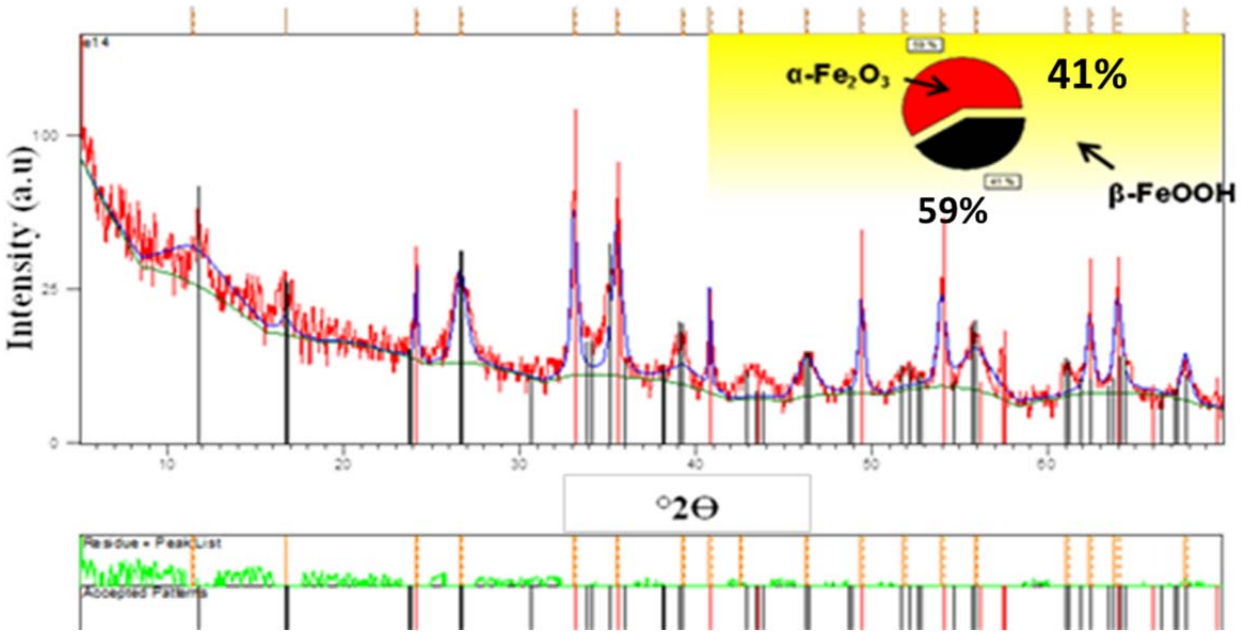

Figure 6.11 Phase quantification of the particles synthesised in EtOH at 135°C

Table 6.7 Effect of temperature on the particle characteristics

Solvent	Temperature	ϕ_{AV}(nm)	L_{AV} (nm)	Phase	Morphology	Average aspect ratio
Ethanol	90	3 ± 1	17 ± 3	β-FeOOH	Rods	6
	100	5 ± 2	22 ± 5	β-FeOOH	Rods	4
	120	7± 2	30 ± 7	β-FeOOH+ α-Fe_2O_3	Rods	4
	135	6± 3	36 ± 8	β-FeOOH+ α-Fe_2O_3	Rods + pseudo cube	6
	150	1100 ±56	-	α-Fe_2O_3	Pseudo cube/ rhombohedral	-
Methanol	90	3 ± 2	15 ± 3	β-FeOOH	Rods	5
	100	3.4 ± 2	18 ± 3	β-FeOOH	Rods	5
	120	349 ± 3	-	α-Fe_2O_3	Pseudo cubes	5
	135	384 ± 3	-	α-Fe_2O_3	pseudo cube	7
	150	322 ± 90	-	α-Fe_2O_3	Pseudo cube/ rhombohedral	-

6.3.4 Role of alcohol on the dehydration properties of β-FeOOH particles

Thermal stability of β-FeOOH particles were evaluated using TGA (Figure 6.12 a), performed up to 300°C. β-FeOOH particles, lose 12%, 14%, 15% and 18% of mass at 300˚C, synthesised in BuOH, PrOH, EtOH and MeOH respectively. The % mass loss, as shown in Figure 6.12 b, is linearly dependent on the number of carbon present in the linear alkyl chain of the solvent. Verdon et al. (1995) have reported that EtOH enhanced the dehydration properties of the CeO_2 nanocrystallite. The improvement of dehydration of akaganeite nanoparticles with increasing carbon number is related azeotrope formation. MeOH – H_2O does not form any azeotrope, however EtOH - H_2O, PrOH - H_2O and BuOH - H_2O form azeotrope, increasing the dehydration properties of the synthesised akaganeite nanoparticles. However, the underlying mechanism has to be further evaluated.

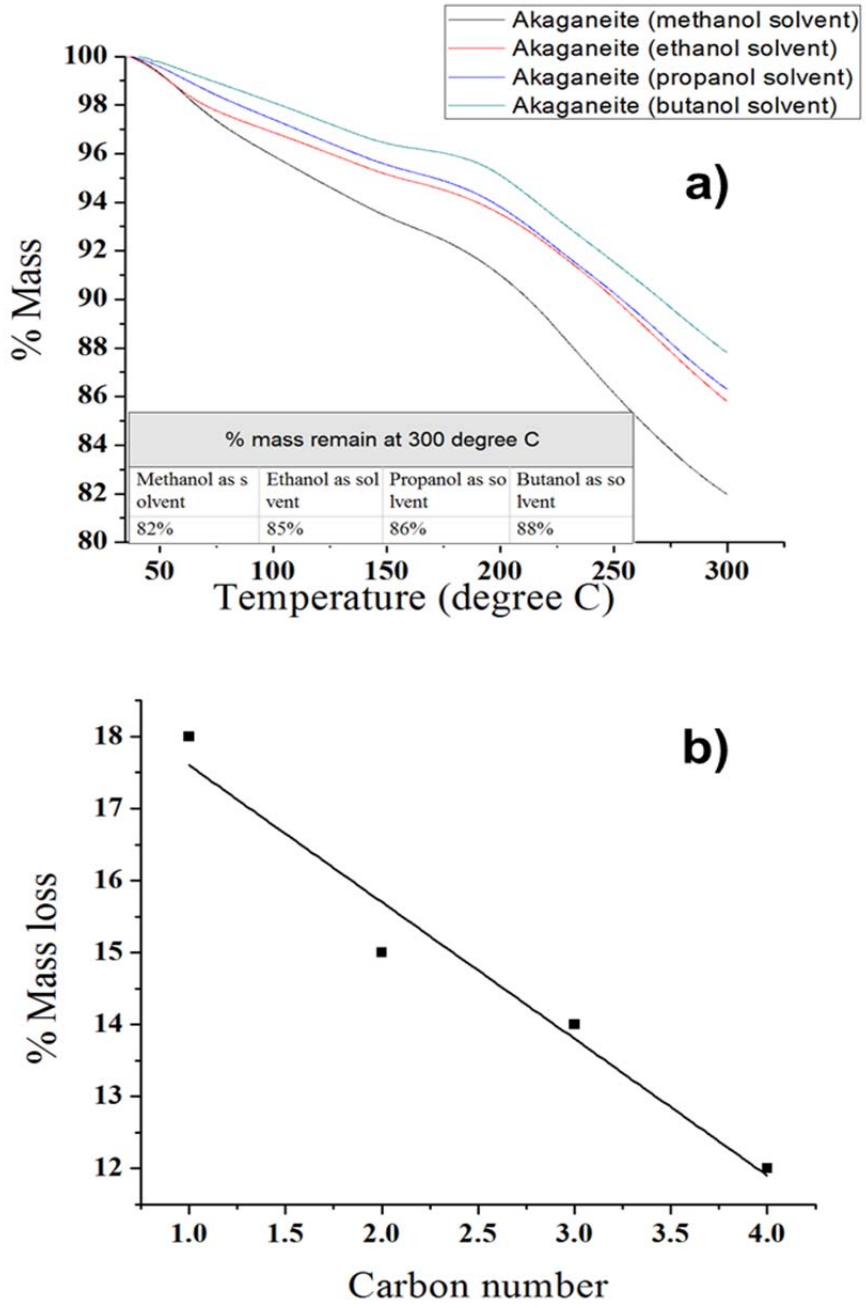

Figure 6.12 a) Thermogravimetric analysis of the synthesised nanorods and b) relationship between % mass loss and carbon number in the linear alkyl chain of the solvents

6.3.5 Magnetic properties of the β-FeOOH nanorods

The magnetic properties of the β-FeOOH nanorods were measured in lightly compressed powders using an Oxford Instruments Vibrating Sample Magnetometer (VSM) from 4 to 290 K and with a sensitivity of 50 μemu.As prepared β-FeOOH nanorods do not show ferromagnetism at any temperature down to 4 K but they have a high positive linear susceptibility of about $1.3x10^{-3}$ constant up to 5 T, giving a magnetic moment per unit mass of about 1 – 1.5 Am^2/kg at 5 T (Figure 6.13). The zero field cooled curve measured (inset Figure 6.13) at 100 mT does not show a blocking temperature, which is different from previous measurements in long akaganeite amorphous nanowires (Zhang et al., 2006). This high susceptibility and the absence of a ferromagnetic phase at low temperatures are probably due to the small size of the particles and the presence of anti-ferromagnetic interactions. However solvent nature had no effect on the magnetic properties of the β-FeOOH particles.

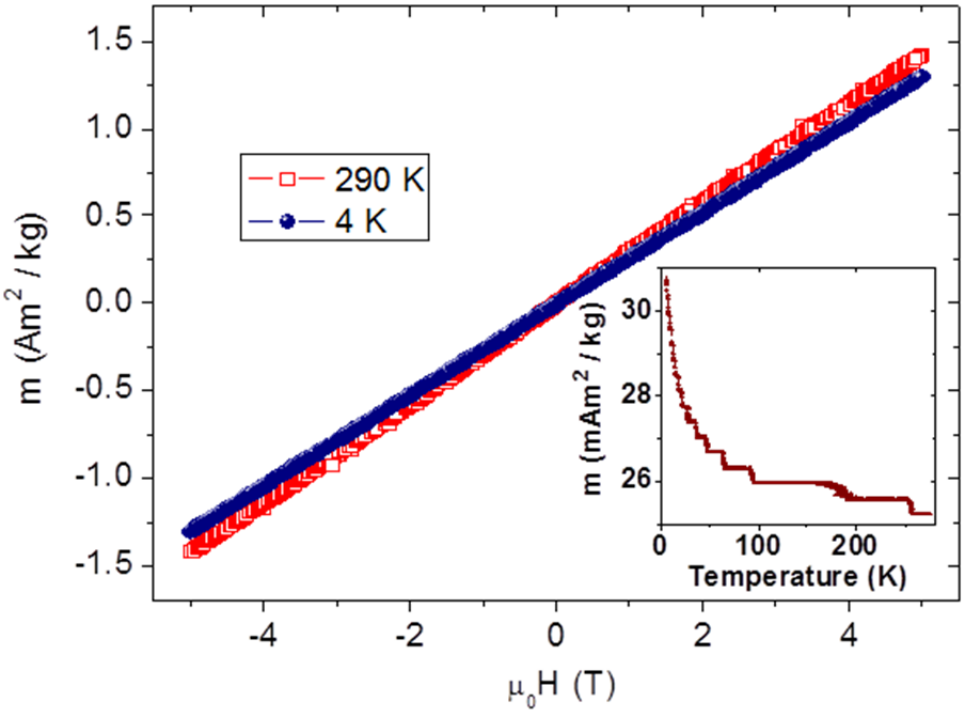

Figure 6.13 Magnetic moment per unit mass of the β-FeOOH nanoparticles in fields up to 5 T. The samples have a large linear susceptibility without hysteresis down to 4 K. Inset: zero field cooled curve measured at 100 mT

6.3.6 Mathematical relationship between experimental conditions and particle size

The effects of three different parameters (Effect of [$FeCl_3$], T and t) were evaluated using a two level factorial trial experimental design. Particle aspect ratios were used as response for the two level factorial trials to keep consistency and simplicity in the analysis. Figure 6.14 presents the effect of the parameters and interaction effect between parameters on aspect ratio obtained for the particles. Evaluation of the effect of principal factors revealed that these parameters have positive effects on the aspect ratios. Alcohol-to-water ratio and time shows the most significant effect to achieve maximum aspect ratio.

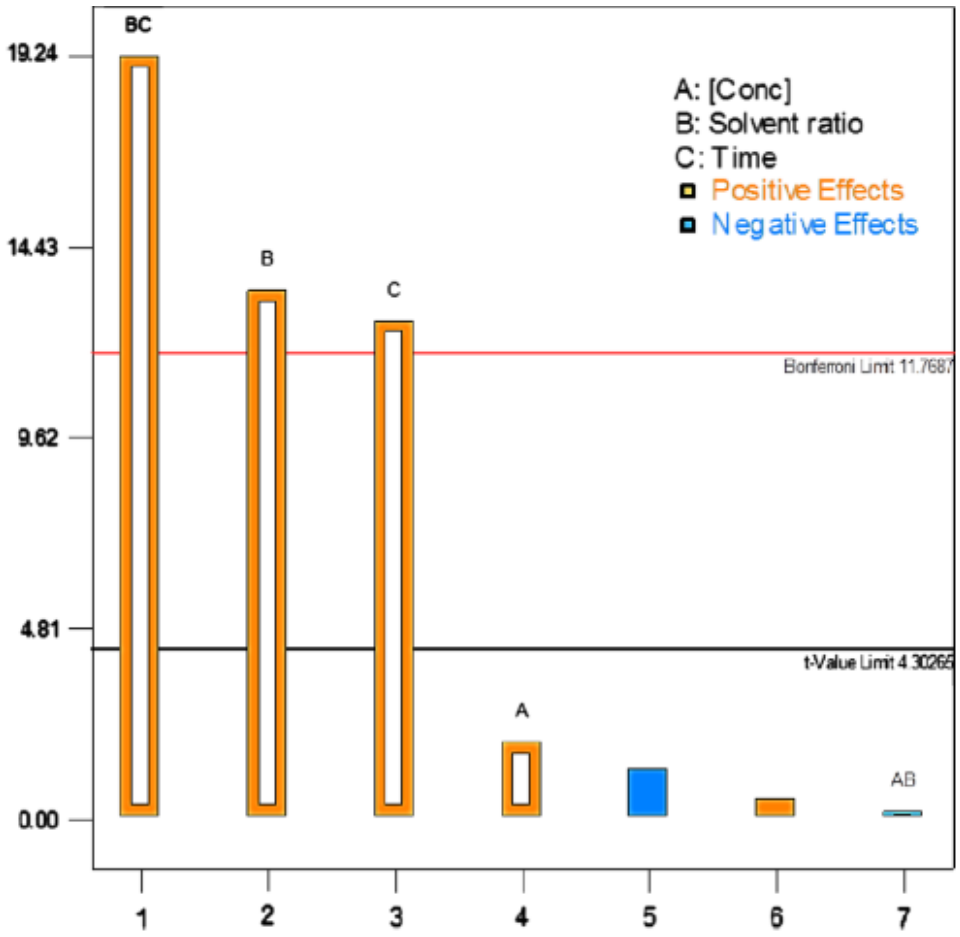

Figure 6.14 Estimated effects of factors on particle aspect ratio using factorial design

A generalized correlation is proposed based on the significance of effects of the parameters and relationship between solvent surface tension and particle characteristics on the particle growth.

$$Y = \beta_o \sigma + \sum_{i=A} \beta_i X_i + \sum_{i=A} \sum_{j=A \neq i} \beta_{ij} XiXj + \varepsilon \qquad \text{Equation 6.1}$$

Where, Y, is the predicted response (aspect ratio in this case), X_i, the un-coded or coded values of the factors (concentration denoted by A, % alcohol to water ratio is denoted by B and time is denoted by C), β_o, a constant, σ, the surface tension of alcohol used, β_i, the main effect coefficients for each variable and β_{ij}, the interaction effect coefficients. The corresponding response model for the aspect ratio of the particles which are valid for un-coded factor is:

$$Y = 0.25\sigma + [A] - 0.29[B] - 0.50[C] + 0.07[AB] + 0.009[BC] \qquad \text{Equation 6.2}$$

Statistical analysis performed in design-expert® software revealed that Equation 6.2 has an F-Test / Model F-value of 141.91, implying that the model is statistically significant and there is a 0.70% chance that a Model F-value this high is due to data noise. The P-value of the model was found to be less than 0.05 indicating model terms are significant. The term B, C and BC in Equation 6.2 is statistically the most significant model terms. Figure 6.2 presents the comparison between predicted and actual aspect ratio obtained. The average percentage uncertainty between the predicted and the actual aspect ratio was found to be between ± 2%.

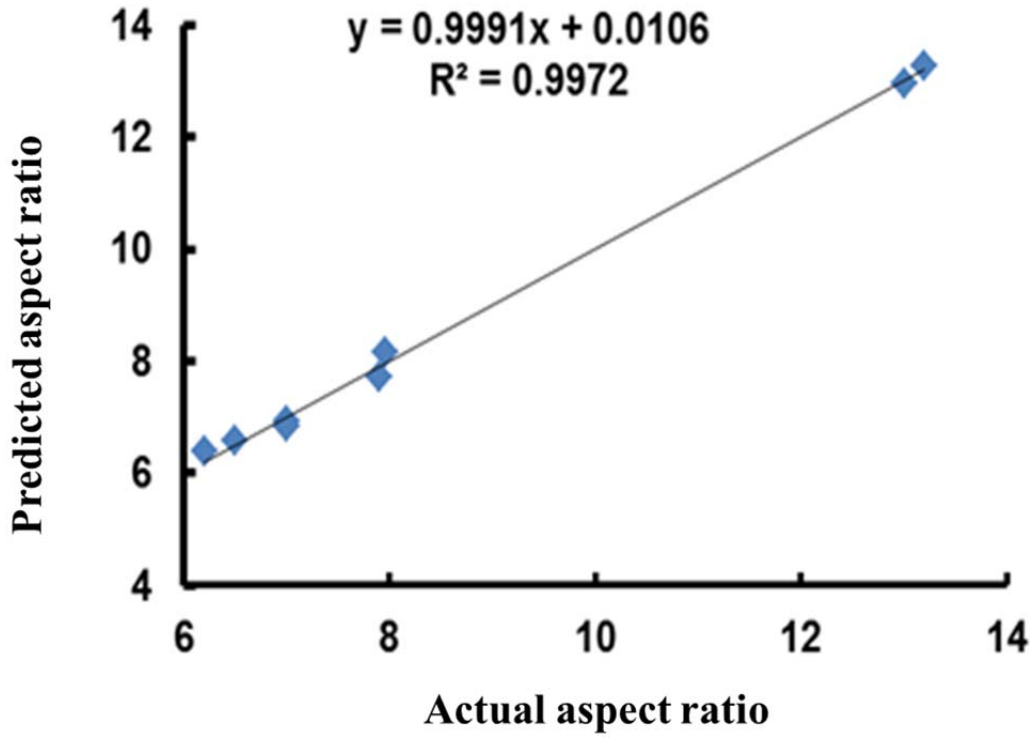

Figure 6.15Comparison between experimental and predicted aspect ratio

Independent experiments at random sequence were conducted to further validate the model. BuOH, PrOH and EtOH were used as solvent for validating the relationships between solvent surface tension and particle growth. Figure 6.163 presents a comparison between experimental data and the model. It can be seen from Figure 6.16 that the model predicts the particle aspect ratio very well, and the uncertainty range is within ±25% in all cases. Considering the nanoscale of the materials this model should be considered reliable under the reported conditions.

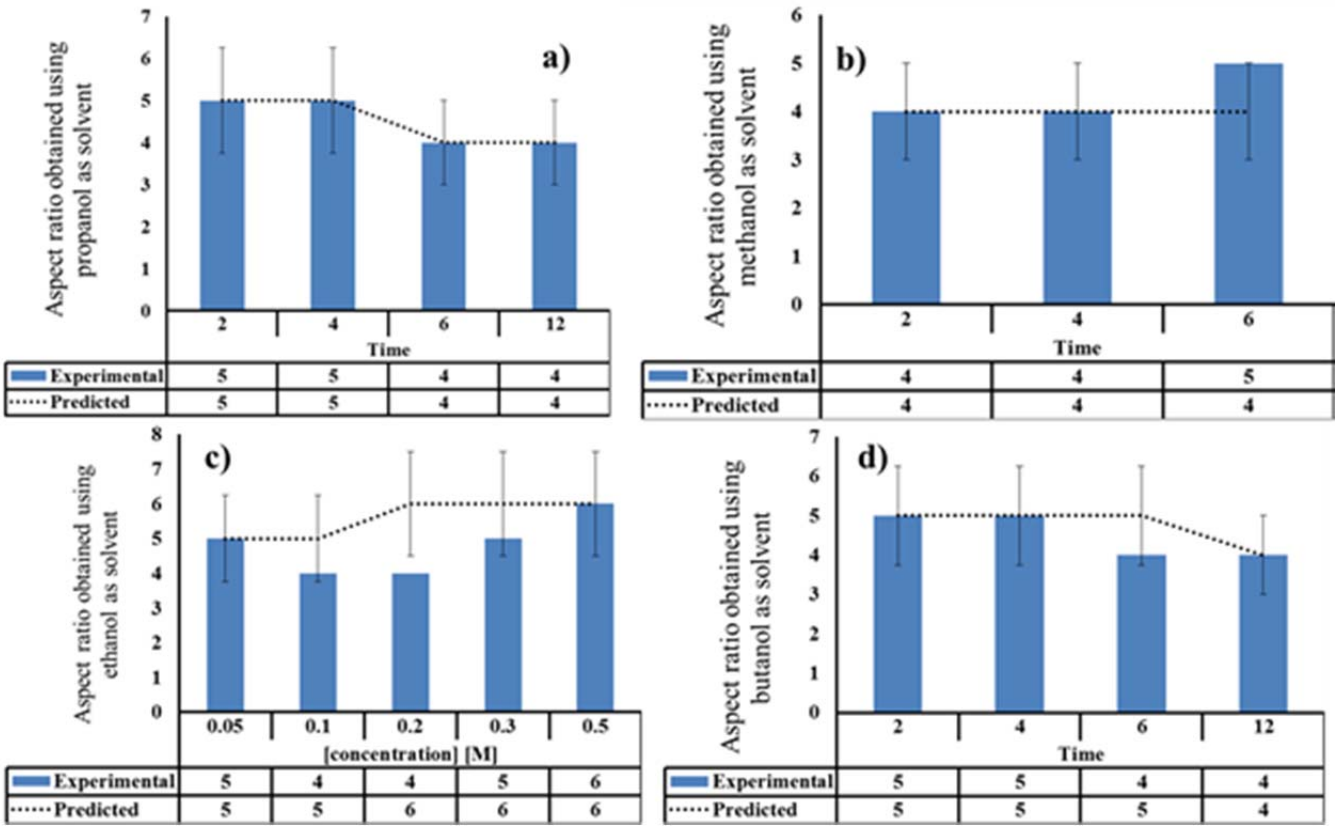

Figure 6.16 Comparison between experimental and predictive data

6.4 Conclusion

The effect of HS processing parameters on the β-FeOOH particle characteristics have been evaluated and presented. The effect of alcohol nature on the particle morphology was found to be more pronounced at higher $FeCl_3$ concentrations (>0.5M). Selective choice of solvent can initiate crystal splitting of β-FeOOH nanorods. Surfactant-free synthesis of nanoribbon is not reported widely in the literature and therefore, their synthesis under supersaturation in selective solvent might be an alternative approach. Significant reduction (98% reduction compared to literature) in synthesis time for hydronium iron jarosite was achieved by controlling solution pH. Transformation of β-FeOOH to α-Fe_2O_3 is strongly dependent on the nature of solvent. In addition, the nature of the solvent affects the dehydration property of the particles. Required transformation temperature and dehydration property increases with the increase in carbon chain length in the solvent. A generalized correlation was developed from statistically designed experiments for the first time to predict β-FeOOH

nanorod growth empirically. The developed correlation takes three different process parameters into account to predict particle aspect ratio with acceptable confidence.

Chapter 7

Summary and conclusions

7.1 Introduction

Solvent dependent morphological evolution and growth mechanisms of the β-FeOOH nanorods were investigated in depth and the findings are reported in this study. A summary and conclusions are presented here.

7.2 Summary

In Chapter 4, the main aspects concerning the effect of alcohol-to-water ratio are discussed. The use of a controlled ROH/H_2O to control particle size is new approach in the synthesis and processing of materials. Prior literature always utilized the dielectric constant properties of the mixed solvent only, to relate particle nucleation and growth. In this study by means of kinetic equation it was illustrated that the solvent surface tension can also be used to relate to particle growth. It was found that there is a linear relationship between surface tension and particle size that holds approximately independent of the nature of the alcohol used to synthesise the particles.

The effect of solvents on the growth kinetics of the β-FeOOH nanorods was evaluated in Chapter 5. Lacunae still exist regarding the growth mechanism of nanoparticles under mixed solvent conditions. Time evolution experiments were conducted under different mixed solvent conditions to investigate the growth of the akaganeite nanorods. A mechanism for the growth of nanorods via the OA mechanism is also presented. The shape of the particle size distribution was linked with the growth mechanism of the nanorods. A quantitative and / or qualitative relationship was established between particle growth rate constants and surface tension and was further validated by an independent study.

In Chapter 6, the effect of HS processing parameters on the morphological and structural evolution of β-FeOOH particles were evaluated to delimit the boundaries for β-FeOOH precipitation. The particle morphology as well as dehydration properties were strongly dependent on solvent nature. A generalized correlation derived from statistically designed experiments predicted particle sizes with acceptable confidence.

7.3 Conclusion

This study relates the role of solvent surface tension with the growth of the particles, which is original.

It revealed that:

- Particle morphology is strongly dependent on the solvent nature;
- the growth kinetics of the β-FeOOH nanorods are solvent dependent;
- selective choice of solvent can give control over particle sizes and
- a quantitative and / or qualitative relationship exists between solvent surface tension and particle growth.

7.4 Significant contribution

The findings in this study obtained from both theoretical and experimental work, provides insight into solvent surface tension and particle growth interactions, producing new vital information that will further promote understanding of the formation mechanisms of β-FeOOH growth.

7.5 Future research contribution

The following comprise some suggestions for future work:

- *In situ* observation of the growth kinetics of the β-FeOOH nanorods via ultrasound method
- The effect of H-bonding on the nanoparticle formation
- The use of polar aprotic and non-polar solvent in the synthesis of β-FeOOH particles

References

ADSCHIRI , T, T MOUSAVAND, S TAKAMI et al. 2005. Supercritical hydrothermal synthesis of advanced metal oxide nanoparticles. *In*: H WAKAYAMA, (ed). *Materials Chemistry in Supercritical Fluids*.

ADSCHIRI, T, K KANAZAWA, and K ARAI. 1992. Rapid and continuous hydrothermal synthesis of metal oxide particles in supercritical water. *Journal of American Ceramic Society*. **75**, pp.1019-1022.

ALMEIDA, T. 2010. *Hydrothermal synthesis of α-Fe2O3 nanorods*. University of Nottingham.

ALMEIDA, T. 2010. *Hydrothermal synthesis of α-Fe2O3 nanorods*. Nottingham: University of Nottingham.

AL-SAYARI, S, A F CARLEY, S H TAYLOR, and G J HUTCHINGS. 2007. Au/ZnO and Au/Fe2O3 catalysts for CO oxidation at ambient temperature: comments on the effect of synthesis conditions on the preparation of high activity catalysts prepared by coprecipitation. *Topics in Catalysis*. **44**, pp.123-128.

AMINE, K, H YASUDA, and M YAMACHI. 1999. β-FeOOH, a new positive electrode material for lithium secondary batteries. *Journal of Power Sources*. **81-82**, pp.221-223.

ARAI, Y, T SAKO, and Y TAKEBAYASHI. 2002. *Supercritical Fluids: Molecular, Interactions, Physical Properties And New Applications*. New York: Springer-Verlag, Nerlin Heidelberg.

ARONNIEMI, M, J LAHTINEN, and P HAUTOJARVI. 2003. Characterization of iron oxide thin films. *Surface And Interface Analysis*. **36**, pp.1004 - 1006.

AZHAR, S. 2007. *Synthesis of well defined hematite films and their use for sintering studies*. Lulea university of technology.

AZHAR UDDIN, M, H TSUDA, S WU, and E SASAOKA. 2008. Catalytic decomposition of biomass tars with iron oxide catalysts. *Fuel*. **87**, pp.451-459.

BAIKER, A and R WANDELER. 2000. Supercritical fluids: opportunities in heterogeneous catalysis. *CATTECH*. **4**(1), pp.128-143.

BALARAMAN, D. 2005. *Ultra-thin ceramic films for low temperature embedding of decoupling capacitors into organic printed wiring boards*. Georgia: Georgia Institute of Technology.

BANDARA, J, U KLEHM, and J KIWI. 2007. Raschig rings-Fe2O3 composite photocatalyst activate in the degradation of 4-chlorophenol and Orange II under daylight irradiation. *Applied Catalysis B: Environmental*. **76**, pp.73-81.

BARRIOS, E, L HERNAN, J MORALES, and J L TIRADO. 1986. Effect of grinding in synthetic akaganeite. *Journal of Colloid and Interface Science*. **113**, pp.212-217.

BARUWATI, B, K M REDDY , and S V MANORAMA. 2006. Synthesis of Nanostructured Hydroxides and Oxides of Iron: Control over morphology and physical properties. *Journal of American Ceramic Society*. **89**, pp.2602 – 2605.

BASHIR, S, R W MCCABE , C BOXALL , and M S LEAVE. 2009. Synthesis of a- and b-FeOOH iron oxide nanoparticles in non-ionic surfactant medium. *Journal of Nanoparticle Research*. **11**, pp.701-706.

BEACH, Elvin R. 2009. *Picoliter drop deposition of oxide nanoparticles: a route to high performance microsensor arrays*. Ohio: The ohio state university.

BENZIGER, J B and I A AKSAY. 1999. *Notes on data analysis: Chemical engineering 346 spring term*. Princeton, Newjersey: Department of Chemical Engineering, Princeton university.

BERNARDI , M IB, C A C FEITOSA , C A PASKOCIMAS et al. 2009. Development of metal oxide nanoparticles by soft chemical method. *Ceramics International*. **35** , pp.463-466.

BO, Tang, Wang GUANGLI, Zhuo LINHAI et al. 2006. Facile route to α-FeOOH and and α-Fe2O3 nanorods and magnetic property. *Inorganic Chemistry*. **45**(13), pp.5196-5200.

BORG, R J and J G DIENES. 1992. *The physical chemistry of solids*. Boston: Academic press.

BRADLEY, D C. 1989. Metal Alkoxides as Precursors for Electronic and Ceramic Materials. *Chemical Reviews*. **89**, pp.1317-1322.

BRINKER, C J and G W SCHERER. 1990. *Sol-gel science the physics and chemistry of sol-gel processing*. San Diego: Academic Press.

BYRAPPA, K. 2005. *In*: *Kirke Othmer encyclopedia of chemical technology*, London: John wiley and Sons.

BYRAPPA, K. 2005. Hydrothermal processing. *In*: *Kirke Othmer encyclopedia of chemical technology*, London: John wiley and Sons.

BYRAPPA, K and T ADSCHIRI. 2007. Hydrothermal technology for nanotechnology. *Progress in Crystal Growth and Characterization of Materials*. **53**.

BYRAPPA, K and M YOSHIMURA. 2001. *handbook of hydrothermal technology: a technology for crystal growth and materials processing*. New York: Noyes publications.

CAHN, R W, P HAASEN, and E J CREMER. 1991. *Materials science technology: phase transformations in materials*. Weiheim: WCH Press.

CAI, J, J LIU, Z GAO et al. 2001. Synthesis and anion exchange of tunnel structure akaganeite. *Chemistry of Materials*. **13**(12), pp.4595-4602.

CAMPBELL, C T, S C PARKER, and D E STARR. 2002. The effect of size-dependent nanoparticle energetics on catalyst sintering. *Science*. **298**, pp.811-814.

CANSELL, F, B CHEVALIER, A DEMOURGUES et al. 1999. Supercritical fluid processing: a new route for materials synthesis. *Journal of Materials Chemistry*. **9**, pp.67–75.

CASTRO, C, J RAMOS, A MILLAN et al. 2000. Production of magnetic nanoparticles in imine polymer matrixes. *Chemistry of Materials*. **12**, pp.3681-3688.

CAURANTA, D, N BAFFIERA, B GARCIAA , and J P PEREIRA-RAMOS. 1996. Synthesis by a soft chemistry route and characterization of LiNixCo1−xO2 ($0 \leq x \leq 1$) cathode materials. *Solid State Ionics*. **91**, pp.45-54.

CELE, Nonhlanhla Precious. 2010. *Preparation and characterization of nafion-based nanocomposite membranes for fuel cell applications*. Kwazulu Natal: University of Zululand.

CHEN, Huey Ing and Hung Yi CHANG. 2004. Homogeneous precipitation of cerium dixoide nanoparticles in alcohol/water mixed solvents. *Colloids and surfaces A: physicochem. Eng. Aspects*. **242**, pp.61-69.

CHEN, Ming, Jianhua JIANG, Xiaoming ZHOU, and Guowang DIAO. 2008. Preparation of akaganeite nanorods and their transformation to sphere shape hematite. *Journal of Nanoscience and Nanotechnology*. **8**, pp.3942-3948.

CHIU, Chao An, Kiril D HRISTOVSKI, Richard DOCKERY et al. 2012. Modeling temperature and reaction time impacts on hematite nanoparticle size during forced hydrolysis of ferric chloride. *Chemical Engineering Journal*. **210**, pp.357-362.

CORNELL, R M and U SCHWERTMANN. 2000. *Iron oxides in the laboratory: preparation and charcaterization*. Wiley VCH.

CORNELL, R M and U SCHWERTMANN. 2003. *The iron oxides: structure, propoerties, reactions, occurences and uses*. Wiley VCH.

COTE, L J, A S TEJA, A P WILKINSON, and Z J ZHANG. 2003. Continuous hydrothermal synthesis and crystallization of CoFe2O4 nanoparticles. *Fluid Phase Equlibrium*. **210**, pp.307-317.

DARR, J A and M POLIAKOFF. 1999. New directions in inorganic and metal-organic coordination chemistry in supercritical fluids. *Chemical Revision*., pp.495-541.

DAWSON, W J. 1988. Hydrothermal synthesis of advanced ceramic powders. *American Ceramic Society Bulletin*. **67**(10), pp.1673-1678.

DAWSON, W J and M K HAN. 1993. Development and scale-up of hydrothermal processes for synthesis of high performance materials. *In*: J B HISKEY and G W WARREN, (eds). *Hydrometallurgy Fundamentals, Technology And Innovations*, SME Inc.

DE YOREO, JJ and P VEKILOV. 2003. Principles of crystal nucleation and growth. *In*: PM DOVE , JJ DE YOREO , and S WEINER , (eds). *Biomineralization*, Washington, DC: Mineralogical society of america, pp.57-93.

DELIYANNI, E A, D N BAKOYANNAKIS, A I ZOUBOULIS et al. 2001. Akaganeite β-FeO(OH) type nanocrystals: preparation and characterization. *Microporous and Mesoporous Materials*. **42**, pp.49-57.

DENARDO, S J, G L DENARDO, and L A MIERS. 2005. Development of Tumor Targeting Bioprobes(111 in-chemaric L6 Monoclonal Antibody Nanoparticles) for alternating magnetic field cancer therapy. *Clinical Cancer Research*. **11**, pp.7087-7092.

DENG, Z, D CHEN, F TANG et al. 2007. Oriented attachment assisted selfassembly of of Sb2O3 nanorods and nanowires: End to End vs Side by side. *Journal of Physcial Chemistry C*. **111**, pp.5325-5330.

DIMITRIEV, Y, Y IVANOVA, and R IORDANOVA. 2008. History of Sol-Gel Science and Technology (Review). *Journal of the University of Chemical Technology and Metallurgy*. **43**, pp.181-192.

DING, Z Y, M A FRISCH, L LI, and E F GLOYNA. 1996. Catalytic oxidation in supercritical water. *Industrial and Engineering Chemistry Research*. **35**, pp.3257-3279.

DRONSKWOSKI, R. 2001. ChemInform Abstract: The little maghemite story. A classic functional material. *Advanced Functional Materials*. **11**, pp.27-29.

EARLE, S A, A P RAMIREZ, and R J CAVA. 1999. The effect of gallium substituion for iron on themagnetic properties of hydronium iron jarosite. *Physica B*. **262**, pp.199-204.

FESTER, V G, P T SLATTER, S BIGGS, and G KALE. 2008. Significance of alcohols in the synthesis of iron oxide nanorods. *In*: *Green chemietry & engineering, process intensification & nanotechnology conference*. Albany,New York: BHR group, pp.231-236.

FLYNN, C M. 1984. Hydrolysis of inorganic Iron(III) salts. *Chemical Reviews*. **84**, pp.31-41.

FRANDSEN, C, C R BAHL, B LEBECH et al. Oriented attachment coupling of a-Fe2O3 nanoparticles. *Physical review B: Condensed Matter Material Phyics*. **72**, p.214406.

GABBOT, paul. 2008. *Prinicple and applications of thermal analysis*. New Delhi: Blackwell publishing.

GALKIN, A A, B G KOSTYUK, N N KUZNETSOVA et al. 2001. Unusual approache to the preparation of heterogeneous catalysts and supports using water in subcritical and supercritical states. *Kinetics and Catalysis*. **42**, pp.154-162.

GALLAGHER, K J. 1970. The atomic structure of tubular subcrystals of β-Iron(III) oxide hydroxide. *Nature*. **226**, p.1225.

GARCIA, K E, C A BARRERO, A L MORALES, and J M GRENECHE. 2008. Characterization of akaganiete synthesized in presence of Al3+, Cr3+ and Cu2+ ions and urea. *Materials Chemistry and Physics*. **112**, pp.120-126.

GARRATT-REED, A J and D C BELL. 2003. *Energy-Dispersive X-Ray analysis in the electron microscope*. Oxford: Bios Scientific publishers limited.

GIBBS , J W. 1876. On the equilibrium of heterogeneous substances. *Trans Connect Acta Sci*. **3**, pp.108-248.

GILBERT, Benjamin, Hengzhong ZHANG, Feng HUANG et al. 2003. Special phase transformation and crystal growth pathways observed in nanoparticles. *Geochemical Transaction*. **4**, pp.20-27.

GOODEY, J, O K K MIN , J BROUSSARD et al. 2003. Syntheses, structures, and second-harmonic generating properties in new quaternary tellurites: A2TeW3O12 (A = K, Rb, or Cs). *Journal of Solid State Chemistry*. **175**, pp.3–12.

GOODHEW, P J and F J HUMPHREYS. 1988. *Electron Microscopy and Analysis, 2nd edition*. London: Taylor & Francis.

GRAEF, Marc and Michael E HENRY. 2007. *Structure of materials*. New York: Cambridge press.

GRUTTNER, Cordula, Knut MULLER, Joachim TELLER et al. 2007. Synthesis and antibody conjugation of magnetic nanoparticles with improved specific power absorption rates for alternating magnetic field cancer therapy. *Journal of Magnetism And Magnetic Materials*. **311**, pp.181-186.

GUO, X and P XIAO. 2006. Effects of solvents on properties of nanocrystalline hydroxyapatite produced from hydrothermal process. *Journal of Europian Ceramic Society*. **26**, pp.3383–3391.

GUYODO, Y, A MOSTROM, R L PENN, and S K BANERJEE. 2003. From nanodots to nanorods:Oriented aggregation and magnetic evoution of nanocrystalline geothite. *Geophysical Research Letters*. **30**, p.1512.

HAKUTA, Y, T ADSCHIRI, T SUZUKI et al. 1998. Flow method for rapidly producing barium hexaferrite particles in supercritical water. *Journal of American Ceramic Society*. **81**, pp.2461-2464.

HAKUTA, Y, S ONAI, T ADSCHIRI, and K ARAI. 1998. Production of ultra-fine ceria particles by hydrothermal synthesis under supercritical conditions. *Journal of Materials Science Letters*. **17**, pp.1211-1213.

HAKUTA, Y, K SEINO, H URA et al. 1999. Production of phosphor (YAG:Tb) fine particles by hydrothermal synthesis in supercritical water. *Journal of Materials Chemistry*. **9**, pp.2671-2674.

HAKUTA, Y, H URA, H HAYASHI, and K ARAI. 2005. Continuous production of BaTiO3 nanoparticles by hydrothermal synthesis. *Industrial and Engineering Chemistry Research*. **44**, pp.840-846.

HAN, Jisheng. 2001. *PhD Thesis : A study of α-iron oxide as a gas sensing material*. University of South Australlia.

HANEDA, K and A H MORRISH. 1977. Vacancy ordering in γ-Fe2O3 small particles. *Solid State Communications*. **22**, pp.7797-782.

HAO, Y and A S TEJA. 2003. Continuously hydrothermal crystallization of α-Fe2O3 and Co3O4 anoparticles. *Journal of Materials Research*. **18**, pp.415-422.

HAYASHI , Hiromichi and Yukiya HAKUTA. 2010. Hydrothermal Synthesis of Metal Oxide Nanoparticles in Supercritical Water. *Materials*. **3**, pp.3794-3817.

HAYASHI, H and K TORII. 2003. Hydrothermal synthesis of titania photocatalyst under subcritical and supercritical water conditions. *Journal of Materials Chemistry*. **12**, pp.3671–3676.

HELGASON, O, J M GRENECHE, F J BERRY, and F MOSSELMANS. 2003. The influence of ruthenium on the magnetic properties of γ-Fe2O3 (maghemite) studied by Mössbauer spectroscopy. *Journal of Physics: Condensed Matter*. **15**, pp.2907-2915.

HENDRIKSEN, P V, S LINDEROTH, and P A LINDGA°RD. 1993. Finite-size modifications of the magnetic properties of clusters. *Physical Review B*. **48**, pp.7259-7273.

HOHENBERG , PC and BI HALPERIN. 1977. Theory of dynamic critical phenomena. *Reviews of Modern Physics*. **49**, pp.435-479.

HOLMES, J D, K P JOHNSTON, R C DOTY, and B A KORGEL. 2000. Control of thickness and orientation of solution-grown silicon nanowires. *Science*. **287**, pp.1471-1473.

HOSAKA, M and T MIYATA. 1993. Hydrothermal growth of α-quartz using high-purity α- cristobalite as feed material. *Materials Research Bulletin*. **28**, pp.1201-1208.

HUANG, F, H ZHANG, and J F BANFIELD. 2003. Two-stage crystal growth kinetics observed during hydrothermal coarsening of nanocrystalline ZnS. *Nano Letters*. **3**(3), pp.373-378.

HUNG, I M, H P WANG, W H LAI, and K Z FUNG. 2004. Preparation of mesoporous cerium oxide templated by tri-block copolymer for solid oxide fuel cell. *Electrochemica Acta*. **50**, pp.745-748.

INOUE, M. 2005. Solvothermal synthesis. *In*: B LEE and S KOMARNENI, (eds). *Chemical Processing of Ceramics*, Boca Raton: CRC Press, pp.21-61.

ISHIKAWA, T, S MIYAMOTO, K KANDORI , and T NAKAYAMA. 2005. Influence of anions on the fomration of beta-FeOOH rusts. *Corrosion Science*. **47**(10), pp.2510-2520.

ISRAELACHVILI, Jacob N. 1992. *Intermolecular and surface forces*. Academic press.

JIANG, X C, A B YU, W R YANG et al. 2010. Synthesis and growth of hematite nanodiscs through a facile hydrothermal approach. *Journal of Nanoparticle Research*. **12**, pp.877-893.

JIU, J, Y GE, X LI, and L NIE. 2002. Preparation of CO3PO4 nanoparticles by a polymer combustion route. *Materials Letter*. **54**, pp.260-263.

JOLIVET, J P, E TRONC, and C CHANEAC. 2006. Iron oxides: From molecular clusters to solid. A nice example of chemical versatility. *Comptes Rendus Geoscience*. **338**, pp.488-497.

JUN, Y W, M F CASULA M. F, J H SIM et al. 2003. Surfactant-assisted elimination of a high energy facet as a means of controlling the shapes of TiO2 nanocrystals. *Journal of American Chemical Society*. **125**, pp.15981-15985.

JUN, Y W, J H LEE, and J CHEON. 2007. Nanoparticle contrast agents for molecular magnetic resonance imaging. *In*: *Nanobiotechnology II: More Concepts And Applications*. Weinheim: Wiley-VCH.

KAKIHANA , M and M YOSHIMURA. 1999. Synthesis and characteristics of complex mul-ticomponent oxides prepared by polymer complex method. *Bulletin of The Chemical Society of Japan*. **72**, pp.1427-1443.

KANAMURA, K, T UMEGAKI, K TOYOSHIMA et al. 2000. Preparation and electrochemical characterization of LiCoO2 single crystal particles prepared by supercritical water synthesis (SCWS). *Materilas Research Society Symposium*. **575** , pp.59-64.

KANDORI, K, N YAMAMATO, A YASUKAWA, and T ISHIKAWA. 2002. Preparation and characterization of disk-shaped hematite particles by a forced hydrolysis reaction in the presence of polyvinyl alcohol. *Physical Chemistry Chemical Physics*. **4**, pp.6116-6122.

KANNO, R, T SHIRANE, Y KAWAMOTO et al. 1996. Synthesis, Structure, and Electrochemical Properties of a New Lithium Iron Oxide, LiFeO2, with a Corrugated Layer Structure. *Journal of The Electrochemical Society*. **143**, pp.2435-2442.

KATSUKI, H and S KOMARNENI. 2001. Microwave-hydrothermal synthesis of monodispersed nanophase α-Fe2O3. *Journal of the American Ceramic Society*. **84**, pp.2313-2317.

KAWAI-NAKAMURA, Akiko, Toshiyuki SATO, Kiwamu SUE et al. 2008. Rapid and continuous hydrothermal synthesis of metal and metal oxide nanoparticles with a microtube-reactor at 523 K and 30 MPa. *Materilas Letter*. **62**, pp.3471-3473.

KELLY, K L, E CORONADO, L L ZHAO, and G C SCHATZ. 2003. The optical properties of metal nanoparticles: The influence of size, shape and dielectric environment. *Journal of Physical Chemistry B*. **668-677**.

KHAN, Yaqoob, S k DURRANI, M SIDDIQUE, and Mazhar MEHMOOD. 2011. Hydrothermal synthesis of α-Fe2O3 nanoparticles capped by Tween-80. *Materials Letters*. **65**, pp.2224-2227.

KIM, F, J SONG, and P YANG. 2002. Photochemical synthesis of nanorods. *Journal of the American Chemcial Society*. **124**, pp.14316-14317.

KIRCHNER, H OK. 1971. Coarsening of Grain-Boundary precipitates. *Metallurgical Transactions*. **2**, pp.2861-2864.

KLIER, J, C J TUCKER, T H KALANTAR, and D P GREEN. 2000. Properties and Applications of Microemulsions. *Advanced Materials*. **12**, pp.1751-1757.

KLOTZ, S, G STEINLE-NEUMANN, T STRASSLE et al. 2008. Magnetism and the Verwey transition in Fe3O4 under pressure. *Physical Review*., pp.012411-1 - 012411-4.

KRILL, C E, L HELFEN, D MICHELS et al. 2001. Size dependent grain growth kinetics observed in nanocrystalline Fe. *Physics Review Letters*. **86**, pp.842-845.

KUMAR, R V, Y KOLTYPIN, Y S COHEN et al. 2000. Preparation of amorphous magnetic nanoparticles embedded in polyvinyl alcohol using ultrasonic raidation. *Journal of Materials Chemistry*. **10**, pp.1125-1129.

KUO, Chih-Wei , Yueh-Hsun LEE, Kuan-Zong FUNG, and Moo-Chin WANG. 2005. Effect of Y2O3 addition on the phase transition and growth of YSZ nanocrystallites prepared by a sol–gel process. *Journal of NonCrystalline Solids*. **351**, pp.304-311.

LAM, U T, R MAMMUCARI, K SUZUKI, and N R FOSTER. 2008. Processing of iron oxide nanoparticles by supercritical fluids. *Industrial And Engineering Chemistry Research*. **47**, pp.599-614.

LEE, Y W. 5–9 August 2006. Formation of nano particles in supercritical fluids. *In*: *Proceedings of ISHR & ICSTR*. Sendai, Japan.

LEE, Y C, Y L CHUEH, C H HSIEH et al. 2007. p-Type α-Fe2O3 nanowires and their n-Type transition in a reductive ambient. *Small*. **3**, pp.1356-1361.

LEE, J and A TEJA. 2006. Synthesis of LiFePO4 micro and nanoparticles in supercritical water. *Materials Letter*. **60**, pp.2105-2109.

LESTER, E, P BLOOD, J DENYER et al. 2006. Reaction engineering: the supercritical water hydrothermal synthesis of nanoparticles. *Journal of Supercritical Fluids*., pp.209-214.

LIANG, Ming-Tsai, Shih-Han WANG, Yu-Lun CHANG et al. 2010. Iron oxide synthesis using a continuous hydrothermal and solvothermal system. *Ceramics International*. **36**, pp.1131-1135.

LIANG, H, H ZHAO, D ROSSOUW et al. 2012. Silver nanorice structures:Oriented attavhment dominated growth, high environmental sensitivity and real-space visualization of multipolar resonances. *Chemistry of Materials*. **24**, pp.2239-2246.

LIEBER, C M. 2003. Nanoscale science and technolgy: Building a big future from small things. *Materials Research Society*. **28**, p.486.

LIN, Jun, Min YU, Cuikun LIN, and Xiaoming LIU. 2007. Multiform Oxide Optical Materials Via the Versatile Pechini-Type Sol-Gel Process: Synthesis and Characteristics. *Journal of Physical Chemistry C*. **111**, pp.5835-5845.

LIU, L, H-Z KOU, W MO et al. 2006. Surfactant-assisted synthesis of α-Fe2O3 nanotubes and nanorods with shape dependent magnetic properties. *Journal of Physical Chemistry B*. **110**, pp.15218-15223.

LODHIA, J, G MANDARANO, N J FERRIS et al. 2010. Development and use of iron oxide nanoparticles (Part 1): Synthesis of iron oxide nanoparticles for MRI. *Biomedical Imaging And Intervention Journal*. **6** , pp.doi: 10.2349/biij.6.2.e12.

MACKAY, A L. 1960. Mossbauer and X-ray data on β-FeOOH (akaganeite). *Mineralogical Magazine*, pp.545-557.

MACKAY, A L. 1962. β-ferric oxyhydroxide-akaganeite. *Mineralogical Magazine*, pp.270-280.

MAJEWSKI, P. 2008. *Encyclopaedia britannica online*. [online].

MAMBOTE, R C M, M A REUTER, P KRIJGSMAN, and R D SCHUILING. 2000. Hydrothermal metallurgy: an overview of basic concepts and applications. *Minerals Engineering*. **13**, pp.803-822.

MANNA, L, D J MILLIRON, A MEILSEL et al. 2003. Controlled growth of tetrapod-branched inorganic nanocrystal. *Nature Materials*. **2**(6), pp.382-385.

MARGULIES, D T, F T PARKER, M L RUDEE et al. 1997. Origin of the anomalous magnetic behavior in single crystal Fe3O4 films. *Physical Review Letters*. **79**, pp.5162-5165.

MATIJEVIC, E. 1985. Production of monodispersed colloidal particles. *Annual Review of Materials Science*. **15**, pp.483-516.

MATIJEVIC, E and P SCHEINER. 1978. Ferric hydrous oxide sols: III. preparation of uniform particles by hydrolysis of Fe(III)-chloride, -nitrate, and -perchlorate solutions. *Journal of Colloid And Interface Science*. **63**, pp.509-522.

MATSON, D W, J C LINEBAN, J G DARAB et al. A flow-through hydrothermal method for the synthesis of active nanocrystalline catalysts. *In*: *Advanced catalysts and nanostructured materials:modern synthetic methods*, California: Academic press.

MEISEN, U and H KATHREIN. 2000. The influence of particle size, shape and particle size distribution on propertiesof magnetites for the production of toners. *Journal of Imaging Science And Technology*. **44**, pp.508-513.

MILLOT, N, B XIN, C PIGHINI, and D AYMES. 2005. Hydrothermal synthesis of nanostructured inorganic powders by a continuous process under supercritical conditions. *Journal of the European Ceramic Society*. **25**, pp.2013-2016.

MOLDOVAN, D, V Y YAMAKOV, D WOLF, and S R PHILLPOT. 2002. Scaling behaviour of of grain-rotation induced grain growth. *Physical Review Letters*. **89**, p.206101.

MORRISH, A H and J A EATON. 1971. Magnetic transition in rhodium-doped hematite single crystals. *Journal of Appplied Physics*. **42**, pp.1495-1496.

MORRISH, A H, G B JOHNSTON, and N A CURRY. 1963. Magnetic transition in pure and Ga doped -Fe2O3. *Physics Letters*. **7**, pp.177-178.

MULLIN, J W. 2011. *Crystallization*. Butterworth Heinmann.

MURAD, E. 1979. Mossbauer and X-ray data on beta-FeOOH. *Calay Minerals*. **14**, pp.273-283.

MURAD, E. 1985. *In*: J W STUCKI, B A GOODMAN, and U SCHWERTMANN, (eds). *Series C: Mathematical and physical sceinces*, D. Reidel.

MURRAY, C B, D J NORRIS, and M G BAWENDI. 1993. Synthesis and characterization of nearly monodisperse CdE (E = sulfur, selenium, tellurium) semiconductor nanocrystallites. *Journal of American Chemical Society*. **115**, pp.8706-8715.

NESTEROVA, M, J MOREAUAND, and J F BANFIELD. 2003. Model biomimitec studies of templated growth and assembly of nanocrystalline FeOOH. *Geochimica et Cosmochimica Acta*. **67**, pp.1185-1187.

NEUBERGER, T, B SCHOPF, H HOFMANN et al. 2005. Superparamagnetic nanoparticles for biomedical applications: possibilities and limitations of a new drug delivery system. *Journal of Magnetism And Magnetic Materials*. **293**, pp.483-496.

NIEDERBERGER, M, G GARNWEITNER, J BUHA et al. 2006. Nonaqueous synthesis of metal oxide nanoparticles: review and indium oxide as case study for the dependence of particle morphology on precursors and solvents. *Journal of Sol-Gel Science And Technology*. **40**, pp.259-266.

NIEDERBERGER, M, F KRUMEICH, K HEGETSCHWEILER, and R NESPER. 2002. An iron polyolate complex as a precursor for the controlled synthesis of mono dispersed iron oxide colloids. *Chemistry of Materials*. **2002**, pp.78-82.

PAN, Z W, Z R DAI, and Z L WANG. 2001. Nanobelts of semiconducitng oxides. *Science*. **291**, pp.1947-1949.

PAULING, L and S B HENDRIKS. 1925. The crystla structures of hematite and corundum. *Journal Of The American Chemical Society*. **47**, pp.781-790.

PENG, X, L MANNA , W YANG et al. 2000. Shape Control Of CdSe Nanocrystals. *Nature*. **404**, pp.59-61.

PENN, R L. 2004. Kinetics of oriented aggregation. *Journal of Physcial Chemistry B*. **108**, pp.12707-12712.

PENN, R L and J F BANFIELD. 1998. Oriented attachment and growth, twinning, polytypism and formation metastable phase: Insights from nanocrystalline TiO2. *American Mineralogist*. **83**, pp.1077-1082.

PENN, R L and J F BANFIELD. 1999. Morphology development and crystal growth in nanocrystalline aggregates under hydrothermal conditions:insights from titania. *Geochimica Et Cosmochimica Acta*. **63**, pp.1549-1557.

PENN, R L, J J ERBS, and M GULLIVER. 2006. Controlled growth of alpha-FeOOh nanorods by exploiting oriented aggreagation. *Journal of Crystal Growth*. **293**, pp.1-4.

PENN, R L, G OSKAM, T J STRATHMANN et al. 2001. Epitaxial assembly in aged colloids. *Journal of Physical Chemistry. B*. **105**, pp.2177-2182.

PERSSON, A I, M W LARSSON, S STRENSTORM et al. 2004. Solid-phase diffusion mechanism for GaAs nanowire growth. *Nature Materials*. **3**, p.677.

PU, Z, M CAO, J YANG et al. 2006. Controlled synthesis and growth mechanism of hematite nanorhombohedra, nanorods and nanocubes. *Nanotechnology*. **17**, pp.799-804.

PUNTES, V F, K M KRISHNAN, and A P ALIVISATOS. 2001. Colloidal nanocrystal shape and size control: the case of cobalt. *Science*. **291**, pp.2115-2117.

PUNTES, V F, D ZANCHET , C K ERDONMEZ, and A P ALIVISATOS. 2002. Synthesis of hcp-Co nanodisks. *Journal of American Chemcial Society*. **124**, pp.12874-12880.

REDL, F X, K S CHO, C B MURRAY, and S O'BRIEN. 2003. Three-dimensional binary superlattices of magnetic nanocrystlas nad semiconductor quantam dots. *Nature*. **423**, pp.968-971.

REGUER, S, D NEFF, Bellot GURLET, and P DILLMANN. 2007. Deterioration of iron archaeological artefacts: micro-Raman investigation on Cl-containing corrosion products. *Journal of Raman Spectroscopy*. **38**, p.389.

RIVEROS , P A and J E DUTRIZAC. 1997. The precipitation of hematite from ferric chloride media. *Hydrometallurgy*. **46**, pp.85-104.

ROSEN, M J. 1989. *Surfactants and Interfacial Phenomena*. New York: Wiley-Interscience.

ROUSSEAU, R W. 1992. Crystallization processes. *In*: *Encyclopedia of physical science and technology*, Academic press, Inc.

SAKKA, S. 2003. Sol-Gel technology as reflected in journal of sol-gel science and technology. *Journal of Sol-Gel Science And Technology*. **26** , pp.29-33.

SCAMEHORN, J. 1986. An overview of Phenomena Involving Surfactant Mixtures. *In*: *Phenomena in Mixed Surfactant Systems*, Washington, DC.: American chemical society.

SCHMIDT, H. 2006. Considerations about the sol-gel process: from the classical sol-gel route to advanced chemical nanotechnologies. *Journal of SolGel Science And Technology*. **40** , pp.115-130.

SEGAL, D. 1997. Chemical synthesis of ceramic materials. *Journal of Materials Chemistry*. **7**, pp.1297-1305.

SENA, S P, R A LINDLEY, H J BLYTHE et al. 1997. Investigation of magnetite thin films produced by pulsed laser deposition. *Journal of Magnetism And Magnetic Materials*. **176**, pp.111-126.

SHAO, Hua-Feng, Xue-Feng QIAN, Jie YIN, and Zi-Kang ZHU. 2005. Controlled morphology synthesis of b-FeOOH and the phase transition to Fe2O3. *Journal of Solid State Chemistry*. **178**, pp.3130-3136.

SHI , J and H VERWEIJ. 2005. Synthesis and purification of oxide nanoparticle dispersions by modified emulsion precipitation. *Langmuir*. **21**, pp.5570-5575.

SOHNEL, O and J W MULLIN. 1978. A method for the determination of precipitation induction periods. *Journal of Crystal Growth*. **44**, p.377.

SOMIYA, S and R ROY. 2000. Hydrothermal synthesis of fine oxide powders. *Bulletinf of Matreial Science*. **23**, pp.453-460.

SPADA, F E, A E BERKOWITZ, and N T PROKEY. 1991. Hc enhancement in partially reduced γ-Fe2O3 via surface treatment with sodium polyphosphate (revisited). *Journal of Applied Physics*. **69**, pp.4475-4477.

SPALDIN, N. 2003. *Magnetic materials: Fundamentals and device applications*. Cambridge: Cambridge University press.

SPANHEL, L and M ANDERSON. 1991. Semiconductor clusters in the Sol-gel process: quantized aggregation, gelation, and crystal growth in concentrated ZnO Col-loids. *Journal of the American Chemical Society*. **113** , pp.2826-2833.

STADTLÄNDER, CT K-H. 2007. Scanning electron microscopy and transmission electron microscopy of mollicutes: challenges and opportunities. *In*: A MÉNDEZ-VILAS and J DÍAZ, (eds). *Modern research and educational topics in microscopy*, Clemson: Formatex, pp.122-131.

STAHL, K, K NIELSEN, J JIANG et al. 2003. On the akaganeite crystal structure, phase transformations and possible role in post-excavational corrosion of iron artifacts. *Corrosion Science*. **45**, p.2563.

SUE, K, K KINURA, and K ARAI. 2004. Hydrothermal synthesis of ZnO nanocrystals using microreactor. *Materials Letters*. **58**, pp.3229-3231.

SUZUKI, E. 2002. High-resolution scanning electron microscopy of immunogold-labelled cells by the use of thin plasma coating of osmium. *Journal of Microscopy*. **208**, pp.153-157.

SVÁB, E and E KRÉN. 1979. Neutron diffraction study of substituted hematite. *Journal of Magnetism And Magnetic Materials*. **14**, pp.184-186.

TANG, Jing and A Paul ALIVISATOS. 2006. Crystal Splitting in the Growth of Bi2S3. *Nano Letters*. **6**(12), pp.2701-2706.

TANG, Z Y, N A KOTOV, and M GIERSIG. 2002. Spontaneous organization of single CdTe nanoparticles into luminescent nanowires. *Science*. **297**, pp.237-240.

TARTAJ, P, M P MORALES, T GONZALVEZ-CARRENO et al. 2003. The preparation of magnetic nanoparticles for applications in biomedicine. *Journal of Physics D: Applied Physics*. **36**(13), pp.183-197.

TEJA, A S and Pei-Yoong KOH. 2009. Production of magnetic oxide nanoparticles. *Synthesis, properties, and applications of magnetic iron oxide nanoparticles*. **55**, pp.22-45.

TRONC, E, A EZZIR, R CHERKAOUI et al. 2000. Surface-related properties of γ-Fe2O3 nanoparticles. *Journal of Magnetism And Magnetic Materials*. **221**, pp.63-79.

USKOKOVIC , V and M DROFENIK. 2005. Synthesis of materials within reverse micelle. *Surface Review And Letters*. **12**, pp.239-277.

VAYSSIERES, L, N BEERMANN, S E LINDQUIST, and A HAGFELDT. 2001. Controlled aqueous chemical growth of oriented three-dimensional crystalline nanorod arrays: Application to iron (III) oxides. *Chemistry Of Materials*. **13**, pp.233-235.

VAYSSIERES, L, C SATHE, S M BUTORIN et al. 2005. One-dimensional quantum confinement effect in α-Fe2O3 ultrafine nanorods arrays. *Advance Materials*. **17**, p.2320.

VAZQUEZ, G, E ALVAREZ, and J M NAVAZA. 1995. Surface tension of alcohol+ water from 20 to 50 degree C. *Journal of Chemical Engineering Data*. **40**, pp.611-614.

VERDON, E, M DEVALETTE, and G DEMAZEAU. 1995. Solvothermal synthesis of cerium dioxide microcrystallites:effect of the solvent. *Materials Letters*. **25**, pp.127-131.

VISWANATHAN, R and R B GUPTA. 2003. Formation of zinc oxide nanoparticles in supercritical water. *Journal of Supercritical Fluids*. **27**, pp.187–193.

VORKAPIC, Danijela and Themis MATSOUKAS. 1998. Effect of temperature and alcohols in the preparation of titania nanoparticles from alkoxides. *Journal of American ceramic society*. **11**, pp.2815-2820.

WANDELER, R and A BAIKER. 2000. Supercritical fluids: opportunities in heterogeneous catalysis. *Cattech*. **4**, pp.34-50.

WANG, G, X GOU, J HORVAT, and J PARK. 2008. Facile synthesis and characterization of iron oxide semiconductor nanowires for gas sensing appliction. *The Journal of Physical Chemistry C*. **112**, pp.15220-15225.

WANG, X and Y LI. 2002. Selected-control hydrothermal Synthesis of alpha- and β -MnO2 single crystal nanowires. *Journal of American Chemical Society*. **124**, pp.2880-2881.

WATSON, JH L and R R CARDELL. 1962. The internal structure of colloidal crystals of β-FeOOH and remarks on their assemblies in schiller layers. *The Journal of Physical Chemistry*. **66**, pp.1757-1763.

WAYCHUNAS, G A. 2001. Structure, aggregation and charracterization of nanoparticles. *In*: J F BANFIELD and A NAVROTSKY, (eds). *Nanoparticles And The Environment*, Washington,DC: Minerological society of America, pp.105-166.

WEI, Chengzhen and Zhaodong NAN. 2011. Effects of experimental conditions on One-dimensional single-crystla nanoxtruxture of b-FeOOH. *Materials Chemistry And Physics*. **127**, pp.220-226.

WHITE, A F. 1990. Heterogeneous electrochemical reactions associated with oxidation of ferrous oxide and silicate surfaces. *In*: M F HOCHELLA and A F WHITE, (eds). *Mineral-Water Interface Geochemistry*, Reviews in Mineralogy, pp.467-505.

WILLIAMS, D B. 1984. *Practical analytical electron microscopy in materials science*. Deerfield beach, Florida: Electron optics publishing group.

XIONG, Y J, Y XIE, S W CHEN, and Z Q LI. 2003. Fabrication of Self-Supported Patterns of Aligned β-FeOOH Nanowires by a Low-Temperature Solution Reaction Chem. Eur. J. 9 (2003) 4991. *Chemistry-A European Journal*. **9**, pp.4991-4996.

XU, Chunbao, Jaewon LEE, and Amyn S TEJA. 2008. Continuous hydrothermal synthesis of lithium iron phosphate particles in subcritical and supercritical water. *Journal of Supercritical Fluids*. **44**, pp.92-97.

XU, Chunabo and Amyn S TEJA. 2008. Continuos hydrothermal synthesis of iron oxide and PVA-protected iron oxide nanoparticles. *Journal of Supercritical Fluids*. **44**, pp.85-91.

YADONG, Yin and A P ALIVISATOS. 2005. Colloidal nanocrystal synthesis and the organic–inorganic interface. *Nature*. **437**, pp.664-670.

YANG, S, y SONG, P Y ZAVALIJ, and M Whittingham STANLEY. 2001. Hydrothermal synthesis of lithium iron phosphate cathodes. *Electrochemistry Communications*. **3** , pp.505-508.

YOSHIMURA , M, W SUCHANEK, and K BYRAPPA. 2000. Soft processing for advanced inorganic materials. *Material Research Society Bulletin*. **25**, pp.17-24.

YU, S H. 2001. Hydrothermal/Solvothermal processing of advanced ceramic materials. *Journal of The Ceramic Society of Japan*. **109** , pp.S65-S75.

YUAN, Qingchun, Nita ARYANTI, Ruozhou HOU, and Richard WILLIAMS. 2009. Performance of slotted pores in particle manufacture using rotating membrane emulsification. *Particulogy*. **7**(2), pp.114-120.

YUE, Jeffrey, Xuchuan JIANG, and Aibing YU. 2011. Experimental and theoretical study on the β-FeOOH nanorods: Growth and conversion. *Journal of Nanoparticle Research*. **13**, pp.3961-3974.

ZHANG, H and BANFIELD. 1999. New kinetic model for the nanocrystalline anatase-to-rutile transformation revealing rate dependence on number of particles. *American Mineral*. **84**, pp.528-535.

ZHANG, H and J F BANFIELD. 2002. Kinetics of crystallization and crystal growth of nanocrystalline anatase in nanometer-sized amorphous titania. *Chemistry of Materials*. **14**, pp.4145-4154.

ZHANG, Jing, Feng HUANG, and Zhang LIN. 2010. Progress of nanocrystalline growth kinetics based on oriented attachment. *Nanoscale*. **18**, pp.18-34.

ZHANG, J, Z LIN, Y LAN et al. 2006. A multistep oriented attachement kinetics: Coarsening of ZnS nanoparticles in concentrated NaOH. *Journal of American Chemical Society*. **128**, pp.12981-12987.

ZHANG, J, Y WANG, J ZHENG et al. 2007. Oriented attachment kinetics for ligand capped nanocrystals: coarsening of thiol-PbS nanoparticles. *Journal of Physical Chemistry B*. **111**, pp.1449-1454.

ZHENG, Zhanfeng. 2009. *Synthesis and modifications of metal oxide nanostructures and their applications*. Queensland university of technology.

ZHONG, Z Y, J LIN, S P TEH et al. 2007. A rapid and efficient method to deposit gold particles on catalyst supports and its application for CO oxidation at low temperatures. *Advanced Functional Materials*. **17**, pp.1402-1408.

ZHUANG, Z, J ZHANG, F HUANG et al. 2009. Pure multistep oriented attachment growth kinetics of surfactant-free SnO2 nanocrystals. *Physical Chemistry Chemical Physics*. **11**, pp.8516-8521.

ZYSLER, R D, D FIORANI, and A M TESTA. 2001. Investigation of magnetic properties of interacting Fe2O3 nanoparticles. *Journal of Magnetism And Magnetic Materials*. **224**, pp.5-11.

Appendices

Appendix A

Mineralogical, chemical and structural information for β-FeOOH particles (JCPDS card no: 42-1315)

a) Name and formula

Reference code:	00-042-1315
Mineral name:	Akaganeite-*M*
PDF index name:	Iron Oxide Chloride Hydroxide
Empirical formula:	$Cl_{1.3}Fe_8H_{9.7}O_{16}$
Chemical formula:	Fe_{8+3} (O , OH)$_{16}Cl_{1.3}$

b) Crystallographic parameters

Crystal system:	Monoclinic
Space group:	I2/m
Space group number:	12
a (Å):	10.6030

b (Å):	3.0350
c (Å):	10.5120
Alpha (°):	90.0000
Beta (°):	90.2200
Gamma (°):	90.0000
Calculated density (g/cm^3):	3.68
Volume of cell (10^6 pm^3):	338.27
Z:	1.00
RIR:	1.32

c) Subfiles and Quality

Subfiles:	Inorganic
	Mineral
	Corrosion
Quality:	Indexed (I)

d) Comments

Color:	Orange-brown
Sample source:	Specimen from corrosion rind on Campo del Cielo meteorite, Argentina.
Analysis:	Microprobe analysis: $Fe_{7.6}Ni_{0.4}O_{6.35}(OH)_{9.65}Cl_{1.25}$.
Additional pattern:	See ICSD 69606 (PDF 80-1770).

e) References

Primary reference: Post, J., National Museum of Natural History, Smithsonian Institution, Washington, DC, USA, *ICDD Grant-in-Aid*, (1989)

f) Peak list

No.	h	k	l	d [A]	2Theta[deg]	I [%]
1	1	0	-1	7.46800	11.841	100.0
2	2	0	0	5.30100	16.711	37.0
3	0	0	2	5.25600	16.855	35.0
4	2	0	-2	3.74000	23.772	4.0
5	2	0	2	3.72500	23.869	4.0
6	3	0	-1	3.34500	26.628	74.0
7	1	0	-3	3.33400	26.717	74.0
8	1	1	0	2.91700	30.624	1.0
9	4	0	0	2.65000	33.797	14.0
10	0	0	4	2.62700	34.102	14.0
11	2	1	-1	2.55100	35.151	86.0
12	3	0	-3	2.49200	36.011	6.0
13	4	0	2	2.35800	38.134	6.0
14	2	0	4	2.35300	38.218	3.0
15	3	1	0	2.30300	39.081	27.0
16	0	1	3	2.29400	39.241	27.0
17	3	1	-2	2.10600	42.909	8.0
18	5	0	-1	2.07900	43.495	2.0

19	1	0	-5	2.06300	43.849	2.0
20	4	1	-1	1.96080	46.264	15.0
21	1	1	-4	1.95290	46.462	15.0
22	4	0	-4	1.86980	48.657	2.0
23	4	0	4	1.86270	48.855	2.0
24	6	0	0	1.76720	51.684	8.0
25	0	0	6	1.75200	52.166	8.0
26	5	1	0	1.73780	52.624	4.0
27	3	1	-4	1.73290	52.785	4.0
28	6	0	-2	1.67700	54.688	2.0
29	5	1	-2	1.64940	55.682	27.0
30	2	1	-5	1.64340	55.903	30.0
31	0	2	0	1.51750	61.010	13.0
32	6	1	-1	1.51360	61.184	11.0
33	7	0	1	1.49840	61.872	4.0
34	5	0	5	1.48770	62.367	4.0
35	6	0	-4	1.46420	63.483	2.0
36	4	0	6	1.45900	63.736	4.0
37	5	1	-4	1.45190	64.085	12.0
38	4	1	5	1.44560	64.398	12.0
39	2	2	-2	1.40590	66.447	1.0
40	3	1	6	1.39230	67.182	2.0
41	7	0	3	1.38840	67.395	4.0
42	3	2	-1	1.38090	67.811	7.0

g) Stick Pattern

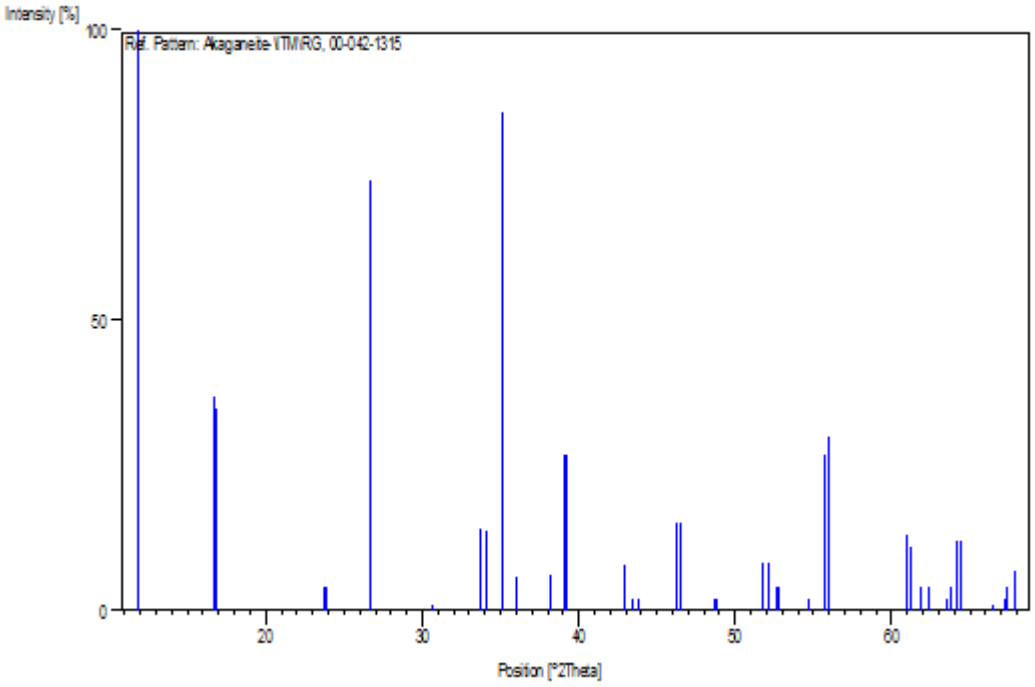

Minerological, chemical and structural information for α-Fe_2O_3 particles (JCPDS card no: 33-0664)

a) Name and formula

Reference code:	00-033-0664
Mineral name:	Hematite, syn
Common name:	burnt ochre

PDF index name:	Iron Oxide
Empirical formula:	Fe_2O_3
Chemical formula:	Fe_2O_3

b)

c) Crystallographic parameters

Crystal system:	Rhombohedral
Space group:	R-3c
Space group number:	167
a (Å):	5.0356
b (Å):	5.0356
c (Å):	13.7489
Alpha (°):	90.0000
Beta (°):	90.0000
Gamma (°):	120.0000
Calculated density (g/cm^3):	5.27
Measured density (g/cm^3):	5.26
Volume of cell (10^6 pm^3):	301.93
Z:	6.00
RIR:	2.40

d) Subfiles and Quality

Subfiles:	Inorganic
	Mineral
	Alloy, metal or intermetalic
	Corrosion
	Common Phase
	Educational pattern
	Forensic
	NBS pattern
	Pharmaceutical
	Pigment/Dye
Quality:	Star (S)

e) Comments

Color:	Dark reddish brown
General comments:	Opaque mineral optical data on specimen from Elba, R_1R_0=30.2, RR_2R_e=26.1, Disp.=16, VHN=1038 (mean at 100, 200, 300), Color values=1 .299, .309, 29.8, 2 .299, .309, 25.7.
	Pattern reviewed by Syvinski, W., McCarthy, G., North Dakota State Univ., Fargo, North Dakota, USA, *ICDD Grant-in-Aid* (1990). Agress well with experimental and calculated patterns.
	Additional weak reflection [indicated by brackets] was observed.
Sample source:	Sample from Pfizer, Inc., New York, USA, heated at 800 C for 3 days.
Optical data:	A=2.94, B=3.22, Sign=-

Additional pattern:	To replace 13-534 and validated by calculated pattern 24-72.
	See ICSD 64599 (PDF 79-7).
Melting point:	1350-1360°
Temperature:	Pattern taken at 25 C.

f) References

Primary reference:	*Natl. Bur. Stand. (U.S.) Monogr. 25*, **18**, 37, (1981)
Optical data:	*Dana's System of Mineralogy, 7th Ed.*, **I**, 529, (1944)

g) Peak list

No.	h	k	l	d [A]	2Theta[deg]	I [%]
1	0	1	2	3.68400	24.138	30.0
2	1	0	4	2.70000	33.153	100.0
3	1	1	0	2.51900	35.612	70.0
4	0	0	6	2.29200	39.277	3.0
5	1	1	3	2.20700	40.855	20.0
6	2	0	2	2.07790	43.519	3.0
7	0	2	4	1.84060	49.480	40.0
8	1	1	6	1.69410	54.091	45.0
9	2	1	1	1.63670	56.152	1.0
10	1	2	2	1.60330	57.429	5.0
11	0	1	8	1.59920	57.590	10.0
12	2	1	4	1.48590	62.451	30.0
13	3	0	0	1.45380	63.991	30.0
14	1	2	5	1.41380	66.028	1.0
15	2	0	8	1.34970	69.601	3.0
16	1	0	10	1.31150	71.937	10.0

17	1	1	9	1.30640	72.262	6.0
18	2	2	0	1.25920	75.431	8.0
19	3	0	6	1.22760	77.730	4.0
20	2	2	3	1.21410	78.760	2.0
21	1	2	8	1.18960	80.711	5.0
22	0	2	10	1.16320	82.940	5.0
23	1	3	4	1.14110	84.916	7.0
24	2	2	6	1.10350	88.542	7.0
25	0	4	2	1.07680	91.345	2.0
26	2	1	10	1.05570	93.715	7.0
27	1	1	12	1.04280	95.239	1.0
28	4	0	4	1.03930	95.663	3.0
29	3	1	8	0.98920	102.285	4.0
30	2	2	9	0.97150	104.914	1.0
31	3	2	4	0.96060	106.623	5.0
32	0	1	14	0.95810	107.025	4.0
33	4	1	0	0.95160	108.090	5.0
34	4	1	3	0.93180	111.518	2.0
35	0	4	8	0.92060	113.594	2.0
36	1	3	10	0.90810	116.045	5.0
37	3	0	12	0.89980	117.758	1.0
38	2	0	14	0.89540	118.697	3.0
39	4	1	6	0.87890	122.431	6.0
40	2	3	8	0.86480	125.929	1.0
41	4	0	10	0.85430	128.758	3.0
42	1	2	14	0.84360	131.878	5.0
43	3	3	0	0.83920	133.241	3.0

44	3	2	10	0.80890	144.457	4.0
45	2	4	4	0.80140	147.971	4.0

h) Stick Pattern

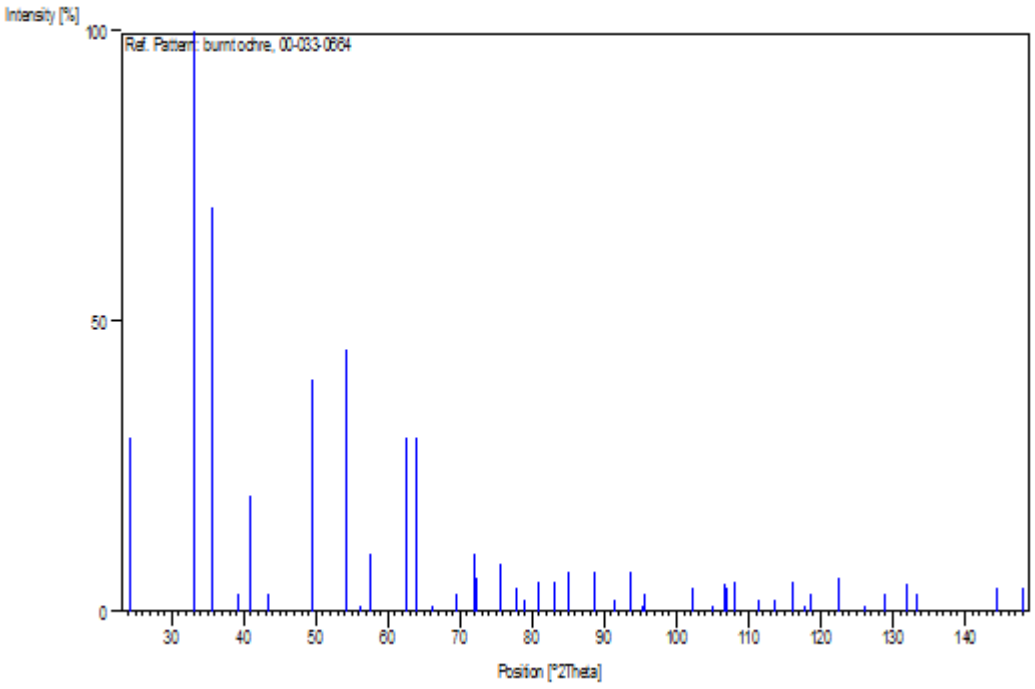

Minerological, chemical and structural information for hydronium iron jarosite particles (JCPDS card no: 21-0932)

a) Name and formula

Reference code:	00-021-0932
Mineral name:	Hydronium jarosite, syn
PDF index name:	Iron Sulfate Hydroxide Hydrate
Empirical formula:	$Fe_3H_9O_{15}S_2$
Chemical formula:	$Fe_3(SO_4)_2(OH)_5 \cdot 2H_2O$

b) Crystallographic parameters

Crystal system:	Rhombohedral
Space group:	R3m
Space group number:	160
a (Å):	7.3559
b (Å):	7.3559
c (Å):	17.0100
Alpha (°):	90.0000
Beta (°):	90.0000
Gamma (°):	120.0000

Calculated density (g/cm^3):	3.00
Volume of cell (10^6 pm^3):	797.09
Z:	3.00
RIR:	-

c) Status, subfiles and quality

Status:	Marked as deleted by ICDD
Subfiles:	Inorganic
	Mineral
Quality:	Indexed (I)

d) Comments

Deleted by:	Deleted by 31-650.
Color:	Golden yellow
General comments:	Rhombohedral axes: a_0=7.085, α=62.56.
	Synthesized by Mme. Walter-Levy (University Caen).
	To replace 2-597 and 18-644.
Additional pattern:	To replace 18-515, 18-653.

e) References

Primary reference:	Technisch Physische Dienst, Delft, Netherlands., *ICDD Grant-in-Aid*, (1968)

Unit cell: *Dana's System of Mineralogy, 7th Ed.*, **2**, 566

f) Peak list

No.	h	k	l	d [A]	2Theta[deg]	I [%]
1	1	0	1	5.97000	14.827	16.0
2	0	0	3	5.67000	15.616	18.0
3	0	1	2	5.10000	17.374	100.0
4	1	1	0	3.68000	24.165	10.0
5	1	0	4	3.54000	25.136	4.0
6	0	2	1	3.13000	28.494	90.0
7	1	1	3	3.09000	28.871	65.0
8	0	1	5	3.00000	29.757	2.0
9	2	0	2	2.98400	29.920	4.0
10	0	0	6	2.83500	31.532	4.0
11	0	2	4	2.54900	35.179	10.0
12	2	0	5	2.32500	38.697	2.0
13	1	2	2	2.31800	38.818	2.0
14	1	0	7	2.27100	39.655	10.0
15	1	1	6	2.24700	40.097	2.0
16	3	0	0	2.12500	42.507	2.0
17	2	1	4	2.09500	43.146	2.0
18	3	0	3	1.99000	45.547	20.0
19	0	2	7	1.93300	46.969	4.0
20	0	0	9	1.89100	48.077	2.0
21	2	2	0	1.83900	49.526	30.0
22	2	0	8	1.76700	51.690	2.0

23	2	2	3	1.74900	52.262	4.0
24	3	1	2	1.73000	52.880	4.0
25	2	1	7	1.71100	53.514	2.0
26	1	3	4	1.63100	56.366	4.0
27	1	2	8	1.59400	57.796	2.0
28	4	0	1	1.58500	58.155	4.0
29	0	4	2	1.56600	58.930	4.0
30	2	2	6	1.54200	59.940	8.0
31	0	2	10	1.50000	61.799	6.0
32	4	0	4	1.49100	62.213	2.0
33	3	2	1	1.45600	63.883	2.0
34	0	4	5	1.44200	64.578	4.0
35	1	3	7	1.42900	65.238	2.0

g) Stick Pattern

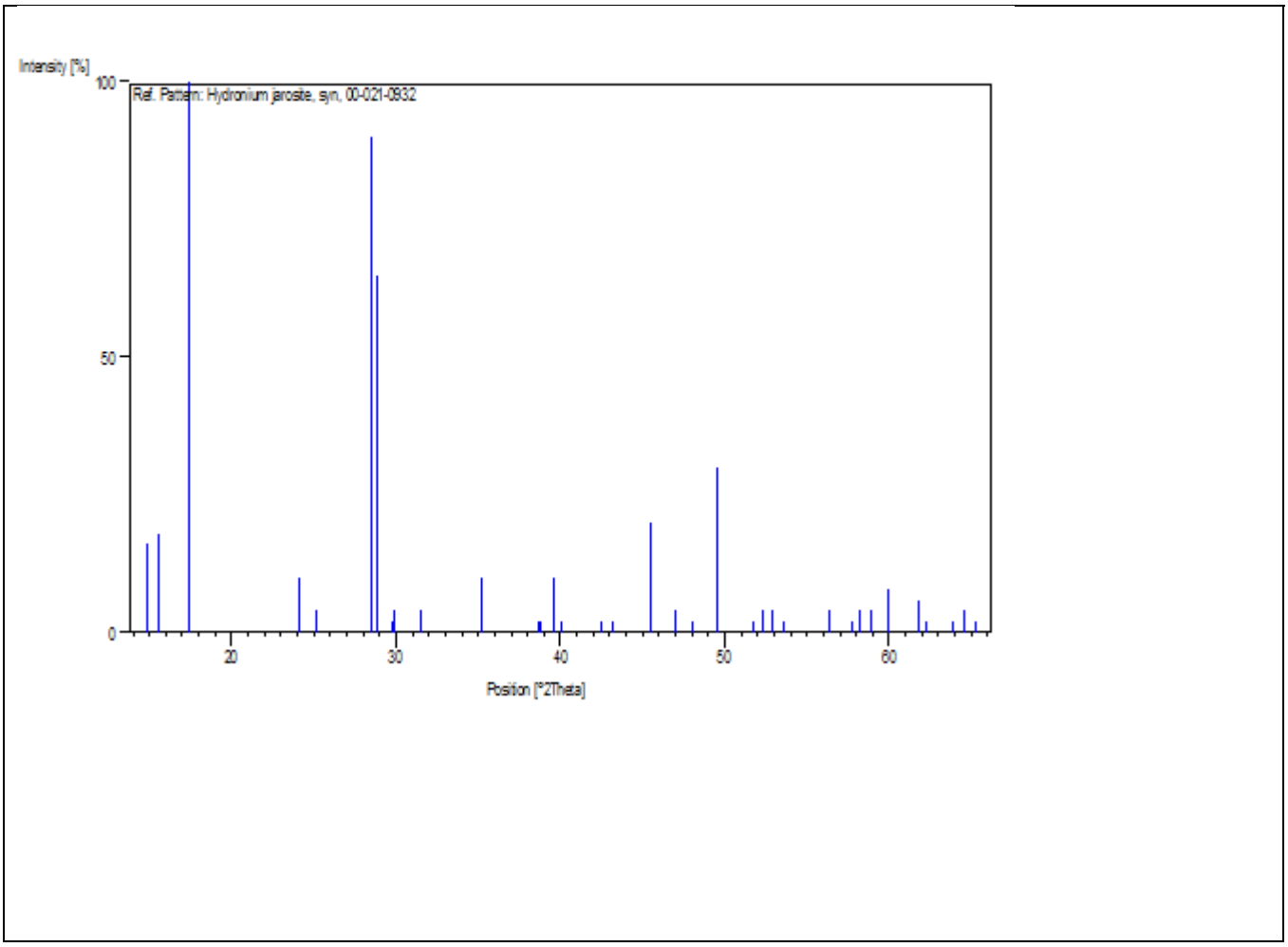

Appendix B

List of Conversation

Contact One:

Dear Mahabubur,

Unfortunately our pending drop apparatus that we have used to make the surface tension determinations that you reference in your email operates only at ambient pressure. This means that we can go easily to temperatures

around 100ºC but we cannot go to pressures of 200-300 kPa (which in the case of alcohol or water mixtures are necessary in order to establish liquid-vapour equilibria inside the chamber). I am sorry that I can not help you.

Good luck with your wok,

Cheers

José Nuno

On Aug 26, 2013, at 1:13 PM, Mahabubur Chowdhury <chowdhurym@cput.ac.za> wrote:

> Good day prof. Lopes,
>
> I hope this email finds you well. I am writing to you in regard of
> measurement of surface tension at high temperature and pressure. I have
> read your paper "High-temperature surface tension and density
> measurements of 1-alkyl-3-methylimidazolium bistriflamide ionic liquids,
> 2010". My research field is in material science. I have submitted a
> paper in the Journal of crystal growth, which evaluates the functional
> relationship between solvent surface tension and particle growth rate.
> However the editor will only accept the paper if i show the surface
> tension of the solvents at hydrothermal conditions (at 100 degree c and
> 200-300 kPa.) I would like to know if you can assist me with measuring
> the surface tension of 4 different alcohols, (Pure alcohol: 1. methanol,
> 2. ethanol, 3. propanol and 4. butanol: and also 50: 50 mixture of the
> same alcohol+water.) at this specific temperature and pressure? You
> Can charge me with the cost to run the experiments or you can co-author

> the paper as it will be accepted once the data is provided and the paper

> is revised. So you can decide how you would like to do this. Please let

> me know. I thank you in advance and hope to hear from you soon.

>

>

> With regards

> Mahabubur

>

>

> M.R.Chowdhury

> Chemical Engineering

> Flow Process Research Centre (FPRC)

> Cape Peninsula University of Technology (CPUT)

> P.O. Box 652, Cape Town 8000 ,South Africa

> Tel: +27 837882309

> Office: +27 (-021)- 4603496

>Email (optional)fahadcapetown@yahoo.com

>http://www.cput.ac.za/flowpro/

> ----------

> and destroy it and any attachments thereto immediately.

> Under no circumstances will the Cape Peninsula University of

> Technology or the sender of this e-mail be liable to any party for

> any direct, indirect, special or other consequential damages for any

> use of this e-mail.

> For the detailed e-mail disclaimer please refer to

>http://www.cput.ac.za/email.php or call +27 (0)21 460 3911

>

> Email secured by Check Point

Email secured by Check Point

Contact two:

Hi,

We do not have the means to measure against pressure.

Kind regards.

Luis Paulo Rebelo

At 13:13 26-08-2013, Mahabubur Chowdhury wrote:

>Good day Prof. Rebelo,

>

>I hope this email finds you well. I am writing to you in regard of

>measurement of surface tension at high temperature and pressure. I have

>read your paper "High-temperature surface tension and density

>measurements of 1-alkyl-3-methylimidazolium bistriflamide ionic liquids,

>2010". My research field is in material science. I have submitted a

>paper in the Journal of crystal growth, which evaluates the functional

>relationship between solvent surface tension and particle growth rate.

>However the editor will only accept the paper if i show the surface

>tension of the solvents at hydrothermal conditions (at 100 degree c and

>200-300 kPa.) I would like to know if you can assist me with measuring

>the surface tension of 4 different alcohols, (Pure alcohol: 1. methanol,

>2. ethanol, 3. propanol and 4. butanol: and also 50: 50 mixture of the

>same alcohol+water.) at this specific temperature and pressure? You

>can charge me with the cost to run the experiments or you can co-author

>the paper as it will be accepted once the data is provided and the paper

>is revised. So you can decide how you would like to do this. Please let

>me know. I thank you in advance and hope to hear from you soon.

>

>

>With regards

Mahabubur

>M.R.Chowdhury

>Chemical Engineering

>Flow Process Research Centre (FPRC)

>Cape Peninsula University of Technology (CPUT)

>P.O. Box 652, Cape Town 8000 ,South Africa

>Tel: +27 837882309

>Office: +27 (-021)- 4603496

>Email (optional)fahadcapetown@yahoo.com

>http://www.cput.ac.za/flowpro/

>----------

>Disclaimer

>This e-mail transmission contains confidential information,

>which is the property of the sender.

>The information in this e-mail or attachments thereto is

>intended for the attention and use only of the addressee.

>Should you have received this e-mail in error, please delete

>and destroy it and any attachments thereto immediately.

>Under no circumstances will the Cape Peninsula University of

>Technology or the sender of this e-mail be liable to any party for

>any direct, indirect, special or other consequential damages for any

>use of this e-mail.

>For the detailed e-mail disclaimer please refer to

>http://www.cput.ac.za/email.php or call +27 (0)21 460 3911

>

>Email secured by Check Point

>

>_____ Information from ESET NOD32 Antivirus, version of virus

>signature database 8729 (20130826) _____

>

>The message was checked by ESET NOD32 Antivirus.

>

>http://www.eset.com

Email secured by Check Point

Contact three:

Dear Sir:

I am sorry to say that I have retired and my lab has been dismantled.
The surface tension equipment has been moved to the lab of Dr Michael
Pegg. I am not sure if he has an available technician to do this work
for you.

I am copying this email to him and he will get back to you if he is
able to do this for you for a fee.

Chris Watts

Quoting Mahabubur Chowdhury <chowdhurym@cput.ac.za>:

> Good day prof. watts,
>
> I hope this email finds you well. I am writing to you in regard of
> measurement of surface tension at high temperature and pressure. I have
> read your paper "Surface tensions of petro-diesel, canola, jatropha and
> soapnut biodiesel fuels at elevated temperatures and pressures, 2013".
> My research field is in material science. I have submitted a paper in
> the Journal of crystal growth, which evaluates the functional

> relationship between solvent surface tension and particle growth rate.

> However the editor will only accept the paper if i show the surface

> tension of the solvents at hydrothermal conditions (at 100 degree c and

> 200-300 kPa) I would like to know if you can assist me with measuring

> the surface tension of 4 different alcohols, (Pure alcohol: 1. methanol,

> 2. ethanol, 3. propanol and 4. butanol: and also 50: 50 mixture of the

> same alcohol + water) at this specific temperature and pressure? You

> can charge me with the cost to run the experiments or you can co-author

> the paper as it will be accepted once the data is provided and the paper

> is revised. And also this experiment will provide novel data as high

> temperature and pressure surface tension measurements of these four

> alcohol is not presented in the literature. So you can decide how you

> would like to do this, either co-authorship or charge me for your

> service. Please let me know. I thank you in advance and hope to hear

> from you soon.

> With regards

> Mahabubur

> M.R.Chowdhury

> Chemical Engineering

> Flow Process Research Centre (FPRC)

> Cape Peninsula University of Technology (CPUT)

> P.O. Box 652, Cape Town 8000 ,South Africa

> Tel: +27 837882309

> Office: +27 (-021)- 4603496

>Email (optional) fahadcapetown@yahoo.com

>http://www.cput.ac.za/flowpro/

> ----------

> Disclaimer

> This e-mail transmission contains confidential information,

> which is the property of the sender.

> The information in this e-mail or attachments thereto is

> intended for the attention and use only of the addressee.

> Should you have received this e-mail in error, please delete

> and destroy it and any attachments thereto immediately.

> Under no circumstances will the Cape Peninsula University of

> Technology or the sender of this e-mail be liable to any party for

> any direct, indirect, special or other consequential damages for any

> use of this e-mail.

> For the detailed e-mail disclaimer please refer to

>http://www.cput.ac.za/email.php or call +27 (0)21 460 3911

>

> Email secured by Check Point

Contact four:

Mahabubur,

Thanks for your interest in our interfacial tension analysis service. However, I regret to say that we do not have capacity to help this autumn. Please, note also that although production of reference data for pure systems like those mentioned is valuable as such, we work on a commercial basis and would have to charge for such services. Our services are aimed at the oil industry and our instruments are designed for very much higher

pressure than 200-300 kPa. If you can find some laboratory at a university doing interfacial tension measurement at the relatively low pressures you request, I think that would be your best option. Such instruments would probably be better suited for the requested pressure range, the work would be less expensive (our services are maybe too expensive to be charged to a private person) and you might find someone who could collaborate with you one the publication instead of charging for the service.

Best regards

Bard Bjorkvik

From: Mahabubur Chowdhury [mailto:chowdhurym@cput.ac.za]

Sent: 04 September 2013 15:58

To: Bård Bjørkvik

Subject: Interfacial tension measurement

Good day,

I hope this email finds you well. I am writing to you in regard of measurement of surface tension at high temperature and pressure. I have read an article from SINTEF regarding the surface tension measurement (I have attached the pdf), My research field is in material science. I have submitted a paper in the Journal of crystal growth, which evaluates the functional relationship between solvent surface tension and particle growth rate. However the editor will only accept the paper if i show the surface tension of the solvents at hydrothermal conditions (at 100 degree c and 200-300 kPa) I would like to know if you can assist me with measuring the surface tension of 4 different alcohols, (Pure alcohol: 1. methanol, 2. ethanol, 3. propanol and 4. butanol: and also 50: 50 mixture of the same alcohol + water) at this specific temperature and pressure? You can charge me with the cost to run the experiments or you can co-author the paper as it will be accepted once the data is provided and the paper is revised. And also this experiment will provide novel data as high temperature and

pressure surface tension measurements of these four alcohol is not presented in the literature. So you can decide how you would like to do this, either co-authorship or charge me for your service. Please let me know. I thank you in advance and hope to hear from you soon.

With regards

Mahabubur

M.R.Chowdhury

Chemical Engineering

Flow Process Research Centre (FPRC)

Cape Peninsula University of Technology (CPUT)

P.O. Box 652, Cape Town 8000 ,South Africa

Tel: +27 837882309

Office: +27 (-021)- 4603496

Email (optional)fahadcapetown@yahoo.com<mailto:fahadcapetown@yahoo.com>

http://www.cput.ac.za/flowpro/

Contact five:

Good day Prof. Lamia and Dr. Piri,

I hope this email finds both of you well. I am writing to you in regard of measurement of surface tension at high temperature and pressure. Your contacts were forwarded to me by Bård Bjørkvik from SINTEF Norway. My research field is in material science. I have submitted a paper in the Journal of crystal growth, which evaluates the functional relationship between solvent surface tension and particle growth rate. However the editor will only accept the paper if i show the surface tensions of the solvents at hydrothermal conditions (at 100

degree c and 200-300 kPa) I would like to know if you can assist me with measuring the surface tension of 4 different alcohols, (Pure alcohol: 1. methanol, 2. ethanol, 3. propanol and 4. butanol: and also 50: 50 mixture of the same alcohol + water) at this specific temperature and pressure? You can charge me with the cost to run the experiments or you can co-author the paper as it will be accepted once the data is provided and the paper is revised. And also this measured experimental data will be novel data as high temperature and pressure surface tension measurements of these four alcohol is not presented in the literature so far. So you can decide how you would like to do this, either co-authorship or charge me for your service. Please let me know. I am in desperate need as the date for the re-submission of the paper is the 6th of October 2013. I thank you in advance and hope to hear from you soon.

With regards

Mahabubur

M.R.Chowdhury

Chemical Engineering

Flow Process Research Centre (FPRC)

Cape Peninsula University of Technology (CPUT)

P.O. Box 652, Cape Town 8000,South Africa

Tel: +27 837882309

Office: +27 (-021)- 4603496

Email (optional)fahadcapetown@yahoo.com

http://www.cput.ac.za/flowpro/

NO response